

## **Abstract**

HARTL, ALEXANDRE EMMANUEL. Bouncing, Sliding and Rolling Dynamics of a Spherical Rover Crossing a Ravine. (Under the direction of Dr. Andre Mazzoleni)

This study presents a numerical simulation model predicting the motion of a tumbleweed rover as it encounters ravines and valleys. The research provides an understanding of the range of tumbleweed design parameters essential for mobility over varied terrain. The study also introduces a numerical model covering the rover's rolling, sliding and bouncing behaviors and the transitions between these modes of movement.

A collision model based on Kane's method of dynamics is used to study the impact between the rover and flat terrain. The model is extended by considering collisions on hills, and a numerical model is created tracking the rover's motion and transition between different terrain types. Rolling and sliding models for a rover in motion are developed for flat and sloping terrains. This study includes several case studies which demonstrate the model's utility as an initial design tool for tumbleweed rovers.

**BOUNCING, SLIDING AND  
ROLLING DYNAMICS OF A  
SPHERICAL ROVER CROSSING A  
RAVINE**

by  
**ALEXANDRE E. HARTL**

**A THESIS SUBMITTED TO THE GRADUATE FACULTY OF NORTH  
CAROLINA STATE UNIVERSITY IN PARTIAL FULFILLMENT OF  
THE REQUIREMENTS FOR THE DEGREE OF MASTER OF  
SCIENCE**

**AEROSPACE ENGINEERING**

**RALEIGH, N.C.  
December, 2006**

**APPROVED BY:**

---

**CHAIR OF ADVISORY COMMITTEE  
DR. ANDRE P. MAZZOLENI**

---

**DR. FRED R. DEJARNETTE**

---

**DR. MANSOOR A. HAIDER**

## **Biography**

Alexandre Emmanuel Hartl was born on June 10, 1981, in Vorhees, N.J. He completed his upper-level education with a bachelor of science degree in Mathematics at the University of North Carolina at Chapel Hill in May 2003. He will complete the requirements for his master of science degree in Aerospace Engineering at North Carolina State University in Raleigh on December 2006.

## Acknowledgements

I want to express my sincere gratitude to my parents, Erwin and Patricia Hartl. Their love, support and generosity sustained the completion of this thesis. I cannot say thank you enough. Also deserving much thanks are my brothers, Boris and Chris. They provided constant encouragement and reminded me there is a life outside of school. Thanks Boris for the kind editing. Moreover, I want to acknowledge my grandmother, Irene, for offering so many kind words over the years. Thank you Heggy Yoon and Justin Newsome for your help.

I owe much thanks to my advisor, Dr. Andre Mazzoleni. He introduced me to the rich field of dynamics while I was a student in his class. His patience and guidance played a significant role in completing this thesis. He always took the time to answer questions and suggest new ideas.

I would also like to thank my committee members, Dr. Mansoor Haider and Dr. Fred Dejarnette, for their help.

# Contents

List of Figures . . . . .	vi
Nomenclature . . . . .	ix
<b>1 Introduction and Background</b>	<b>1</b>
1.1 Notation/Assumptions . . . . .	3
<b>2 Equations of Motion for a Bouncing Sphere</b>	<b>5</b>
2.1 Equations of Motion for a Bouncing Sphere on a Horizontal Plane	5
2.1.1 Background . . . . .	5
2.1.2 Derivation . . . . .	8
2.1.3 Trajectory Model and the Reinitialization of the General- ized Speeds . . . . .	16
2.2 Equations of Motion for a Bouncing Sphere on an Incline Plane .	17
2.2.1 Background . . . . .	17
2.2.2 Derivation . . . . .	20
2.2.3 Trajectory Model and the Reinitialization of the General- ized Speeds . . . . .	28
2.3 Equations of Motion for a Bouncing Sphere on a Decline Plane . .	30
2.3.1 Derivation . . . . .	33
2.3.2 Trajectory Model and the Reinitialization of the General- ized Speeds . . . . .	41
<b>3 Equations of Motion for a Rolling and Sliding Sphere</b>	<b>44</b>
3.1 Rolling and Sliding Model of a Rigid Sphere on a Horizontal Plane	44
3.2 Rolling and Sliding Model of a Rigid Sphere on an Incline Plane .	47
3.3 Rolling and Sliding Model of a Rigid Sphere on a Decline Plane .	51

<b>4</b>	<b>Numerical Simulation Model</b>	<b>56</b>
4.1	Framework . . . . .	56
4.2	Numerical Simulation Example . . . . .	58
4.3	Parametric Study Framework . . . . .	59
<b>5</b>	<b>Parametric Studies</b>	<b>62</b>
5.1	Parametric Study I and II . . . . .	62
5.2	Parametric Study III and IV . . . . .	63
5.3	Parametric Study Figures . . . . .	64
<b>6</b>	<b>Case Studies</b>	<b>97</b>
6.1	Case Study I . . . . .	97
6.2	Case Study II . . . . .	98
6.3	Case Study III . . . . .	99
6.4	Case Study IV . . . . .	101
<b>7</b>	<b>Conclusions</b>	<b>103</b>
	<b>References</b>	<b>104</b>
	Appendix . . . . .	108
<b>A</b>	<b>Example Of The Runge-Kutta Method</b>	<b>109</b>
<b>B</b>	<b>Application Of The Runge-Kutta Method</b>	<b>110</b>
B.1	Numerical Models on the Horizontal Plane . . . . .	110
B.2	Numerical Models on the Incline Plane . . . . .	114
B.3	Numerical Models on the Decline Plane . . . . .	119

# List of Figures

1.1	Artist’s concept of a Tumbleweed Rover (1) . . . . .	2
2.1	Reference Frame (Horizontal Plane) . . . . .	6
2.2	Reference Frame (Incline Plane) . . . . .	18
2.3	Rotation Matrix (Incline Plane) . . . . .	30
2.4	Reference Frame (Decline Plane) . . . . .	31
2.5	Rotation Matrix (Decline Plane) . . . . .	43
3.1	Free Body Diagram (Horizontal Plane) . . . . .	45
3.2	Free Body Diagram (Incline Plane) . . . . .	48
3.3	Free Body Diagram (Decline Plane) . . . . .	52
4.1	An example of an arbitrary valley encountered by a tumbleweed rover . . . . .	57
4.2	A two-dimensional simulation representation . . . . .	59
4.3	A three-dimensional simulation representation (view I) . . . . .	60
4.4	A three-dimensional simulation representation (view II) . . . . .	61
5.1	Percentage crossed for varying design parameter sets and velocity range ( $2 - 7m/s$ ) on Mars. . . . .	65
5.2	Percentage crossed for varying design parameter sets and velocity range ( $2 - 7m/s$ ) on Earth. . . . .	66
5.3	Average tumbleweed height for varying design parameter sets and velocity range ( $5 - 10m/s$ ) on Mars. Note $J/m = 0.1b^2$ . . . . .	67
5.4	Average tumbleweed height for varying design parameter sets and velocity range ( $5 - 10m/s$ ) on Mars. Note $J/m = 0.2b^2$ . . . . .	68

5.5	Average tumbleweed height for varying design parameter sets and velocity range (5 – 10m/s) on Mars. Note $J/m = 0.3b^2$ . . . . .	69
5.6	Average tumbleweed height for varying design parameter sets and velocity range (5 – 10m/s) on Mars. Note $J/m = 0.4b^2$ . . . . .	70
5.7	Average tumbleweed height for varying design parameter sets and velocity range (5 – 10m/s) on Mars. Note $J/m = 0.5b^2$ . . . . .	71
5.8	Average tumbleweed height for varying design parameter sets and velocity range (5 – 10m/s) on Mars. Note $J/m = 0.6b^2$ . . . . .	72
5.9	Average tumbleweed height for varying design parameter sets and velocity range (5 – 10m/s) on Mars. Note $J/m = 0.67b^2$ . . . . .	73
5.10	Average tumbleweed height for varying design parameter sets and velocity range (5 – 10m/s) on Mars. . . . .	74
5.11	Tumbleweed height for varying design parameter sets and velocity profiles (5 – 10m/s) on Mars. Note $J/m = 0.1b^2$ . . . . .	75
5.12	Tumbleweed height for varying design parameter sets and velocity profiles (5 – 10m/s) on Mars. Note $J/m = 0.2b^2$ . . . . .	76
5.13	Tumbleweed height for varying design parameter sets and velocity profiles (5 – 10m/s) on Mars. Note $J/m = 0.3b^2$ . . . . .	77
5.14	Tumbleweed height for varying design parameter sets and velocity profiles (5 – 10m/s) on Mars. Note $J/m = 0.4b^2$ . . . . .	78
5.15	Tumbleweed height for varying design parameter sets and velocity profiles (5 – 10m/s) on Mars. Note $J/m = 0.5b^2$ . . . . .	79
5.16	Tumbleweed height for varying design parameter sets and velocity profiles (5 – 10m/s) on Mars. Note $J/m = 0.6b^2$ . . . . .	80
5.17	Tumbleweed height for varying design parameter sets and velocity profiles (5 – 10m/s) on Mars. Note $J/m = 0.67b^2$ . . . . .	81
5.18	Average tumbleweed height for varying design parameter sets and velocity range (5 – 10m/s) on Earth. Note $J/m = 0.1b^2$ . . . . .	82
5.19	Average tumbleweed height for varying design parameter sets and velocity range (5 – 10m/s) on Earth. Note $J/m = 0.2b^2$ . . . . .	83
5.20	Average tumbleweed height for varying design parameter sets and velocity range (5 – 10m/s) on Earth. Note $J/m = 0.3b^2$ . . . . .	84

5.21	Average tumbleweed height for varying design parameter sets and velocity range ( $5 - 10m/s$ ) on Earth. Note $J/m = 0.4b^2$ . . . . .	85
5.22	Average tumbleweed height for varying design parameter sets and velocity range ( $5 - 10m/s$ ) on Earth. Note $J/m = 0.5b^2$ . . . . .	86
5.23	Average tumbleweed height for varying design parameter sets and velocity range ( $5 - 10m/s$ ) on Earth. Note $J/m = 0.6b^2$ . . . . .	87
5.24	Average tumbleweed height for varying design parameter sets and velocity range ( $5 - 10m/s$ ) on Earth. Note $J/m = 0.67b^2$ . . . . .	88
5.25	Average tumbleweed height for varying design parameter sets and velocity range ( $5 - 10m/s$ ) on Earth. . . . .	89
5.26	Tumbleweed height for varying design parameter sets and velocity profiles ( $5 - 10m/s$ ) on Earth. Note $J/m = 0.1b^2$ . . . . .	90
5.27	Tumbleweed height for varying design parameter sets and velocity profiles ( $5 - 10m/s$ ) on Earth. Note $J/m = 0.2b^2$ . . . . .	91
5.28	Tumbleweed height for varying design parameter sets and velocity profiles ( $5 - 10m/s$ ) on Earth. Note $J/m = 0.3b^2$ . . . . .	92
5.29	Tumbleweed height for varying design parameter sets and velocity profiles ( $5 - 10m/s$ ) on Earth. Note $J/m = 0.4b^2$ . . . . .	93
5.30	Tumbleweed height for varying design parameter sets and velocity profiles ( $5 - 10m/s$ ) on Earth. Note $J/m = 0.5b^2$ . . . . .	94
5.31	Tumbleweed height for varying design parameter sets and velocity profiles ( $5 - 10m/s$ ) on Earth. Note $J/m = 0.6b^2$ . . . . .	95
5.32	Tumbleweed height for varying design parameter sets and velocity profiles ( $5 - 10m/s$ ) on Earth. Note $J/m = 0.67b^2$ . . . . .	96
6.1	A two-dimensional simulation representation on Mars. . . . .	100
6.2	A two-dimensional simulation representation on Earth. . . . .	102

# Nomenclature<sup>1</sup>

$b$	Radius
$m$	Mass
$J$	Principal Moment of Inertia
$e$	Coefficient of Restitution
$\mu$	Coefficient of Static Friction
$\mu'$	Coefficient of Kinetic Friction
$\vec{\omega}$	Angular Velocity
$\vec{v}$	Translational Velocity
$u$	Generalized Speeds
$\vec{v}^P$	Partial Velocity of P
$\vec{R}$	Contact Force
$S$	Component of Contact Force
$\vec{v}$	Normal Impulse
$\vec{\tau}$	Tangential Impulse
$I$	Generalized Impulse
$p$	Generalized Momentum
$K$	Kinetic Energy
$\vec{F}$	Force
$\vec{N}$	Normal Force
$\vec{\alpha}$	Angular Acceleration
$\vec{a}$	Translational Acceleration
$\vec{g}$	Gravitational Acceleration
$\beta$	Angle of Decline Plane
$\theta$	Angle of Incline Plane
$dh$	Height of Decline Plane
$pl$	Length of Horizontal Plane

---

<sup>1</sup>Any symbol which is not a vector is assumed to be a magnitude or scalar

# Chapter 1

## Introduction and Background

The evidence of water on Mars and the idea of using the Moon as a staging ground for future planetary missions has increased interest in these regions. Future missions will require the exploration of large areas on these surfaces since areas of scientific interest are far away from the landing sites. Because of the inherent dangers with manned missions, rovers provide a viable option for future investigations on these regions.

NASA currently employs wheeled rovers, including the Mars Exploration Rovers, to examine the Martian surface. These rovers are intricate and expensive, with limited ability to navigate rough terrain. This complicates gathering scientific data on Martian climate and geology, and renders answering questions on the existence of water and life difficult.

A vehicle prepared to explore large areas of terrain is the tumbleweed rover. A tumbleweed is a spherical (wind-driven or self-propelled) rover designed to provide superior mobility and greater accessibility on the surface of Mars and the Moon, see figure 1.1. Compared with conventional wheeled rovers, a tumbleweed can cover vast distances faster and reach previously inaccessible areas of scientific interest, such as canyons and valleys. Since a tumbleweed is significantly less expensive than traditional rovers, multiple tumbleweeds can be deployed across the Martian or Lunar surface for scientific surveys. The tumbleweed's design is also well suited for polar missions since the rover can seek out water sources beneath a surface desert or an ice sheet, a task that cannot be done accurately

from orbit. For these reasons a model describing and predicting a tumbleweed's motion across the Martian or Lunar terrain is valuable.



Figure 1.1: Artist's concept of a Tumbleweed Rover (1)

The tumbleweed rover is based on concepts going back to the 1970's, where Jacques Blamont of the National Center for Space Studies developed the notion for wind-driven rovers. The concept has been pursued by several investigators at the NASA Langley Research Center (LaRC) and at the Jet Propulsion Laboratory (JPL). LaRC is focusing on concepts based on lightweight deployable structures, while JPL is focusing on inflatable concepts based on airbag landing technology. Other organizations, including Texas Technical University (TTU), North Carolina State University (NCSU) and the Swiss Federal Institute of Technology are also examining wind-driven rover concepts.

Research into the tumbleweed rover's dynamics, however, is in its early stages. Feasibility studies of wind-driven mobility on the surface of Mars have been exam-

ined (2) – (10), and other studies have presented dynamic models for particular tumbleweed concepts (11) – (17). Researchers at NASA Langley have investigated the dynamics of a tumbleweed rover rolling on a flat surface and on a slope (2). A simplified dynamic analysis of a rover bouncing and impacting a rock have also been presented (3). Kolacinski and Quinn investigated the numerical modeling of wind-driven Martian rovers, and developed techniques for numerically modeling the rover’s dynamics (15). Work done by Rose et al. have produced a detailed dynamic model using Martian wind driven sensor platform concepts (11), (12).

Several areas have been identified where the existing research can be expanded. Particularly, a numerical simulation model predicting a tumbleweed’s motion for arbitrary terrains is needed. Also required are dynamic models describing the tumbleweed’s behaviors on these terrains, which include flat planes, hills, gullies and valleys.

This study presents a numerical simulation model predicting the motion of a tumbleweed rover as it encounters real terrain scenarios. The research provides an understanding of the range of tumbleweed design parameters essential for mobility over varied terrain. The study also introduces a numerical model covering the tumbleweed’s rolling, sliding and bouncing behaviors and the transitions between these modes of movement.

A collision model based on Kane’s method of dynamics is used to study the impact between the tumbleweed and flat terrain. The model is extended by considering collisions on hills, and a numerical model is created tracking the tumbleweed’s motion and transition between different terrain types. Rolling and sliding models for a tumbleweed in motion are developed for flat and sloping terrains. This study includes several case studies which demonstrate the model’s utility as an initial design tool for tumbleweed rovers.

## 1.1 Notation/Assumptions

Kane’s equations and the Newton-Euler method are adopted for the modeling of the equations of motion. The choice of notation to employ is based on the application. For complex systems, including the collision dynamics of a bouncing

sphere, Kane's equations provides a concise approach for deriving equations of motion, resulting in efficient algorithms. For basic applications, including the equations of motion for free-fall and rolling, the Newton-Euler method is preferred. Throughout the study the tumbleweed is modeled as a sphere, and it is assumed the tumbleweed is non-rigid during collisions with the terrain. It is also assumed the tumbleweed rover is sufficiently rigid while rolling so that elastic considerations may be ignored. Due to the thin Martian atmosphere, the effects of drag and the Magnus force are neglected. Note the words "sphere" and "tumbleweed rover" are used interchangeably in the study.

# Chapter 2

## Equations of Motion for a Bouncing Sphere

Kane's collision model for a bouncing sphere on a horizontal plane provides a direct method for computing a sphere's generalized speeds after impact(18). We extend the model to include collisions on the incline and decline planes. As a result an efficient set of algorithms are constructed for numerical simulations. For completeness, the collision models for the horizontal, incline and decline planes are independently derived, and these models may be used to analysis the sphere's motion for varied terrains.

### 2.1 Equations of Motion for a Bouncing Sphere on a Horizontal Plane

#### 2.1.1 Background

Consider a sphere of mass  $m$  and radius  $b$ , whose motion is unconstrained on a horizontal plane defined by three mutually perpendicular unit vectors  $(\vec{n}_1, \vec{n}_2, \vec{n}_3)$ , where  $\vec{n}_2$  is perpendicular to the plane, see figure 2.1. The sphere has six degrees of freedom, three angles defining its orientation and three components defining its position. Consequently, the sphere's angular and translational velocities may

be expressed in terms of the generalized speeds  $u_1, \dots, u_6$  as

$$\vec{\omega} = u_1 \vec{n}_1 + u_2 \vec{n}_2 + u_3 \vec{n}_3 \quad (2.1)$$

and

$$\vec{v} = u_4 \vec{n}_1 + u_5 \vec{n}_2 + u_6 \vec{n}_3 \quad (2.2)$$

where  $\vec{v}$  denotes the velocity of the sphere's center of mass.

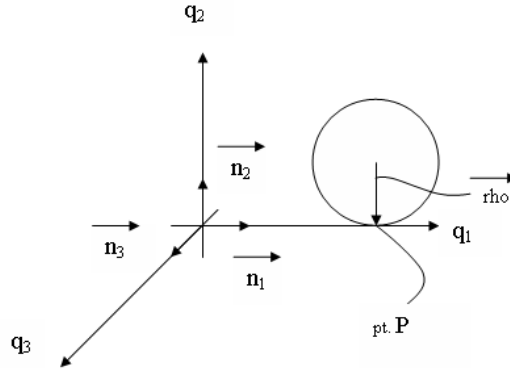


Figure 2.1: Reference Frame (Horizontal Plane)

From equations (2.1) and (2.2), we define the velocity of the point P of the sphere that comes into contact with the surface as

$$v^{\vec{P}} = \vec{v} + \vec{\omega} \times \vec{\rho} \quad (2.3)$$

where  $\vec{\rho} = -bn_2$ .

Then from equation (2.3), the partial velocities of P are determined by inspection and are simply the coefficients for each generalized speed.

Operating under the aforementioned system, Kane's collision model enables us to investigate the collision of a sphere as it impacts a flat surface beginning at

time  $t_1$  and ending at time  $t_2$ . Two dynamical equations essential to the model are the generalized impulse  $I_r$  and the generalized momentum  $p_r$ . The generalized impulse is defined as

$$I_r = v_r^P(\vec{t}_1) \cdot \int_{t_1}^{t_2} \vec{R} dt \quad (r = 1, \dots, 6) \quad (2.4)$$

where  $v_r^P(\vec{t}_1)$  is the partial velocity of the sphere at the point of contact with the surface at time  $t_1$ , and  $\int_{t_1}^{t_2} \vec{R} dt$  is the contact force exerted on the sphere by the surface at their contact point during the time interval  $[t_1, t_2]$ . Moreover, if we let  $S_i = \vec{n}_i \cdot \int_{t_1}^{t_2} \vec{R} dt$  ( $i=1,2,3$ ), then we can define  $\int_{t_1}^{t_2} \vec{R} dt$  as

$$\int_{t_1}^{t_2} \vec{R} dt = S_1 \vec{n}_1 + S_2 \vec{n}_2 + S_3 \vec{n}_3 \quad (2.5)$$

The generalized momentum<sup>1</sup> is defined as follows:

$$p_r = \frac{\partial K}{\partial u_r} \quad (r = 1, \dots, 6) \quad (2.6)$$

where  $K$  is the kinetic energy of the sphere and  $u_r$  are the generalized speeds. Integrating equation (2.4) results in the following approximation connecting the generalized impulse to the generalized momentum<sup>2</sup>:

$$I_r \approx p_r(t_2) - p_r(t_1) \quad (r = 1, \dots, 6) \quad (2.7)$$

In order to capture the sphere's motion at time  $t_2$ , two assumptions supplement the use of equation (2.7) together with a complete description of the sphere's motion at time  $t_1$ . The first assumption is the normal components of the velocity of approach  $\vec{v}_A$  and separation  $\vec{v}_S$  of the sphere, with respect to the surface, have opposite directions, where the magnitudes are related by the following equation:

$$\vec{n}_2 \cdot \vec{v}_S = -e \vec{n}_2 \cdot \vec{v}_A \quad (2.8)$$

In equation (2.8),  $e$  is called the coefficient of restitution,  $\vec{v}_A = \vec{v}^P(t_1)$  and  $\vec{v}_S = \vec{v}^P(t_2)$ , where it is assumed the surface's velocity is zero during and after colliding with the sphere. The second assumption determines if the sphere encounters no

<sup>1</sup>See page 226 of (18) for a proof of this definition

<sup>2</sup>See pages 226-227 of (18) for a proof of this definition

slipping or slipping at the point of contact with the surface. If there is no slipping at  $t_2$ , the following inequality must be satisfied:

$$|\vec{\tau}| < \mu |\vec{\nu}| \quad (2.9)$$

where  $\vec{\tau}=S_1\vec{n}_1 + S_3\vec{n}_3$  is the tangential impulse,  $\vec{\nu}=S_2\vec{n}_2$  is the normal impulse and  $\mu$  is the coefficient of static friction. Consequently,

$$\vec{n}_2 \times (\vec{v}_S \times \vec{n}_2) = 0 \quad (2.10)$$

The equation states the tangential component of the velocity of separation is zero.

If inequality (2.8) is violated, slipping occurs at  $t_2$ , and  $\vec{\tau}$  is expressed as

$$\vec{\tau} = -\mu' |\vec{\nu}| \frac{\vec{n}_2 \times (\vec{v}_S \times \vec{n}_2)}{|\vec{n}_2 \times (\vec{v}_S \times \vec{n}_2)|} \quad (2.11)$$

where the constant  $\mu'$  is the coefficient of kinetic friction.

The model requires the physical parameters  $b$ ,  $m$ ,  $J$ ,  $e$ ,  $\mu$  and  $\mu'$ , and the generalized speeds at time  $t_1$  are known. Then the motion of the sphere at time  $t_2$  is fully defined by invoking equations (2.7), (2.8), (2.9), (2.10) and (2.11).

## 2.1.2 Derivation

This section provides a complete derivation of Kane's collision model for a bouncing uniform sphere on a horizontal plane. Assume the following physical parameters are known:  $b$ ,  $m$ ,  $J$ ,  $e$ ,  $\mu$  and  $\mu'$ . Also assume that the generalized speeds at time  $t_1$  are known and are given in the form of equations (2.1) and (2.2). The generalized speeds at time  $t_2$  are the quantities to be determined.

The velocity of the point P of the sphere that comes into contact with the surface is given by equation (2.3):

$$\begin{aligned} \vec{v}^P &= \vec{v} + \vec{\omega} \times \vec{\rho} \\ &= u_4\vec{n}_1 + u_5\vec{n}_2 + u_6\vec{n}_3 + (u_1\vec{n}_1 + u_2\vec{n}_2 + u_3\vec{n}_3) \times -b\vec{n}_2 \\ &= u_4\vec{n}_1 + u_5\vec{n}_2 + u_6\vec{n}_3 + bu_3\vec{n}_1 - bu_1\vec{n}_3 \\ &= (u_4 + bu_3)\vec{n}_1 + u_5\vec{n}_2 + (u_6 - bu_1)\vec{n}_3 \end{aligned} \quad (2.12)$$

The partial velocities of P at time  $t_1$  are determined by inspection of equation (2.12) and are listed below:

$$v_1^P(\vec{t}_1) = -b\vec{n}_3 \quad (2.13)$$

$$v_2^P(\vec{t}_1) = 0 \quad (2.14)$$

$$v_3^P(\vec{t}_1) = b\vec{n}_1 \quad (2.15)$$

$$v_4^P(\vec{t}_1) = \vec{n}_1 \quad (2.16)$$

$$v_5^P(\vec{t}_1) = \vec{n}_2 \quad (2.17)$$

$$v_6^P(\vec{t}_1) = \vec{n}_3 \quad (2.18)$$

From equations (2.4) and (2.5) and employing equations (2.13) through (2.18), the generalized impulse at the point of contact is expressed as

$$I_r = v_r^P(\vec{t}_1) \cdot (S_1\vec{n}_1 + S_2\vec{n}_2 + S_3\vec{n}_3) \quad (r = 1, \dots, 6) \quad (2.19)$$

where

$$\begin{aligned} I_1 &= -b\vec{n}_3 \cdot (S_1\vec{n}_1 + S_2\vec{n}_2 + S_3\vec{n}_3) \\ &= -bS_3 \end{aligned} \quad (2.20)$$

$$\begin{aligned} I_2 &= 0 \cdot (S_1\vec{n}_1 + S_2\vec{n}_2 + S_3\vec{n}_3) \\ &= 0 \end{aligned} \quad (2.21)$$

$$\begin{aligned} I_3 &= b\vec{n}_1 \cdot (S_1\vec{n}_1 + S_2\vec{n}_2 + S_3\vec{n}_3) \\ &= bS_1 \end{aligned} \quad (2.22)$$

$$\begin{aligned} I_4 &= \vec{n}_1 \cdot (S_1\vec{n}_1 + S_2\vec{n}_2 + S_3\vec{n}_3) \\ &= S_1 \end{aligned} \quad (2.23)$$

$$\begin{aligned} I_5 &= \vec{n}_2 \cdot (S_1\vec{n}_1 + S_2\vec{n}_2 + S_3\vec{n}_3) \\ &= S_2 \end{aligned} \quad (2.24)$$

$$\begin{aligned}
I_6 &= \vec{n}_3 \cdot (S_1 \vec{n}_1 + S_2 \vec{n}_2 + S_3 \vec{n}_3) \\
&= S_3
\end{aligned} \tag{2.25}$$

The kinetic energy of the sphere is equal to the sum of the kinetic energy due to the rotational and translational velocities about the center of mass. So, we can write:

$$K_{sphere} = K_\omega + K_v \tag{2.26}$$

where

$$\begin{aligned}
K_\omega &= \frac{1}{2} \vec{\omega} \cdot \vec{L} \cdot \vec{\omega} \\
&= \frac{1}{2} \{\omega\}^T [L] \{\omega\} \\
&= \frac{1}{2} (L_{11}u_1^2 + L_{22}u_2^2 + L_{33}u_3^2) - L_{12}u_1u_2 - L_{13}u_1u_3 - L_{23}u_2u_3
\end{aligned} \tag{2.27}$$

and

$$\begin{aligned}
K_v &= \frac{1}{2} m \vec{v} \cdot \vec{v} \\
&= \frac{1}{2} m \{v\}^T \{v\} \\
&= \frac{1}{2} m (u_4^2 + u_5^2 + u_6^2)
\end{aligned} \tag{2.28}$$

Since the coordinate axes are selected as the principal axes, the expression for the rotational kinetic energy in equation (2.27) simplifies to

$$\begin{aligned}
K_\omega &= \frac{1}{2} (L_{11}u_1^2 + L_{22}u_2^2 + L_{33}u_3^2) \\
&= \frac{1}{2} J (u_1^2 + u_2^2 + u_3^2)
\end{aligned} \tag{2.29}$$

where  $J = L_{11} = L_{22} = L_{33}$ . Therefore, the kinetic energy of the sphere is

$$K_{sphere} = \frac{1}{2} J (u_1^2 + u_2^2 + u_3^2) + \frac{1}{2} m (u_4^2 + u_5^2 + u_6^2) \tag{2.30}$$

Substituting equation (2.30) into equation (2.6), results in expressions for the generalized momentum:

$$p_1 = J u_1 \tag{2.31}$$

$$p_2 = Ju_2 \quad (2.32)$$

$$p_3 = Ju_3 \quad (2.33)$$

$$p_4 = mu_4 \quad (2.34)$$

$$p_5 = mu_5 \quad (2.35)$$

$$p_6 = mu_6 \quad (2.36)$$

With expressions developed for the generalized impulse and momentum, substituting equations (2.20) through (2.25) and equations (2.31) through (2.36) into equation (2.7), we develop the following expressions:

$$-bS_3 \approx J[u_1(t_2) - u_1(t_1)] \quad (2.37)$$

$$0 \approx J[u_2(t_2) - u_2(t_1)] \quad (2.38)$$

$$bS_1 \approx J[u_3(t_2) - u_3(t_1)] \quad (2.39)$$

$$S_1 \approx m[u_4(t_2) - u_4(t_1)] \quad (2.40)$$

$$S_2 \approx m[u_5(t_2) - u_5(t_1)] \quad (2.41)$$

$$S_3 \approx m[u_6(t_2) - u_6(t_1)] \quad (2.42)$$

From equation (2.38), we can immediately solve for  $u_2(t_2)$ :

$$u_2(t_2) \approx u_2(t_1) \quad (2.43)$$

Studying equations (2.37) and (2.39)–(2.42), we have five equations and eight unknowns:  $u_1(t_2)$ ,  $u_3(t_2)$ ,  $u_4(t_2)$ ,  $u_5(t_2)$ ,  $u_6(t_2)$ ,  $S_1$ ,  $S_2$  and  $S_3$ . We use equations (2.8)–(2.11) to supplement the preceding equations. To use equation (2.8) we first define the velocity of approach and separation. Assuming the velocity of the surface is zero during and after colliding with the sphere, the velocity of approach and separation are determined from equation (2.12) where:

$$\begin{aligned} \vec{v}_A &= v^P \vec{t}_1 \\ &= [u_4(t_1) + bu_3(t_1)]\vec{n}_1 + u_5(t_1)\vec{n}_2 + [u_6(t_1) - bu_1(t_1)]\vec{n}_3 \end{aligned} \quad (2.44)$$

and

$$\begin{aligned}\vec{v}_S &= v^P \vec{t}_2 \\ &= [u_4(t_2) + bu_3(t_2)]\vec{n}_1 + u_5(t_2)\vec{n}_2 + [u_6(t_2) - bu_2(t_2)]\vec{n}_3\end{aligned}\quad (2.45)$$

Then by equation (2.8), we solve for  $u_5(t_2)$ :

$$u_5(t_2) = -eu_5(t_1) \quad (2.46)$$

Furthermore,  $S_2$  in equation (2.41) may be replaced by the following expression when employing equation (2.46):

$$S_2 \approx -m(1 + e)u_5(t_1) \quad (2.47)$$

To solve for the remaining six unknowns,  $u_1(t_2)$ ,  $u_3(t_2)$ ,  $u_4(t_2)$ ,  $u_6(t_2)$ ,  $S_1$  and  $S_3$ , we must determine if the sphere encounters no slipping or slipping at the point of contact with the surface. We first define several quantities relevant to both cases. From equation (2.5) the normal impulse  $\vec{v}$  and the tangential impulse  $\vec{\tau}$  are given below:

$$\vec{v} = S_2 \vec{n}_2 \quad (2.48)$$

and

$$\vec{\tau} = S_1 \vec{n}_1 + S_3 \vec{n}_3 \quad (2.49)$$

Next, the tangential component of the velocity of separation is

$$\begin{aligned}\vec{n}_2 \times (\vec{v}_S \times \vec{n}_2) &= \vec{n}_2 \times ([u_4(t_2) + bu_3(t_2)]\vec{n}_1 + u_5(t_2)\vec{n}_2 + [u_6(t_2) - bu_1(t_2)]\vec{n}_3 \times \vec{n}_2) \\ &= \vec{n}_2 \times (-[u_6(t_2) - bu_1(t_2)]\vec{n}_1 + [u_4(t_2) + bu_3(t_2)]\vec{n}_3) \\ &= [u_4(t_2) + bu_3(t_2)]\vec{n}_1 + [u_6(t_2) - bu_1(t_2)]\vec{n}_3\end{aligned}\quad (2.50)$$

At time  $\vec{t}_2$  the sphere may experience no slipping or slipping. We consider no slipping first when determining the remaining six unknowns. From equations (2.10) and (2.50) and from equations (2.9), (2.48) and (2.49) respectively, we see that

$$u_4(t_2) + bu_3(t_2) = 0 \quad (2.51)$$

$$u_6(t_2) - bu_1(t_2) = 0 \quad (2.52)$$

and

$$(S_1^2 + S_3^2)^{1/2} < \mu |S_2| \quad (2.53)$$

Eliminating  $S_1$  from equations (2.39) and (2.40) and removing  $S_3$  from equations (2.37) and (2.42), we obtain the following expressions:

$$bm[u_4(t_2) - u_4(t_1)] \approx J[u_3(t_2) - u_3(t_1)] \quad (2.54)$$

and

$$-bm[u_6(t_2) - u_6(t_1)] \approx J[u_1(t_2) - u_1(t_1)] \quad (2.55)$$

We solve for  $u_3(t_2)$  and  $u_4(t_2)$  using equations (2.51) and (2.54). Solving for  $u_4(t_2)$  in equation (2.51) and  $u_3(t_2)$  in equation (2.54) respectively, we obtain

$$u_4(t_2) = -bu_3(t_2) \quad (2.56)$$

and

$$u_3(t_2) \approx u_3(t_1) + \frac{bm}{J}[u_4(t_2) - u_4(t_1)] \quad (2.57)$$

Substituting equation (2.56) into equation (2.57) gives

$$u_3(t_2) \approx \frac{Ju_3(t_1) + mb[-bu_3(t_2) - u_4(t_1)]}{J} \quad (2.58)$$

Solving explicitly for  $u_3(t_2)$  in equation (2.58) results in

$$u_3(t_2) \approx \frac{Ju_3(t_1) - mbu_4(t_1)}{mb^2 + J} \quad (2.59)$$

Substituting equation (2.59) into equation (2.56) determines the value of  $u_4(t_2)$

$$u_4(t_2) = -bu_3(t_2) \quad (2.60)$$

Similarly, we solve for  $u_1(t_2)$  and  $u_6(t_2)$  using equations (2.52) and (2.55). Solving for  $u_6(t_2)$  in equation (2.52) and  $u_1(t_2)$  in equation (2.55) respectively, we obtain

$$u_6(t_2) = bu_1(t_2) \quad (2.61)$$

and

$$u_1(t_2) \approx u_1(t_1) - \frac{bm}{J}[u_6(t_2) - u_6(t_1)] \quad (2.62)$$

Substituting equation (2.61) into equation (2.62) gives

$$u_1(t_2) \approx \frac{Ju_1(t_1) - mb[bu_1(t_2) - u_6(t_1)]}{J} \quad (2.63)$$

Solving explicitly for  $u_1(t_2)$  in equation (2.63) results in

$$u_1(t_2) \approx \frac{Ju_1(t_1) + mbu_6(t_1)}{mb^2 + J} \quad (2.64)$$

Substituting equation (2.64) into equation (2.61) determines the value of  $u_6(t_2)$

$$u_6(t_2) = bu_1(t_2) \quad (2.65)$$

$S_1$  and  $S_3$  are determined by substituting equations (2.60) and (2.65) into equations (2.40) and (2.42) respectively.

Hence, successive use of equations (2.43), (2.46), (2.59), (2.60), (2.64) and (2.65) result in a set of values for  $u_1, \dots, u_6$  at time  $t_2$ . These values are valid if and only if inequality (2.53) is satisfied for values of  $S_1$ ,  $S_2$  and  $S_3$  given by equations (2.40), (2.41) and (2.42).

Otherwise, if inequality (2.53) is violated, then the sphere is slipping at time  $t_2$ , and the quantities  $u_1(t_2)$ ,  $u_3(t_2)$ ,  $u_4(t_2)$ ,  $u_6(t_2)$ ,  $S_1$  and  $S_3$  must be recalculated. Note  $u_1(t_2)$ ,  $u_5(t_2)$  and  $S_2$  are given by equations (2.43), (2.46) and (2.59) respectively, regardless if the sphere experiences no slipping or slipping at time  $t_2$ .

If there is slipping at time  $t_2$ , then from equations (2.11), (2.48), (2.49) and (2.50) we see that

$$S_1 = -\mu' |S_2| \frac{u_4(t_2) + bu_3(t_2)}{\{[u_4(t_2) + bu_3(t_2)]^2 + [u_6(t_2) - bu_1(t_2)]^2\}^{1/2}} \quad (2.66)$$

$$S_3 = -\mu' |S_2| \frac{u_6(t_2) - bu_1(t_2)}{\{[u_4(t_2) + bu_3(t_2)]^2 + [u_6(t_2) - bu_1(t_2)]^2\}^{1/2}} \quad (2.67)$$

Next, we solve for equations (2.37), (2.39), (2.40) and (2.42) in terms of the generalized speeds at time  $t_2$ , giving

$$u_1(t_2) \approx u_1(t_1) - bS_3/J \quad (2.68)$$

$$u_3(t_2) \approx u_3(t_1) + bS_1/J \quad (2.69)$$

$$u_4(t_2) \approx u_4(t_1) + S_1/m \quad (2.70)$$

$$u_6(t_2) \approx u_6(t_1) + S_3/m \quad (2.71)$$

We notice  $u_1(t_2)$ ,  $u_3(t_2)$ ,  $u_4(t_2)$  and  $u_6(t_2)$  are in terms of their corresponding generalized speed at time  $t_1$ , which are known quantities, and either  $S_1$  or  $S_3$ , which are unknown quantities. To determine  $S_1$  and  $S_3$  respectively, we recast expressions involving generalized speeds at time  $t_2$  in equations (2.66) and (2.67) in terms of generalized speeds at time  $t_1$ . Consequently, we form the following two expressions using equations (2.69) and (2.70) and equations (2.68) and (2.71):

$$u_4(t_2) + bu_3(t_2) \approx u_4(t_1) + bu_3(t_1) + \left(\frac{1}{m} + \frac{b^2}{J}\right) S_1 \quad (2.72)$$

$$u_6(t_2) - bu_1(t_2) \approx u_6(t_1) - bu_1(t_1) + \left(\frac{1}{m} + \frac{b^2}{J}\right) S_3 \quad (2.73)$$

For convenience, we define the constants  $\alpha_1$ ,  $\gamma_1$  and  $k_1$  as

$$\alpha_1 = u_4(t_1) + bu_3(t_1) \quad (2.74)$$

$$\gamma_1 = u_6(t_1) - bu_1(t_1) \quad (2.75)$$

$$k_1 = \frac{1}{m} + \frac{b^2}{J} \quad (2.76)$$

Substituting equations (2.74) through (2.76) into equations (2.66) and (2.67) results in

$$S_1 \approx -\mu' |S_2| \frac{\alpha_1 + k_1 S_1}{[(\alpha_1 + k_1 S_1)^2 + (\gamma_1 + k_1 S_3)^2]^{1/2}} \quad (2.77)$$

and

$$S_3 \approx -\mu' |S_2| \frac{\gamma_1 + k_1 S_3}{[(\alpha_1 + k_1 S_1)^2 + (\gamma_1 + k_1 S_3)^2]^{1/2}} \quad (2.78)$$

Dividing equation (2.77) by (2.78) leads to

$$\frac{S_1}{S_3} \approx \frac{\alpha_1 + k_1 S_1}{\gamma_1 + k_1 S_3} \quad (2.79)$$

which implies that

$$S_3 \approx \frac{\gamma_1}{\alpha_1} S_1 \quad (2.80)$$

Substituting equation (2.80) into equation (2.77) gives

$$\begin{aligned} S_1 &\approx -\mu' |S_2| \frac{\alpha_1 + k_1 S_1}{\{(\alpha_1 + k_1 S_1)^2 + [\gamma_1 + k_1(\gamma_1/\alpha_1)S_1]^2\}^{1/2}} \\ &= -\mu' |S_2| \frac{\alpha_1 + k_1 S_1}{|\alpha_1 + k_1 S_1| [1 + (\gamma_1/\alpha_1)^2]^{1/2}} \end{aligned} \quad (2.81)$$

For slipping at time  $t_2$ , successive use of equations (2.74), (2.75), (2.76), (2.81), (2.80), (2.68), (2.69), (2.70), (2.71), (2.43) and (2.46) result in a set of values for  $u_1, \dots, u_6$  at time  $t_2$ .

In conclusion, the model initially assumes no slipping at time  $t_2$  for each bounce of the sphere. A set of values for  $u_1, \dots, u_6$  at time  $t_2$  are produced, and are valid if and only if inequality (2.53) is satisfied for values of  $S_1$ ,  $S_2$  and  $S_3$  given by equations (2.40), (2.41) and (2.42). If inequality (2.53) is violated, then a new set of values for  $u_1, \dots, u_6$  at time  $t_2$  are developed under the assumption of slipping. The process is repeated until the bouncing ends. The method for reinitializing the generalized speeds after each bounce is discussed in the next section.

### 2.1.3 Trajectory Model and the Reinitialization of the Generalized Speeds

A trajectory model tracking the sphere's motion after each bounce is developed and incorporated into Kane's collision model. By employing this model, the sphere's generalized speeds are reinitialized after each bounce. As a starting point, we define the equations of motion for the sphere's trajectory after experiencing a collision.

From basic dynamics, the equations of motion for a sphere in free-fall in the  $\vec{n}_1, \vec{n}_2, \vec{n}_3$  directions are

$$\sum F_{q_1} = ma_{q_1} = 0 \quad (2.82)$$

$$\sum F_{q_2} = ma_{q_2} = -mg \quad (2.83)$$

$$\sum F_{q_3} = ma_{q_3} = 0 \quad (2.84)$$

where air resistance and the Mangus Force are neglected.

Since the Mangus Force is neglected between bounces, we can reinitialize the angular velocities for the next bounce by setting  $u_1(t_1) = u_1(t_2)$ ,  $u_2(t_1) = u_2(t_2)$  and  $u_3(t_1) = u_3(t_2)$ . Notice the velocities in the  $\vec{n}_1$  and  $\vec{n}_3$  directions, namely  $u_4(t_2)$  and  $u_6(t_2)$  respectively are constant since the acceleration term in equations (2.82) and (2.84) are both zero. This implies that the horizontal speed is unchanged between bounces, and permits us to set  $u_4(t_1) = u_4(t_2)$  and  $u_6(t_1) = u_6(t_2)$  for the next bounce. Because of the conservation of mechanical energy between bounces, the velocity in the  $\vec{n}_2$  direction changes sign and allows us to set  $u_5(t_1) = -u_5(t_2)$  for the next bounce. Bouncing continues until  $u_5(t_1)$  equals 0 m/s.

Note the above method for reinitializing the generalized speeds is valid only for collisions occurring on the horizontal plane. A more general and flexible method is to employ a numerical model to reinitialize the generalized speeds since it can detect collisions occurring on all types of planes. This approach also handles a sphere transitioning between different planes. Consequently, the latter method is chosen for this study. Note the collision model reduces to a two-dimensional model if the following initial generalized speeds are zero:  $u_1, u_2$  and  $u_6$ .

## 2.2 Equations of Motion for a Bouncing Sphere on an Incline Plane

### 2.2.1 Background

Consider a sphere of mass  $m$  and radius  $b$ , whose motion is unconstrained on an incline plane defined by three mutually perpendicular unit vectors  $(\vec{c}_1, \vec{c}_2, \vec{c}_3)$ , where  $\vec{c}_2$  is perpendicular to the plane, see figure 2.2. The sphere has six degrees of freedom, three angles defining its orientation and three components defining its position. Consequently, the sphere's angular and translational velocities may be expressed in terms of the generalized speeds  $u_{11}, \dots, u_{66}$  as

$$\vec{\omega} = u_{11}\vec{c}_1 + u_{22}\vec{c}_2 + u_{33}\vec{c}_3 \quad (2.85)$$

and

$$\vec{v} = u_{44}\vec{c}_1 + u_{55}\vec{c}_2 + u_{66}\vec{c}_3 \quad (2.86)$$

where  $\vec{v}$  denotes the velocity of the sphere's center of mass.

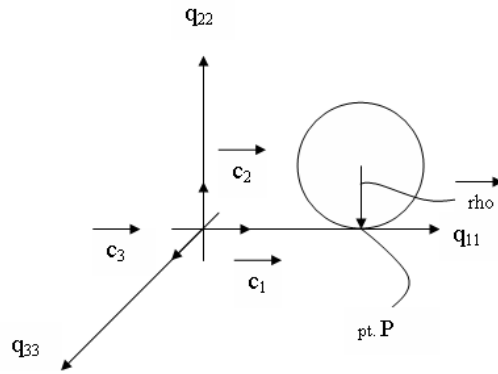


Figure 2.2: Reference Frame (Incline Plane)

From equations (2.85) and (2.86), we define the velocity of the point P of the sphere that comes into contact with the surface as

$$v^{\vec{P}} = \vec{v} + \vec{\omega} \times \vec{\rho} \quad (2.87)$$

where  $\vec{\rho} = -b\vec{c}_2$ .

Then from equation (2.87), the partial velocities of P are determined by inspection, and are simply the coefficients for each generalized speed.

Operating under the aforementioned system, Kane's collision model enables us to investigate the collision of a sphere as it impacts a flat surface beginning at time  $t_1$  and ending at time  $t_2$ . Two dynamical equations essential to the model are the generalized impulse  $I_{rr}$  and the generalized momentum  $p_{rr}$ . The generalized

impulse is defined as

$$I_{rr} = v_{rr}^P(\vec{t}_1) \cdot \int_{t_1}^{t_2} \vec{R} dt \quad (rr = 1, \dots, 6) \quad (2.88)$$

where  $v_{rr}^P(\vec{t}_1)$  is the partial velocity of the sphere at the point of contact with the surface at time  $t_1$ , and  $\int_{t_1}^{t_2} \vec{R} dt$  is the contact force exerted on the sphere by the surface at their contact point during the time interval  $[t_1, t_2]$ . Moreover, if we let  $S_{ii} = \vec{c}_i \cdot \int_{t_1}^{t_2} \vec{R} dt$  ( $i=ii=1,2,3$ ), then we can define  $\int_{t_1}^{t_2} \vec{R} dt$  as

$$\int_{t_1}^{t_2} \vec{R} dt = S_{11}\vec{c}_1 + S_{22}\vec{c}_2 + S_{33}\vec{c}_3 \quad (2.89)$$

The generalized momentum<sup>1</sup> is defined as follows:

$$p_{rr} = \frac{\partial K}{\partial u_{rr}} \quad (rr = 1, \dots, 6) \quad (2.90)$$

where  $K$  is the kinetic energy of the sphere and  $u_{rr}$  are the generalized speeds. Integrating equation (2.88) results in the following approximation connecting the generalized impulse to the generalized momentum<sup>2</sup>:

$$I_{rr} \approx p_{rr}(t_2) - p_{rr}(t_1) \quad (rr = 1, \dots, 6) \quad (2.91)$$

In order to capture the sphere's motion at time  $t_2$ , two assumptions supplement the use of equation (2.91) together with a complete description of the sphere's motion at time  $t_1$ . The first assumption is the normal components of the velocity of approach  $\vec{v}_A$  and separation  $\vec{v}_S$  of the sphere, with respect to the surface, have opposite directions, where the magnitudes are related by the following equation:

$$\vec{c}_2 \cdot \vec{v}_S = -e\vec{c}_2 \cdot \vec{v}_A \quad (2.92)$$

In equation (2.92),  $e$  is called the coefficient of restitution,  $\vec{v}_A = \vec{v}^P(t_1)$  and  $\vec{v}_S = \vec{v}^P(t_2)$ , where it is assumed the surface's velocity is zero during and after colliding with the sphere. The second assumption determines if the sphere encounters no slipping or slipping at the point of contact with the surface. If there is no slipping at  $t_2$ , the following inequality must be satisfied:

$$|\vec{\tau}| < \mu |\vec{v}| \quad (2.93)$$

<sup>1</sup>See page 226 of (18) for a proof of this definition

<sup>2</sup>See pages 226-227 of (18) for a proof of this definition

where  $\vec{\tau}=S_{11}\vec{c}_1 + S_{33}\vec{c}_3$  is the tangential impulse,  $\vec{\nu}=S_{22}\vec{c}_2$  is the normal impulse and  $\mu$  is the coefficient of static friction. Consequently,

$$\vec{c}_2 \times (\vec{v}_S \times \vec{c}_2) = 0 \quad (2.94)$$

The equation states the tangential component of the velocity of separation is zero.

If inequality (2.92) is violated, slipping occurs at  $t_2$ , and  $\vec{\tau}$  is expressed as

$$\vec{\tau} = -\mu' |\vec{\nu}| \frac{\vec{c}_2 \times (\vec{v}_S \times \vec{c}_2)}{|\vec{c}_2 \times (\vec{v}_S \times \vec{c}_2)|} \quad (2.95)$$

where the constant  $\mu'$  is the coefficient of kinetic friction.

The model requires that the physical parameters  $b$ ,  $m$ ,  $J$ ,  $e$ ,  $\mu$  and  $\mu'$  and the generalized speeds at time  $t_1$  are known. Then the motion of the sphere at time  $t_2$  is fully defined by invoking equations (2.91), (2.92), (2.93), (2.94) and (2.95).

## 2.2.2 Derivation

This section provides a complete derivation of a collision model for a bouncing uniform sphere on an incline plane. Assume the following physical parameters are known:  $b$ ,  $m$ ,  $J$ ,  $e$ ,  $\mu$ , and  $\mu'$ . Also assume the generalized speeds at time  $t_1$  are known and are given in the form of equations (2.85) and (2.86). The generalized speeds at time  $t_2$  are the quantities to be determined.

The velocity of the point P of the sphere that comes into contact with the surface is given by equation (2.87):

$$\begin{aligned} v^{\vec{P}} &= \vec{v} + \vec{\omega} \times \vec{\rho} \\ &= u_{44}\vec{c}_1 + u_{55}\vec{c}_2 + u_{66}\vec{c}_3 + (u_{11}\vec{c}_1 + u_{22}\vec{c}_2 + u_{33}\vec{c}_3) \times -b\vec{c}_2 \\ &= u_{44}\vec{c}_1 + u_{55}\vec{c}_2 + u_{66}\vec{c}_3 + bu_{33}\vec{c}_1 - bu_{11}\vec{c}_3 \\ &= (u_{44} + bu_{33})\vec{c}_1 + u_{55}\vec{c}_2 + (u_{66} - bu_{11})\vec{c}_3 \end{aligned} \quad (2.96)$$

The partial velocities of P at time  $t_1$  are determined by inspection of equation (2.96) and are listed below:

$$v_{11}^{\vec{P}}(t_1) = -b\vec{c}_3 \quad (2.97)$$

$$v_{22}^{\vec{P}}(t_1) = 0 \quad (2.98)$$

$$v_{33}^P(\vec{t}_1) = b\vec{c}_1 \quad (2.99)$$

$$v_{44}^P(\vec{t}_1) = \vec{c}_1 \quad (2.100)$$

$$v_{55}^P(\vec{t}_1) = \vec{c}_2 \quad (2.101)$$

$$v_{66}^P(\vec{t}_1) = \vec{c}_3 \quad (2.102)$$

From equations (2.88) and (2.89) and employing equations (2.97) through (2.102), the generalized impulse at the point of contact is expressed as

$$I_{rr} = v_{rr}^P(\vec{t}_1) \cdot (S_{11}\vec{c}_1 + S_{22}\vec{c}_2 + S_{33}\vec{c}_3) \quad (rr = 1, \dots, 6) \quad (2.103)$$

where

$$\begin{aligned} I_{11} &= -b\vec{c}_3 \cdot (S_{11}\vec{c}_1 + S_{22}\vec{c}_2 + S_{33}\vec{c}_3) \\ &= -bS_{33} \end{aligned} \quad (2.104)$$

$$\begin{aligned} I_{22} &= 0 \cdot (S_{11}\vec{c}_1 + S_{22}\vec{c}_2 + S_{33}\vec{c}_3) \\ &= 0 \end{aligned} \quad (2.105)$$

$$\begin{aligned} I_{33} &= b\vec{c}_1 \cdot (S_{11}\vec{c}_1 + S_{22}\vec{c}_2 + S_{33}\vec{c}_3) \\ &= bS_{11} \end{aligned} \quad (2.106)$$

$$\begin{aligned} I_{44} &= \vec{c}_1 \cdot (S_{11}\vec{c}_1 + S_{22}\vec{c}_2 + S_{33}\vec{c}_3) \\ &= S_{11} \end{aligned} \quad (2.107)$$

$$\begin{aligned} I_{55} &= \vec{c}_2 \cdot (S_{11}\vec{c}_1 + S_{22}\vec{c}_2 + S_{33}\vec{c}_3) \\ &= S_{22} \end{aligned} \quad (2.108)$$

$$\begin{aligned} I_{66} &= \vec{c}_3 \cdot (S_{11}\vec{c}_1 + S_{22}\vec{c}_2 + S_{33}\vec{c}_3) \\ &= S_{33} \end{aligned} \quad (2.109)$$

The kinetic energy of the sphere is equal to the sum of the kinetic energy due to the rotational and translational velocities about the center of mass. So, we can write:

$$K_{sphere} = K_{\omega} + K_v \quad (2.110)$$

where

$$\begin{aligned}
K_\omega &= \frac{1}{2} \vec{\omega} \cdot \vec{L} \cdot \vec{\omega} \\
&= \frac{1}{2} \{\omega\}^T [L] \{\omega\} \\
&= \frac{1}{2} (L_{11}u_{11}^2 + L_{22}u_{22}^2 + L_{33}u_{33}^2) - L_{12}u_{11}u_{22} - L_{13}u_{11}u_{33} - L_{23}u_{22}u_{33}
\end{aligned} \tag{2.111}$$

and

$$\begin{aligned}
K_v &= \frac{1}{2} m \vec{v} \cdot \vec{v} \\
&= \frac{1}{2} m \{v\}^T \{v\} \\
&= \frac{1}{2} m (u_{44}^2 + u_{55}^2 + u_{66}^2)
\end{aligned} \tag{2.112}$$

Since the coordinate axes are selected as the principal axes, the expression for the rotational kinetic energy in equation (2.111) simplifies to

$$\begin{aligned}
K_\omega &= \frac{1}{2} (L_{11}u_{11}^2 + L_{22}u_{22}^2 + L_{33}u_{33}^2) \\
&= \frac{1}{2} L (u_{11}^2 + u_{22}^2 + u_{33}^2)
\end{aligned} \tag{2.113}$$

where  $J = L_{11} = L_{22} = L_{33}$ . Therefore, the kinetic energy of the sphere is

$$K_{sphere} = \frac{1}{2} J (u_{11}^2 + u_{22}^2 + u_{33}^2) + \frac{1}{2} m (u_{44}^2 + u_{55}^2 + u_{66}^2) \tag{2.114}$$

Substituting equation (2.114) into equation (2.90), results in expressions for the generalized momentum:

$$p_{11} = J u_{11} \tag{2.115}$$

$$p_{22} = J u_{22} \tag{2.116}$$

$$p_{33} = J u_{33} \tag{2.117}$$

$$p_{44} = m u_{44} \tag{2.118}$$

$$p_{55} = m u_{55} \tag{2.119}$$

$$p_{66} = m u_{66} \tag{2.120}$$

With expressions developed for the generalized impulse and momentum, substituting equations (2.104) through (2.109) and equations (2.115) through (2.120) into equation (2.91), we develop the following expressions:

$$-bS_{33} \approx J[u_{11}(t_2) - u_{11}(t_1)] \quad (2.121)$$

$$0 \approx J[u_{22}(t_2) - u_{22}(t_1)] \quad (2.122)$$

$$bS_{11} \approx J[u_{33}(t_2) - u_{33}(t_1)] \quad (2.123)$$

$$S_{11} \approx m[u_{44}(t_2) - u_{44}(t_1)] \quad (2.124)$$

$$S_{22} \approx m[u_{55}(t_2) - u_{55}(t_1)] \quad (2.125)$$

$$S_{33} \approx m[u_{66}(t_2) - u_{66}(t_1)] \quad (2.126)$$

From equation (2.122), we can immediately solve for  $u_{22}(t_2)$ :

$$u_{22}(t_2) \approx u_{22}(t_1) \quad (2.127)$$

Studying equations (2.121) and (2.123)–(2.126), we have five equations and eight unknowns:  $u_{11}(t_2)$ ,  $u_{33}(t_2)$ ,  $u_{44}(t_2)$ ,  $u_{55}(t_2)$ ,  $u_{66}(t_2)$ ,  $S_{11}$ ,  $S_{22}$  and  $S_{33}$ . We use equations (2.92)–(2.95) to supplement the preceding equations. To use equation (2.92), we first define the velocity of approach and separation. Assuming the velocity of the surface is zero during and after colliding with the sphere, the velocity of approach and separation are determined from equation (2.96) where:

$$\begin{aligned} \vec{v}_A &= v^P \vec{t}_1 \\ &= [u_{44}(t_1) + bu_{33}(t_1)]\vec{c}_1 + u_{55}(t_1)\vec{c}_2 + [u_{66}(t_1) - bu_{11}(t_1)]\vec{c}_3 \end{aligned} \quad (2.128)$$

and

$$\begin{aligned} \vec{v}_S &= v^P \vec{t}_2 \\ &= [u_{44}(t_2) + bu_{33}(t_2)]\vec{c}_1 + u_{55}(t_2)\vec{c}_2 + [u_{66}(t_2) - bu_{22}(t_2)]\vec{c}_3 \end{aligned} \quad (2.129)$$

Then by equation (2.92), we solve for  $u_{55}(t_2)$ :

$$u_{55}(t_2) = -eu_{55}(t_1) \quad (2.130)$$

Furthermore,  $S_{22}$  in equation (2.125) may be replaced by the following expression when employing equation (2.130):

$$S_{22} \approx -m(1+e)u_{55}(t_1) \quad (2.131)$$

To solve for the remaining six unknowns,  $u_{11}(t_2)$ ,  $u_{33}(t_2)$ ,  $u_{44}(t_2)$ ,  $u_{66}(t_2)$ ,  $S_{11}$  and  $S_{33}$ , we must determine if the sphere encounters no slipping or slipping at the point of contact with the surface. We first define several quantities relevant to both cases. From equation (2.89) the normal impulse  $\vec{v}$  and the tangential impulse  $\vec{\tau}$  are given below:

$$\vec{v} = S_{22}\vec{c}_2 \quad (2.132)$$

and

$$\vec{\tau} = S_{11}\vec{c}_1 + S_{33}\vec{c}_3 \quad (2.133)$$

Next, the tangential component of the velocity of separation is

$$\begin{aligned} \vec{c}_2 \times (\vec{v}_S \times \vec{c}_2) &= \vec{c}_2 \times ([u_{44}(t_2) + bu_{33}(t_2)]\vec{c}_1 + u_{55}(t_2)\vec{c}_2 + [u_{66}(t_2) - bu_{11}(t_2)]\vec{c}_3 \times \vec{c}_2) \\ &= \vec{c}_2 \times (-[u_{66}(t_2) - bu_{11}(t_2)]\vec{c}_1 + [u_{44}(t_2) + bu_{33}(t_2)]\vec{c}_3) \\ &= [u_{44}(t_2) + bu_{33}(t_2)]\vec{c}_1 + [u_{66}(t_2) - bu_{11}(t_2)]\vec{c}_3 \end{aligned} \quad (2.134)$$

At time  $t_2$  the sphere may experience no slipping or slipping. We consider the case of no slipping first when determining the remaining six unknowns. From equations (2.94) and (2.134) and from equations (2.93), (2.132) and (2.133) respectively, we see that

$$u_{44}(t_2) + bu_{33}(t_2) = 0 \quad (2.135)$$

$$u_{66}(t_2) - bu_{11}(t_2) = 0 \quad (2.136)$$

and

$$(S_{11}^2 + S_{33}^2)^{1/2} < \mu |S_{22}| \quad (2.137)$$

Eliminating  $S_{11}$  from equations (2.123) and (2.124) and removing  $S_{33}$  from equations (2.121) and (2.126), we obtain the following expressions:

$$bm[u_{44}(t_2) - u_{44}(t_1)] \approx J[u_{33}(t_2) - u_{33}(t_1)] \quad (2.138)$$

and

$$-bm[u_{66}(t_2) - u_{66}(t_1)] \approx J[u_{11}(t_2) - u_{11}(t_1)] \quad (2.139)$$

We solve for  $u_{33}(t_2)$  and  $u_{44}(t_2)$  using equations (2.135) and (2.138). Solving for  $u_{44}(t_2)$  in equation (2.135) and  $u_{33}(t_2)$  in equation (2.138) respectively, we obtain

$$u_{44}(t_2) = -bu_{33}(t_2) \quad (2.140)$$

and

$$u_{33}(t_2) \approx u_{33}(t_1) + \frac{bm}{J}[u_{44}(t_2) - u_{44}(t_1)] \quad (2.141)$$

Substituting equation (2.140) into equation (2.141) gives

$$u_{33}(t_2) \approx \frac{Ju_{33}(t_1) + mb[-bu_{33}(t_2) - u_{44}(t_1)]}{J} \quad (2.142)$$

Solving explicitly for  $u_{33}(t_2)$  in equation (2.142) results in

$$u_{33}(t_2) \approx \frac{Ju_{33}(t_1) - mbu_{44}(t_1)}{mb^2 + J} \quad (2.143)$$

Substituting equation (2.143) into equation (2.140) determines the value of  $u_{44}(t_2)$

$$u_{44}(t_2) = -bu_{33}(t_2) \quad (2.144)$$

Similarly, we solve for  $u_{11}(t_2)$  and  $u_{66}(t_2)$  using equations (2.136) and (2.139). Solving for  $u_{66}(t_2)$  in equation (2.136) and  $u_{11}(t_2)$  in equation (2.139) respectively, we obtain

$$u_{66}(t_2) = bu_{11}(t_2) \quad (2.145)$$

and

$$u_{11}(t_2) \approx u_{11}(t_1) - \frac{bm}{J}[u_{66}(t_2) - u_{66}(t_1)] \quad (2.146)$$

Substituting equation (2.145) into equation (2.146) gives

$$u_{11}(t_2) \approx \frac{Ju_{11}(t_1) - mb[bu_{11}(t_2) - u_{66}(t_1)]}{J} \quad (2.147)$$

Solving explicitly for  $u_{11}(t_2)$  in equation (2.147) results in

$$u_{11}(t_2) \approx \frac{Ju_{11}(t_1) + mbu_{66}(t_1)}{mb^2 + J} \quad (2.148)$$

Substituting equation (2.148) into equation (2.145) determines the value of  $u_{66}(t_2)$

$$u_{66}(t_2) = bu_{11}(t_2) \quad (2.149)$$

$S_{11}$  and  $S_{33}$  are determined by substituting equations (2.144) and (2.149) into equations (2.124) and (2.126) respectively.

Hence, successive use of equations (2.127), (2.130), (2.143), (2.144), (2.148) and (2.149) result in a set of values for  $u_{11}, \dots, u_{66}$  at time  $t_2$ . These values are valid if and only if inequality (2.137) is satisfied for values of  $S_{11}$ ,  $S_{22}$  and  $S_{33}$  given by equations (2.124), (2.125) and (2.126).

Otherwise, if inequality (2.137) is violated, then the sphere is slipping at time  $t_2$ , and the quantities  $u_{11}(t_2)$ ,  $u_{33}(t_2)$ ,  $u_{44}(t_2)$ ,  $u_{66}(t_2)$ ,  $S_{11}$  and  $S_{33}$  must be recalculated. Note  $u_{11}(t_2)$ ,  $u_{55}(t_2)$  and  $S_{22}$  are given by equations (2.127), (2.130) and (2.143) respectively, regardless if the sphere experiences no slipping or slipping at time  $t_2$ .

If there is slipping at time  $t_2$ , then from equations (2.95), (2.132), (2.133) and (2.134) we see that

$$S_{11} = -\mu' |S_{22}| \frac{u_{44}(t_2) + bu_{33}(t_2)}{\{[u_{44}(t_2) + bu_{33}(t_2)]^2 + [u_{66}(t_2) - bu_{11}(t_2)]^2\}^{1/2}} \quad (2.150)$$

$$S_{33} = -\mu' |S_{22}| \frac{u_{66}(t_2) - bu_{11}(t_2)}{\{[u_{44}(t_2) + bu_{33}(t_2)]^2 + [u_{66}(t_2) - bu_{11}(t_2)]^2\}^{1/2}} \quad (2.151)$$

Next, we solve for equations (2.121), (2.123), (2.124) and (2.126) in terms of the generalized speeds at time  $t_2$ , giving

$$u_{11}(t_2) \approx u_{11}(t_1) - bS_{33}/J \quad (2.152)$$

$$u_{33}(t_2) \approx u_{33}(t_1) + bS_{11}/J \quad (2.153)$$

$$u_{44}(t_2) \approx u_{44}(t_1) + S_{11}/m \quad (2.154)$$

$$u_{66}(t_2) \approx u_{66}(t_1) + S_{33}/m \quad (2.155)$$

We note  $u_{11}(t_2)$ ,  $u_{33}(t_2)$ ,  $u_{44}(t_2)$  and  $u_{66}(t_2)$  are in terms of their corresponding generalized speed at time  $t_1$ , which are known quantities, and either  $S_{11}$  or

$S_{33}$ , which are unknown quantities. To determine  $S_{11}$  and  $S_{33}$  respectively, we recast expressions involving generalized speeds at time  $t_2$  in equations (2.150) and (2.151) in terms of generalized speeds at time  $t_1$ . Consequently, we form the following two expressions using equations (2.153) and (2.154) and equations (2.152) and (2.155) respectively:

$$u_{44}(t_2) + bu_{33}(t_2) \approx u_{44}(t_1) + bu_{33}(t_1) + \left(\frac{1}{m} + \frac{b^2}{J}\right) S_{11} \quad (2.156)$$

$$u_{66}(t_2) - bu_{11}(t_2) \approx u_{66}(t_1) - bu_{11}(t_1) + \left(\frac{1}{m} + \frac{b^2}{J}\right) S_{33} \quad (2.157)$$

For convenience, we define the constants  $\alpha_{11}$ ,  $\gamma_{11}$  and  $k_{11}$  as

$$\alpha_{11} = u_{44}(t_1) + bu_{33}(t_1) \quad (2.158)$$

$$\gamma_{11} = u_{66}(t_1) - bu_{11}(t_1) \quad (2.159)$$

$$k_{11} = \frac{1}{m} + \frac{b^2}{J} \quad (2.160)$$

Substituting equations (2.158) through (2.160) into equations (2.150) and (2.151) results in

$$S_{11} \approx -\mu' |S_{22}| \frac{\alpha_{11} + k_{11}S_{11}}{[(\alpha_{11} + k_{11}S_{11})^2 + (\gamma_{11} + k_{11}S_{33})^2]^{1/2}} \quad (2.161)$$

and

$$S_{33} \approx -\mu' |S_{22}| \frac{\gamma_{11} + k_{11}S_{33}}{[(\alpha_{11} + k_{11}S_{11})^2 + (\gamma_{11} + k_{11}S_{33})^2]^{1/2}} \quad (2.162)$$

Dividing equation (2.161) by (2.162) leads to

$$\frac{S_{11}}{S_{33}} \approx \frac{\alpha_{11} + k_{11}S_{11}}{\gamma_{11} + k_{11}S_{33}} \quad (2.163)$$

which implies that

$$S_{33} \approx \frac{\gamma_{11}}{\alpha_{11}} S_{11} \quad (2.164)$$

Substituting equation (2.164) into equation (2.161) gives

$$\begin{aligned} S_{11} &\approx -\mu' |S_{22}| \frac{\alpha_{11} + k_{11}S_{11}}{\{(\alpha_{11} + k_{11}S_{11})^2 + [\gamma_{11} + k_{11}(\gamma_{11}/\alpha_{11})S_{11}]^2\}^{1/2}} \\ &= -\mu' |S_{22}| \frac{\alpha_{11} + k_{11}S_{11}}{|\alpha_{11} + k_{11}S_{11}| [1 + (\gamma_{11}/\alpha_{11})^2]^{1/2}} \end{aligned} \quad (2.165)$$

For slipping at time  $t_2$ , successive use of equations (2.158), (2.159), (2.160), (2.165), (2.164), (2.152), (2.153), (2.154), (2.155), (2.127) and (2.130) result in a set of values for  $u_{11}, \dots, u_{66}$  at time  $t_2$ .

In conclusion, the model initially assumes no slipping at time  $t_2$  for each bounce of the sphere. A set of values for  $u_{11}, \dots, u_{66}$  at time  $t_2$  are produced, and are valid if and only if inequality (2.137) is satisfied for values of  $S_{11}$ ,  $S_{22}$  and  $S_{33}$  given by equations (2.124), (2.125) and (2.126). If inequality (2.137) is violated, then a new set of values for  $u_{11}, \dots, u_{66}$  at time  $t_2$  are developed under the assumption of slipping. The process is repeated until the bouncing ends. The method for reinitializing the generalized speeds after each bounce is discussed in the next section.

### 2.2.3 Trajectory Model and the Reinitialization of the Generalized Speeds

A trajectory model tracking the sphere's motion after each bounce is developed and incorporated into the collision model. By employing this model, the sphere's generalized speeds are reinitialized after each bounce. As a starting point, we define the equations of motion for the sphere's trajectory after experiencing a collision.

Resolving the gravitational force into the  $\vec{c}$  frame, results in the following expression:

$$-g\vec{n}_2 = -g(\sin\theta\vec{c}_1 + \cos\theta\vec{c}_2) \quad (2.166)$$

Then the equations of motion in the  $\vec{c}_1, \vec{c}_2, \vec{c}_3$  directions respectively are

$$\begin{aligned} \sum F_{q_{11}} = ma_{q_{11}} &= -mg\vec{c}_1 \cdot (\sin\theta\vec{c}_1 + \cos\theta\vec{c}_2) \\ &= -mg\sin\theta \end{aligned} \quad (2.167)$$

$$\begin{aligned} \sum F_{q_{22}} = ma_{q_{22}} &= -mg\vec{c}_2 \cdot (\sin\theta\vec{c}_1 + \cos\theta\vec{c}_2) \\ &= -mg\cos\theta \end{aligned} \quad (2.168)$$

$$\begin{aligned} \sum F_{q_{33}} = ma_{q_{33}} &= -mg\vec{c}_3 \cdot (\sin\theta\vec{c}_1 + \cos\theta\vec{c}_2) \\ &= 0 \end{aligned} \quad (2.169)$$

where air resistance and the Mangus force are neglected.

Since the Mangus Force is neglected between bounces, we can reinitialize the angular velocities for the next bounce by setting  $u_{11}(t_1) = u_{11}(t_2)$ ,  $u_{22}(t_1) = u_{22}(t_2)$  and  $u_{33}(t_1) = u_{33}(t_2)$ . Notice the velocity in the  $\vec{c}_3$  direction, namely  $u_{66}(t_2)$ , is constant since the acceleration term in equation (2.169) is zero. This implies that the horizontal speed in the  $\vec{c}_3$  direction is unchanged between bounces, and permits us to set  $u_{66}(t_1) = u_{66}(t_2)$  for the next bounce. Because of the conservation of mechanical energy between bounces, the velocity in the  $\vec{c}_2$  direction changes sign, and allows us to set  $u_{55}(t_1) = -u_{55}(t_2)$  for the next bounce. The horizontal velocity in the  $\vec{c}_1$  direction, namely  $u_{44}(t_2)$ , is not constant between bounces because of the gravity component acting in that direction. Hence, to reinitialize  $u_{44}(t_2)$  for the next bounce,  $u_{44}(t_2)$  is determined by numerically integrating equations (2.167) and (2.168) simultaneously using  $u_{44}(t_2)$  and  $u_{55}(t_2)$  as initial conditions. A collision occurs when the velocity in the  $\vec{c}_2$  direction is equal to  $-u_{55}(t_2)$ . At this event, we obtain the final velocity in the  $\vec{c}_1$  direction, which we call  $u_{44}$ . Finally, we may set  $u_{44}(t_1) = u_{44}$  for the next bounce. Bouncing continues until  $u_{55}(t_1)$  equals 0 m/s.

Note the above method for reinitializing the generalized speeds is valid only for collisions occurring on the incline plane. A more general and flexible method is to employ a numerical model to reinitialize all the generalized speeds since it can detect collisions occurring on all types of planes. This approach also handles a sphere transitioning between different planes. Consequently, the latter method is chosen for this study. Note the collision model reduces to a two-dimensional model if the following initial generalized speeds are zero:  $u_{11}$ ,  $u_{22}$  and  $u_{66}$ .

Note the sphere's motion may be resolved into the n-frame, or the horizontal plane, by the following rotation matrix (see figure 2.3):

$$\begin{matrix} & \vec{c}_1 & \vec{c}_2 & \vec{c}_3 \\ \begin{matrix} \vec{n}_1 \\ \vec{n}_2 \\ \vec{n}_3 \end{matrix} & \begin{pmatrix} \cos\theta & -\sin\theta & 0 \\ \sin\theta & \cos\theta & 0 \\ 0 & 0 & 1 \end{pmatrix} & & \end{matrix} \quad (2.170)$$

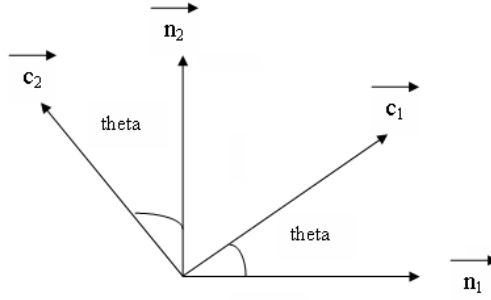


Figure 2.3: Rotation Matrix (Incline Plane)

## 2.3 Equations of Motion for a Bouncing Sphere on a Decline Plane

Consider a sphere of mass  $m$  and radius  $b$ , whose motion is unconstrained on a decline plane defined by three mutually perpendicular unit vectors  $(\vec{a}_1, \vec{a}_2, \vec{a}_3)$ , where  $\vec{a}_2$  is perpendicular to the plane, see figure 2.4. The sphere has six degrees of freedom, three angles defining its orientation and three components defining its position. Consequently, the sphere's angular and translational velocities may be expressed in terms of the generalized speeds  $u_{111}, \dots, u_{666}$  as

$$\vec{\omega} = u_{111}\vec{a}_1 + u_{222}\vec{a}_2 + u_{333}\vec{a}_3 \quad (2.171)$$

and

$$\vec{v} = u_{444}\vec{a}_1 + u_{555}\vec{a}_2 + u_{666}\vec{a}_3 \quad (2.172)$$

where  $\vec{v}$  denotes the velocity of the sphere's center of mass.

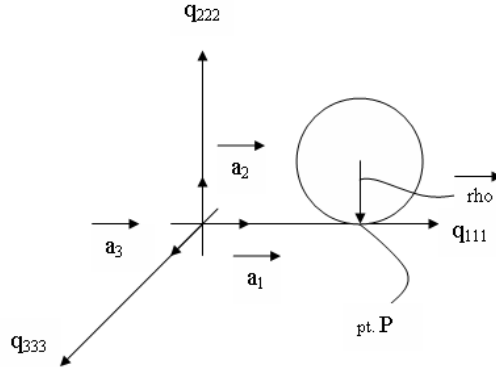


Figure 2.4: Reference Frame (Decline Plane)

From equations (2.171) and (2.172), we define the velocity of the point P of the sphere that comes into contact with the surface as

$$v^{\vec{P}} = \vec{v} + \vec{\omega} \times \vec{\rho} \quad (2.173)$$

where  $\vec{\rho} = -b\vec{a}_2$ .

Then from equation (2.173), the partial velocities of P are determined by inspection, and are simply the coefficients for each generalized speed.

Operating under the aforementioned system, Kane's collision model enables us to investigate the collision of a sphere as it impacts a flat surface beginning at time  $t_1$  and ending at time  $t_2$ . Two dynamical equations essential to the model are the generalized impulse  $I_{rrr}$  and the generalized momentum  $p_{rrr}$ . The generalized impulse is defined as

$$I_{rrr} = v_{rrr}^P(t_1) \cdot \int_{t_1}^{t_2} \vec{R} dt \quad (rrr = 1, \dots, 6) \quad (2.174)$$

where  $v_{rrr}^P(t_1)$  is the partial velocity of the sphere at the point of contact with the surface at time  $t_1$ , and  $\int_{t_1}^{t_2} \vec{R} dt$  is the contact force exerted on the sphere by the

surface at their contact point during the time interval  $[t_1, t_2]$ . Moreover, if we let  $S_{iii} = \vec{a}_i \cdot \int_{t_1}^{t_2} \vec{R} dt$  ( $i=iii=1,2,3$ ), then we can define  $\int_{t_1}^{t_2} \vec{R} dt$  as

$$\int_{t_1}^{t_2} \vec{R} dt = S_{111}\vec{a}_1 + S_{222}\vec{a}_2 + S_{333}\vec{a}_3 \quad (2.175)$$

The generalized momentum<sup>1</sup> is defined as follows:

$$p_{rrr} = \frac{\partial K}{\partial u_{rrr}} \quad (rrr = 1, \dots, 6) \quad (2.176)$$

where  $K$  is the kinetic energy of the sphere and  $u_{rrr}$  are the generalized speeds. Integrating equation (2.174) results in the following approximation connecting the generalized impulse to the generalized momentum<sup>2</sup>:

$$I_{rrr} \approx p_{rrr}(t_2) - p_{rrr}(t_1) \quad (rrr = 1, \dots, 6) \quad (2.177)$$

In order to capture the sphere's motion at time  $t_2$ , two assumptions supplement the use of equation (2.177) together with a complete description of the sphere's motion at time  $t_1$ . The first assumption is the normal components of the velocity of approach  $\vec{v}_A$  and separation  $\vec{v}_S$  of the sphere, with respect to the surface, have opposite directions, where the magnitudes are related by the following equation:

$$\vec{a}_2 \cdot \vec{v}_S = -e\vec{a}_2 \cdot \vec{v}_A \quad (2.178)$$

In equation (2.178),  $e$  is called the coefficient of restitution,  $\vec{v}_A = \vec{v}^P(t_1)$  and  $\vec{v}_S = \vec{v}^P(t_2)$ , where it is assumed the surface's velocity is zero during and after colliding with the sphere. The second assumption determines if the sphere encounters no slipping or slipping at the point of contact with the surface. If there is no slipping at  $t_2$ , the following inequality must be satisfied:

$$|\vec{\tau}| < \mu |\vec{\nu}| \quad (2.179)$$

where  $\vec{\tau} = S_{111}\vec{a}_1 + S_{333}\vec{a}_3$  is the tangential impulse,  $\vec{\nu} = S_{222}\vec{a}_2$  is the normal impulse and  $\mu$  is the coefficient of static friction. Consequently,

$$\vec{a}_2 \times (\vec{v}_S \times \vec{a}_2) = 0 \quad (2.180)$$

<sup>1</sup>See page 226 of (18) for a proof of this definition

<sup>2</sup>See pages 226-227 of (18) for a proof of this definition

The equation states the tangential component of the velocity of separation is zero.

If inequality (2.178) is violated, slipping occurs at  $t_2$ , and  $\vec{\tau}$  is expressed as

$$\vec{\tau} = -\mu' |\vec{v}| \frac{\vec{a}_2 \times (\vec{v}_S \times \vec{a}_2)}{|\vec{a}_2 \times (\vec{v}_S \times \vec{a}_2)|} \quad (2.181)$$

where the constant  $\mu'$  is the coefficient of kinetic friction.

The model requires the physical parameters  $b$ ,  $m$ ,  $J$ ,  $e$ ,  $\mu$  and  $\mu'$  and the generalized speeds at time  $t_1$  are known. Then the motion of the sphere at time  $t_2$  is fully defined by invoking equations (2.177), (2.178), (2.179), (2.180) and (2.181).

### 2.3.1 Derivation

This section provides a complete derivation of a collision model for a bouncing uniform sphere on an incline plane. Assume the following physical parameters are known:  $b$ ,  $m$ ,  $J$ ,  $e$ ,  $\mu$ , and  $\mu'$ . Also assume that the generalized speeds at time  $t_1$  are known and are given in the form of equations (2.171) and (2.172). The generalized speeds at time  $t_2$  are the quantities to be determined.

The velocity of the point P of the sphere that comes into contact with the surface is given by equation (2.173):

$$\begin{aligned} \vec{v}^P &= \vec{v} + \vec{\omega} \times \vec{\rho} \\ &= u_{444}\vec{a}_1 + u_{555}\vec{a}_2 + u_{666}\vec{a}_3 + (u_{111}\vec{a}_1 + u_{222}\vec{a}_2 + u_{333}\vec{a}_3) \times -b\vec{a}_2 \\ &= u_{444}\vec{a}_1 + u_{555}\vec{a}_2 + u_{666}\vec{a}_3 + bu_{333}\vec{a}_1 - bu_{111}\vec{a}_3 \\ &= (u_{444} + bu_{333})\vec{a}_1 + u_{555}\vec{a}_2 + (u_{666} - bu_{111})\vec{a}_3 \end{aligned} \quad (2.182)$$

The partial velocities of P at time  $t_1$  are determined by inspection of equation (2.182) and are listed below:

$$v_{111}^P \vec{a}_1 = -b\vec{a}_3 \quad (2.183)$$

$$v_{222}^P \vec{a}_2 = 0 \quad (2.184)$$

$$v_{333}^P \vec{a}_3 = b\vec{a}_1 \quad (2.185)$$

$$v_{444}^P \vec{a}_1 = \vec{a}_1 \quad (2.186)$$

$$v_{555}^P \vec{a}_2 = \vec{a}_2 \quad (2.187)$$

$$v_{666}^P \vec{a}_3 = \vec{a}_3 \quad (2.188)$$

From equations (2.174) and (2.175) and employing equations (2.183) through (2.188), the generalized impulse at the point of contact is expressed as

$$I_{rrr} = v_{rrr}^P \vec{t}_1 \cdot (S_{111} \vec{a}_1 + S_{222} \vec{a}_2 + S_{333} \vec{a}_3) \quad (rrr = 1, \dots, 6) \quad (2.189)$$

where

$$\begin{aligned} I_{111} &= -b \vec{a}_3 \cdot (S_{111} \vec{a}_1 + S_{222} \vec{a}_2 + S_{333} \vec{a}_3) \\ &= -b S_{333} \end{aligned} \quad (2.190)$$

$$\begin{aligned} I_{222} &= 0 \cdot (S_{111} \vec{a}_1 + S_{222} \vec{a}_2 + S_{333} \vec{a}_3) \\ &= 0 \end{aligned} \quad (2.191)$$

$$\begin{aligned} I_{333} &= b \vec{a}_1 \cdot (S_{111} \vec{a}_1 + S_{222} \vec{a}_2 + S_{333} \vec{a}_3) \\ &= b S_{111} \end{aligned} \quad (2.192)$$

$$\begin{aligned} I_{444} &= \vec{a}_1 \cdot (S_{111} \vec{a}_1 + S_{222} \vec{a}_2 + S_{333} \vec{a}_3) \\ &= S_{111} \end{aligned} \quad (2.193)$$

$$\begin{aligned} I_{555} &= \vec{a}_2 \cdot (S_{111} \vec{a}_1 + S_{222} \vec{a}_2 + S_{333} \vec{a}_3) \\ &= S_{222} \end{aligned} \quad (2.194)$$

$$\begin{aligned} I_{666} &= \vec{a}_3 \cdot (S_{111} \vec{a}_1 + S_{222} \vec{a}_2 + S_{333} \vec{a}_3) \\ &= S_{333} \end{aligned} \quad (2.195)$$

The kinetic energy of the sphere is equal to the sum of the kinetic energy due to the rotational and translational velocities about the center of mass. So, we can write:

$$K_{sphere} = K_{\omega} + K_v \quad (2.196)$$

where

$$\begin{aligned} K_{\omega} &= \frac{1}{2} \vec{\omega} \cdot \vec{L} \cdot \vec{\omega} \\ &= \frac{1}{2} \{\omega\}^T [L] \{\omega\} \\ &= \frac{1}{2} (L_{11} u_{111}^2 + L_{22} u_{222}^2 + L_{33} u_{333}^2) - L_{12} u_{111} u_{222} - L_{13} u_{111} u_{333} - L_{23} u_{222} u_{333} \end{aligned} \quad (2.197)$$

and

$$\begin{aligned}
K_v &= \frac{1}{2} m \vec{v} \cdot \vec{v} \\
&= \frac{1}{2} m \{v\}^T \{v\} \\
&= \frac{1}{2} m (u_{444}^2 + u_{555}^2 + u_{666}^2)
\end{aligned} \tag{2.198}$$

Since the coordinate axes are selected as the principal axes, the expression for the rotational kinetic energy in equation (2.197) simplifies to

$$\begin{aligned}
K_\omega &= \frac{1}{2} (L_{11} u_{111}^2 + L_{22} u_{222}^2 + L_{33} u_{333}^2) \\
&= \frac{1}{2} L (u_{111}^2 + u_{222}^2 + u_{333}^2)
\end{aligned} \tag{2.199}$$

where  $J = L_{11} = L_{22} = L_{33}$ . Therefore, the kinetic energy of the sphere is

$$K_{sphere} = \frac{1}{2} J (u_{111}^2 + u_{222}^2 + u_{333}^2) + \frac{1}{2} m (u_{444}^2 + u_{555}^2 + u_{666}^2) \tag{2.200}$$

Substituting equation (2.200) into equation (2.176), results in expressions for the generalized momentum:

$$p_{111} = J u_{111} \tag{2.201}$$

$$p_{222} = J u_{222} \tag{2.202}$$

$$p_{333} = J u_{333} \tag{2.203}$$

$$p_{444} = m u_{444} \tag{2.204}$$

$$p_{555} = m u_{555} \tag{2.205}$$

$$p_{666} = m u_{666} \tag{2.206}$$

With expressions developed for the generalized impulse and the momentum, substituting equations (2.190) through (2.195) and equations (2.201) through (2.206) into equation (2.177), we develop the following expressions:

$$-bS_{333} \approx J[u_{111}(t_2) - u_{111}(t_1)] \tag{2.207}$$

$$0 \approx J[u_{222}(t_2) - u_{222}(t_1)] \tag{2.208}$$

$$bS_{111} \approx J[u_{333}(t_2) - u_{333}(t_1)] \quad (2.209)$$

$$S_{111} \approx m[u_{444}(t_2) - u_{444}(t_1)] \quad (2.210)$$

$$S_{222} \approx m[u_{555}(t_2) - u_{555}(t_1)] \quad (2.211)$$

$$S_{333} \approx m[u_{666}(t_2) - u_{666}(t_1)] \quad (2.212)$$

From equation (2.208), we can immediately solve for  $u_{222}(t_2)$ :

$$u_{222}(t_2) \approx u_{222}(t_1) \quad (2.213)$$

Studying equations (2.207) and (2.209)– (2.212), we have five equations and eight unknowns:  $u_{111}(t_2)$ ,  $u_{333}(t_2)$ ,  $u_{444}(t_2)$ ,  $u_{555}(t_2)$ ,  $u_{666}(t_2)$ ,  $S_{111}$ ,  $S_{222}$  and  $S_{333}$ . We use equations (2.178)- (2.181) to supplement the preceding equations. To use equation (2.178), we first define the velocity of approach and separation. Assuming the velocity of the surface is zero during and after colliding with the sphere, the velocity of approach and separation are determined from equation (2.182) where:

$$\begin{aligned} \vec{v}_A &= v^P(t_1) \\ &= [u_{444}(t_1) + bu_{333}(t_1)]\vec{a}_1 + u_{555}(t_1)\vec{a}_2 + [u_{666}(t_1) - bu_{111}(t_1)]\vec{a}_3 \end{aligned} \quad (2.214)$$

and

$$\begin{aligned} \vec{v}_S &= v^P(t_2) \\ &= [u_{444}(t_2) + bu_{333}(t_2)]\vec{a}_1 + u_{555}(t_2)\vec{a}_2 + [u_{666}(t_2) - bu_{222}(t_2)]\vec{a}_3 \end{aligned} \quad (2.215)$$

Then by equation (2.178), we solve for  $u_{555}(t_2)$ :

$$u_{555}(t_2) = -eu_{555}(t_1) \quad (2.216)$$

Furthermore,  $S_{222}$  in equation (2.211) may be replaced by the following expression when employing equation (2.216):

$$S_{222} \approx -m(1 + e)u_{555}(t_1) \quad (2.217)$$

To solve for the remaining six unknowns,  $u_{111}(t_2)$ ,  $u_{333}(t_2)$ ,  $u_{444}(t_2)$ ,  $u_{666}(t_2)$ ,  $S_{111}$  and  $S_{333}$ , we must determine if the sphere encounters no slipping or slipping at the point of contact with the surface. We first define several quantities relevant to both cases. From equation (2.175) the normal impulse  $\vec{v}$  and the tangential impulse  $\vec{\tau}$  are given below:

$$\vec{v} = S_{222}\vec{a}_2 \quad (2.218)$$

and

$$\vec{\tau} = S_{111}\vec{a}_1 + S_{333}\vec{a}_3 \quad (2.219)$$

Next, the tangential component of the velocity of separation is

$$\begin{aligned} \vec{a}_2 \times (\vec{v}_S \times \vec{a}_2) &= \vec{a}_2 \times ([u_{444}(t_2) + bu_{333}(t_2)]\vec{a}_1 + u_{555}(t_2)\vec{a}_2 + [u_{666}(t_2) - bu_{111}(t_2)]\vec{a}_3 \times \vec{a}_2) \\ &= \vec{a}_2 \times (-[u_{666}(t_2) - bu_{111}(t_2)]\vec{a}_1 + [u_{444}(t_2) + bu_{333}(t_2)]\vec{a}_3) \\ &= [u_{444}(t_2) + bu_{333}(t_2)]\vec{a}_1 + [u_{666}(t_2) - bu_{111}(t_2)]\vec{a}_3 \end{aligned} \quad (2.220)$$

At time  $t_2$  the sphere may experience no slipping or slipping. We consider the case of no slipping first when determining the remaining six unknowns. From equations (2.180) and (2.220) and from equations (2.179), (2.218) and (2.219) respectively, we see that

$$u_{444}(t_2) + bu_{333}(t_2) = 0 \quad (2.221)$$

$$u_{666}(t_2) - bu_{111}(t_2) = 0 \quad (2.222)$$

and

$$(S_{111}^2 + S_{333}^2)^{1/2} < \mu |S_{222}| \quad (2.223)$$

Eliminating  $S_{111}$  from equations (2.209) and (2.210) and removing  $S_{333}$  from equations (2.207) and (2.212), we obtain the following expressions:

$$bm[u_{444}(t_2) - u_{444}(t_1)] \approx J[u_{333}(t_2) - u_{333}(t_1)] \quad (2.224)$$

and

$$-bm[u_{666}(t_2) - u_{666}(t_1)] \approx J[u_{111}(t_2) - u_{111}(t_1)] \quad (2.225)$$

We solve for  $u_{333}(t_2)$  and  $u_{444}(t_2)$  using equations (2.221) and (2.224). Solving for  $u_{444}(t_2)$  in equation (2.221) and  $u_{333}(t_2)$  in equation (2.224) respectively, we obtain

$$u_{444}(t_2) = -bu_{333}(t_2) \quad (2.226)$$

and

$$u_{333}(t_2) \approx u_{333}(t_1) + \frac{bm}{J}[u_{444}(t_2) - u_{444}(t_1)] \quad (2.227)$$

Substituting equation (2.226) into equation (2.227) gives

$$u_{333}(t_2) \approx \frac{Ju_{333}(t_1) + mb[-bu_{333}(t_2) - u_{444}(t_1)]}{J} \quad (2.228)$$

Solving explicitly for  $u_{333}(t_2)$  in equation (2.228) results in

$$u_{333}(t_2) \approx \frac{Ju_{333}(t_1) - mbu_{444}(t_1)}{mb^2 + J} \quad (2.229)$$

Substituting equation (2.229) into equation (2.226) determines the value of  $u_{444}(t_2)$

$$u_{444}(t_2) = -bu_{333}(t_2) \quad (2.230)$$

Similarly, we solve for  $u_{111}(t_2)$  and  $u_{666}(t_2)$  using equations (2.222) and (2.225). Solving for  $u_{666}(t_2)$  in equation (2.222) and  $u_{111}(t_2)$  in equation (2.225) respectively, we obtain

$$u_{666}(t_2) = bu_{111}(t_2) \quad (2.231)$$

and

$$u_{111}(t_2) \approx u_{111}(t_1) - \frac{bm}{J}[u_{666}(t_2) - u_{666}(t_1)] \quad (2.232)$$

Substituting equation (2.231) into equation (2.232) gives

$$u_{111}(t_2) \approx \frac{Ju_{111}(t_1) - mb[bu_{111}(t_2) - u_{666}(t_1)]}{J} \quad (2.233)$$

Solving explicitly for  $u_{111}(t_2)$  in equation (2.233) results in

$$u_{111}(t_2) \approx \frac{Ju_{111}(t_1) + mbu_{666}(t_1)}{mb^2 + J} \quad (2.234)$$

Substituting equation (2.234) into equation (2.231) determines the value of  $u_{666}(t_2)$

$$u_{666}(t_2) = bu_{111}(t_2) \quad (2.235)$$

$S_{111}$  and  $S_{333}$  are determined by substituting equations (2.230) and (2.235) into equations (2.210) and (2.212) respectively.

Hence, successive use of equations (2.213), (2.216), (2.229), (2.230), (2.234) and (2.235) result in a set of values for  $u_{111}, \dots, u_{666}$  at time  $t_2$ . These values are

valid if and only if inequality (2.223) is satisfied for values of  $S_{111}$ ,  $S_{222}$  and  $S_{333}$  given by equations (2.210), (2.211) and (2.212).

Otherwise, if inequality (2.223) is violated, then the sphere is slipping at time  $t_2$ , and the quantities  $u_{111}(t_2)$ ,  $u_{333}(t_2)$ ,  $u_{444}(t_2)$ ,  $u_{666}(t_2)$ ,  $S_{111}$  and  $S_{333}$  must be recalculated. Note  $u_{111}(t_2)$ ,  $u_{555}(t_2)$  and  $S_{222}$  are given by equations (2.213), (2.216) and (2.229) respectively, regardless if the sphere experiences no slipping or slipping at time  $t_2$ .

If there is slipping at time  $t_2$ , then from equations (2.181), (2.218), (2.219) and (2.220) we see that

$$S_{111} = -\mu' |S_{222}| \frac{u_{444}(t_2) + bu_{333}(t_2)}{\{[u_{444}(t_2) + bu_{333}(t_2)]^2 + [u_{666}(t_2) - bu_{111}(t_2)]^2\}^{1/2}} \quad (2.236)$$

$$S_{333} = -\mu' |S_{222}| \frac{u_{666}(t_2) - bu_{111}(t_2)}{\{[u_{444}(t_2) + bu_{333}(t_2)]^2 + [u_{666}(t_2) - bu_{111}(t_2)]^2\}^{1/2}} \quad (2.237)$$

Next, we solve for equations (2.207), (2.209), (2.210) and (2.212) in terms of the generalized speeds at time  $t_2$ , giving

$$u_{111}(t_2) \approx u_{111}(t_1) - bS_{333}/J \quad (2.238)$$

$$u_{333}(t_2) \approx u_{333}(t_1) + bS_{111}/J \quad (2.239)$$

$$u_{444}(t_2) \approx u_{444}(t_1) + S_{111}/m \quad (2.240)$$

$$u_{666}(t_2) \approx u_{666}(t_1) + S_{333}/m \quad (2.241)$$

We note  $u_{111}(t_2)$ ,  $u_{333}(t_2)$ ,  $u_{444}(t_2)$  and  $u_{666}(t_2)$  are in terms of their corresponding generalized speed at time  $t_1$ , which are known quantities, and either  $S_{111}$  or  $S_{333}$ , which are unknown quantities. To determine  $S_{111}$  and  $S_{333}$  respectively, we recast expressions involving generalized speeds at time  $t_2$  in equations (2.236) and (2.237) in terms of generalized speeds at time  $t_1$ . Consequently, we form the following two expressions using equations (2.239) and (2.240) and equations (2.238) and (2.241):

$$u_{444}(t_2) + bu_{333}(t_2) \approx u_{444}(t_1) + bu_{333}(t_1) + \left(\frac{1}{m} + \frac{b^2}{J}\right) S_{111} \quad (2.242)$$

$$u_{666}(t_2) - bu_{111}(t_2) \approx u_{666}(t_1) - bu_{111}(t_1) + \left(\frac{1}{m} + \frac{b^2}{J}\right) S_{333} \quad (2.243)$$

For convenience, we define the constants  $\alpha_{111}$ ,  $\gamma_{111}$  and  $k_{111}$  as

$$\alpha_{111} = u_{444}(t_1) + bu_{333}(t_1) \quad (2.244)$$

$$\gamma_{111} = u_{666}(t_1) - bu_{111}(t_1) \quad (2.245)$$

$$k_{111} = \frac{1}{m} + \frac{b^2}{J} \quad (2.246)$$

Substituting equations (2.244) through (2.246) into equations (2.236) and (2.237) results in

$$S_{111} \approx -\mu' |S_{222}| \frac{\alpha_{111} + k_{111}S_{111}}{[(\alpha_{111} + k_{111}S_{111})^2 + (\gamma_{111} + k_{111}S_{333})^2]^{1/2}} \quad (2.247)$$

and

$$S_{333} \approx -\mu' |S_{222}| \frac{\gamma_{111} + k_{111}S_{333}}{[(\alpha_{111} + k_{111}S_{111})^2 + (\gamma_{111} + k_{111}S_{333})^2]^{1/2}} \quad (2.248)$$

Dividing equation (2.247) by (2.248) leads to

$$\frac{S_{111}}{S_{333}} \approx \frac{\alpha_{111} + k_{111}S_{111}}{\gamma_{111} + k_{111}S_{333}} \quad (2.249)$$

which implies that

$$S_{333} \approx \frac{\gamma_{111}}{\alpha_{111}} S_{111} \quad (2.250)$$

Substituting equation (2.250) into equation (2.247) gives

$$\begin{aligned} S_{111} &\approx -\mu' |S_{222}| \frac{\alpha_{111} + k_{111}S_{111}}{\{(\alpha_{111} + k_{111}S_{111})^2 + [\gamma_{111} + k_{111}(\gamma_{111}/\alpha_{111})S_{111}]^2\}^{1/2}} \\ &= -\mu' |S_{222}| \frac{\alpha_{111} + k_{111}S_{111}}{|\alpha_{111} + k_{111}S_{111}| [1 + (\gamma_{111}/\alpha_{111})^2]^{1/2}} \end{aligned} \quad (2.251)$$

For slipping at time  $t_2$ , successive use of equations (2.244), (2.245), (2.246), (2.251), (2.250), (2.238), (2.239), (2.240), (2.241), (2.213) and (2.216) result in a set of values for  $u_{111}, \dots, u_{666}$  at time  $t_2$ .

In conclusion, the model initially assumes no slipping at time  $t_2$  for each bounce of the sphere. A set of values for  $u_{111}, \dots, u_{666}$  at time  $t_2$  are produced,

and are valid if and only if inequality (2.223) is satisfied for values of  $S_{111}$ ,  $S_{222}$  and  $S_{333}$  given by equations (2.210), (2.211) and (2.212). If inequality (2.223) is violated, then a new set of values for  $u_{111}, \dots, u_{666}$  at time  $t_2$  are developed under the assumption of slipping. The process is repeated until the bouncing ends. The method for reinitializing the generalized speeds after each bounce is discussed in the next section.

### 2.3.2 Trajectory Model and the Reinitialization of the Generalized Speeds

A trajectory model tracking the sphere's motion after each bounce is developed and incorporated into the collision model. By employing this model, the sphere's generalized speeds are reinitialized after each bounce. As a starting point, we define the equations of motion for the sphere's trajectory after experiencing a collision.

Resolving the gravitational force into the  $\vec{a}$  frame, results in the following expression:

$$-g\vec{n}_2 = -g(-\sin\beta\vec{a}_1 + \cos\beta\vec{a}_2) \quad (2.252)$$

Then the equations of motion in the  $\vec{a}_1, \vec{a}_2, \vec{a}_3$  directions are

$$\begin{aligned} \sum F_{q_{111}} = ma_{q_{111}} &= -mg\vec{a}_1 \cdot (-\sin\beta\vec{a}_1 + \cos\beta\vec{a}_2) \\ &= mg\sin\beta \end{aligned} \quad (2.253)$$

$$\begin{aligned} \sum F_{q_{222}} = ma_{q_{222}} &= -mg\vec{a}_2 \cdot (-\sin\beta\vec{a}_1 + \cos\beta\vec{a}_2) \\ &= -mg\cos\beta \end{aligned} \quad (2.254)$$

$$\begin{aligned} \sum F_{q_{333}} = ma_{q_{333}} &= -mg\vec{a}_3 \cdot (-\sin\beta\vec{a}_1 + \cos\beta\vec{a}_2) \\ &= 0 \end{aligned} \quad (2.255)$$

where air resistance and the Mangus force are neglected.

Since the Mangus Force is neglected between bounces, we can reinitialize the angular velocities for the next bounce by setting  $u_{111}(t_1) = u_{111}(t_2)$ ,  $u_{222}(t_1) = u_{222}(t_2)$  and  $u_{333}(t_1) = u_{333}(t_2)$ . Notice the velocity in the  $\vec{a}_3$  direction, namely

$u_{666}(t_2)$ , is constant since the acceleration term in equation (2.169) is zero. This implies that the horizontal speed in the  $\vec{a}_3$  direction is unchanged between bounces, and permits us to set  $u_{666}(t_1) = u_{666}(t_2)$  for the next bounce. Because of the conservation of mechanical energy between bounces, the velocity in the  $\vec{a}_2$  direction changes sign, and allows us to set  $u_{555}(t_1) = -u_{555}(t_2)$  for the next bounce. The horizontal velocity in the  $\vec{a}_1$  direction, namely  $u_{444}(t_2)$ , is not constant between bounces because of the gravity component acting in that direction. Hence, to reinitialize  $u_{444}(t_2)$  for the next bounce,  $u_{444}(t_2)$  is determined by numerically integrating equations (2.253) and (2.254) simultaneously using  $u_{444}(t_2)$  and  $u_{555}(t_2)$  as initial conditions. A collision occurs when the velocity in the  $\vec{a}_2$  direction is equal to  $-u_{555}(t_2)$ . At this event, we obtain the final velocity in the  $\vec{a}_1$  direction, which we call  $u_{444}$ . Finally, we may set  $u_{444}(t_1) = u_{444}$  for the next bounce. Bouncing continues until  $u_{555}(t_1)$  equals 0 m/s.

Note the above method for reinitializing the generalized speeds is valid only for collisions occurring on the decline plane. A more general and flexible method is to employ a numerical model to reinitialize all the generalized speeds since it can detect collisions occurring on all types of planes. This approach also handles a sphere transitioning between different planes. Consequently, the latter method is chosen for this study. Note the collision model reduces to a two-dimensional model if the following initial generalized speeds are zero:  $u_{111}$ ,  $u_{222}$  and  $u_{666}$ .

Note the sphere's motion may be resolved into the n-frame, or the horizontal plane, by the following rotation matrix (see figure 2.5):

$$\begin{matrix} & \vec{a}_1 & \vec{a}_2 & \vec{a}_3 \\ \vec{n}_1 & \left( \begin{matrix} \cos\beta & \sin\beta & 0 \\ -\sin\beta & \cos\beta & 0 \\ 0 & 0 & 1 \end{matrix} \right) & & \end{matrix} \quad (2.256)$$

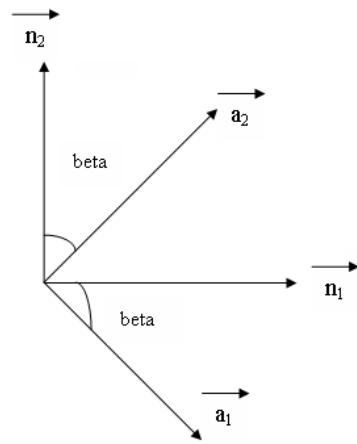


Figure 2.5: Rotation Matrix (Decline Plane)

## Chapter 3

# Equations of Motion for a Rolling and Sliding Sphere

In this chapter we consider the rolling and sliding motion of a sphere on the horizontal, incline and decline planes. For all planes assume the following physical parameters are known:  $b$ ,  $m$ ,  $J$ ,  $e$ ,  $\mu$  and  $\mu'$ . Also assume the sphere is rigid, in motion and the initial generalized speeds are known. Note the sphere is rolling without slipping when  $|v| = |\omega| r$ . Otherwise, the sphere is sliding when  $|v| \neq |\omega| r$ .

### 3.1 Rolling and Sliding Model of a Rigid Sphere on a Horizontal Plane

Consider the two-dimensional rolling and sliding motion of a rigid sphere shown in figure 3.1. The equations of motion are written using the free-body diagram. Note the sense of the frictional force depends on whether the sphere has backspin or topspin. If the sphere has backspin, then the frictional force,  $F_{fr}$ , is directed toward the left. If the sphere has topspin, then the sense of the frictional force depends on the relationship between  $|v|$  and  $|\omega| r$ . The different cases are summarized as follows:

- If  $|v| = |\omega| r$ , then  $F_{fr} = 0$

- If  $|v| < |\omega| r$ , then  $F_{fr}$  is directed toward the right
- If  $|v| > |\omega| r$ , then  $F_{fr}$  is directed toward the left

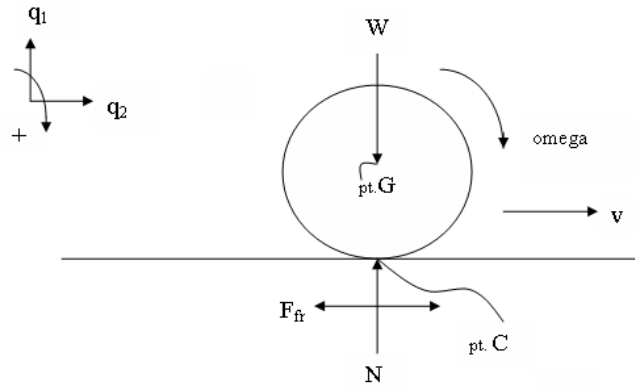


Figure 3.1: Free Body Diagram (Horizontal Plane)

Once the sense of the frictional force is known, the equations of motion may be defined. First, we consider the case of  $F_{fr}$  directed toward the left. Summing the forces in the  $\vec{n}_2$  and  $\vec{n}_1$  directions respectively, we have

$$\begin{aligned}
 \sum F_{q_2} &= ma_{q_2} \\
 &= N - W = 0 \\
 \Rightarrow N &= W = mg
 \end{aligned} \tag{3.1}$$

and

$$\begin{aligned}
 \sum F_{q_1} &= ma_{q_1} \\
 &= -F_{fr} = ma_{q_1} \\
 &= -\mu' N = ma_{q_1}
 \end{aligned}$$

$$\begin{aligned}
&= -\mu' mg = ma_{q_1} \\
\Rightarrow a_{q_1} &= -\mu' g \tag{3.2}
\end{aligned}$$

Summing moments about point G, with the clockwise direction as positive, we have

$$\begin{aligned}
\sum M_G &= J_G \alpha_n \\
&= F_{fr} b = J_G \alpha_n \\
&= \mu' m g b = J_G \alpha_n \\
\Rightarrow \alpha_n &= \frac{\mu' g b}{J_G/m} \tag{3.3}
\end{aligned}$$

Then equations (3.1), (3.2) and (3.3) define the motion of a rolling sphere with  $F_{fr}$  directed toward the left.

Next, we consider the case of  $F_{fr}$  directed toward the right. Summing the forces in the  $\vec{n}_2$  and  $\vec{n}_1$  directions respectively, we have

$$\begin{aligned}
\sum F_{q_2} &= ma_{q_2} \\
&= N - W = 0 \\
\Rightarrow N &= W = mg \tag{3.4}
\end{aligned}$$

and

$$\begin{aligned}
\sum F_{q_1} &= ma_{q_1} \\
&= F_{fr} = ma_{q_1} \\
&= \mu' N = ma_{q_1} \\
&= \mu' mg = ma_{q_1} \\
\Rightarrow a_{q_1} &= \mu' g \tag{3.5}
\end{aligned}$$

Summing moments about point G, with the clockwise direction as positive, we have

$$\begin{aligned}
\sum M_G &= J_G \alpha_n \\
&= -F_{fr} b = J_G \alpha_n \\
&= -\mu' m g b = J_G \alpha_n \\
\Rightarrow \alpha_n &= -\frac{\mu' g b}{J_G/m} \tag{3.6}
\end{aligned}$$

Then equations (3.4), (3.5) and (3.6) define the motion of a rolling sphere with  $F_{fr}$  directed toward the right.

Now, we consider the case of  $F_{fr}$  equal to zero, which implies the sphere is rolling without slipping. Summing moments about point C, with the clockwise direction as positive, we have

$$\begin{aligned} \sum M_C &= J_C \alpha_n \\ &= 0 = J_C \alpha_n \\ \Rightarrow \alpha_n &= 0 \end{aligned} \tag{3.7}$$

Since the sphere is rolling without slipping, the following kinematic expression applies:

$$a_{q1} = b\alpha_n = 0 \tag{3.8}$$

Then equations (3.7) and (3.8) define the motion of a rolling sphere with  $F_{fr}$  equal to zero.

The model determines if the sphere is initially rolling without slipping or if the sphere is initially sliding. If the sphere is initially rolling without slipping, then the motion will continue until the sphere impacts the terrain. If the sphere is initially sliding, then two potential cases arise. For the first case, the sphere impacts the terrain while sliding. For the second case, the sphere's motion will transition from sliding to rolling without slipping before impacting the terrain.

In this study we vary the sphere's density, where the principal moment of inertial can range from  $J_G = 0.1mb^2$  to  $J_G = 2/3mb^2$  for a thin spherical shell. Note the minimum value of the coefficient of static friction compatible with rolling in the horizontal plane is  $\mu_{min} = \frac{F_{fr}}{N} = \frac{0}{mg} = 0$ . Hence, the equations derived above are valid if and only if  $\mu > \mu_{min}$ .

## 3.2 Rolling and Sliding Model of a Rigid Sphere on an Incline Plane

Consider the two dimensional rolling and sliding motion of a rigid sphere shown in figure 3.2. The equations of motion are written using the free-body diagram.

Note the sense of the frictional force depends on whether the sphere has backspin or topspin. If the sphere has backspin, then the frictional force,  $F_{fr}$ , is directed toward the left. If the sphere has topspin, then the sense of the frictional force depends on the relationship between  $|v|$  and  $|\omega| r$ . The different cases are summarized as follows:

- If  $|v| = |\omega| r$ , then  $F_{fr}$  is directed toward the right
- If  $|v| < |\omega| r$ , then  $F_{fr}$  is directed toward the right
- If  $|v| > |\omega| r$ , then  $F_{fr}$  is directed toward the left

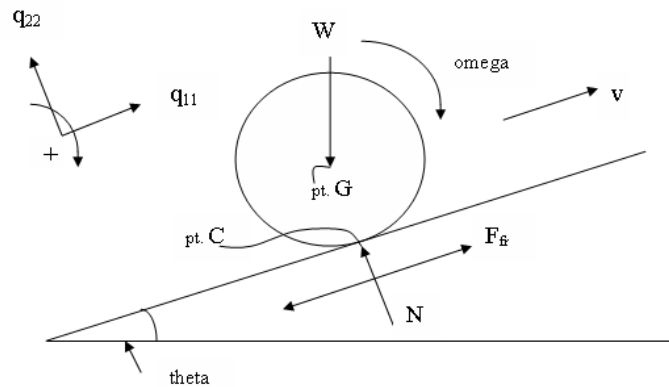


Figure 3.2: Free Body Diagram (Incline Plane)

Once the sense of the frictional force is known, the equations of motion may be defined. First, we consider the case of  $F_{fr}$  directed toward the left and  $|v| \neq |\omega| r$ . Summing the forces in the  $\vec{c}_2$  and  $\vec{c}_1$  directions respectively, we have

$$\sum F_{q22} = ma_{q22}$$

$$\begin{aligned}
&= N - W \cos\theta = 0 \\
&= N - mg \cos\theta = 0 \\
\Rightarrow N &= mg \cos\theta
\end{aligned} \tag{3.9}$$

and

$$\begin{aligned}
\sum F_{q11} &= ma_{q11} \\
= -F_{fr} - W \sin\theta &= ma_{q11} \\
= -\mu' N - mg \sin\theta &= ma_{q11} \\
= -\mu' mg \cos\theta - mg \sin\theta &= ma_{q11} \\
\Rightarrow a_{q11} &= -g(\mu' \cos\theta + \sin\theta)
\end{aligned} \tag{3.10}$$

Summing moments about point G, with the clockwise direction as positive, we have

$$\begin{aligned}
\sum M_G &= J_G \alpha_c \\
= F_{fr} b &= J_G \alpha_c \\
= \mu' mg b \cos\theta &= J_G \alpha_c \\
\Rightarrow \alpha_c &= \frac{\mu' g b \cos\theta}{J_G/m}
\end{aligned} \tag{3.11}$$

Then equations (3.9), (3.10) and (3.11) define the motion of a rolling sphere with  $F_{fr}$  directed toward the left.

Next, we consider the case of  $F_{fr}$  directed toward the right and  $|v| < |\omega| r$ . Summing the forces in the  $\vec{c}_2$  and  $\vec{c}_1$  directions respectively, we have

$$\begin{aligned}
\sum F_{q22} &= ma_{q22} \\
= N - W \cos\theta &= 0 \\
= N - mg \cos\theta &= 0 \\
\Rightarrow N &= mg \cos\theta
\end{aligned} \tag{3.12}$$

and

$$\begin{aligned}
\sum F_{q11} &= ma_{q11} \\
= F_{fr} - W \sin\theta &= ma_{q11}
\end{aligned}$$

$$\begin{aligned}
&= \mu' N - mg \sin \theta = ma_{q_{11}} \\
&= \mu' mg \cos \theta - mg \sin \theta = ma_{q_{11}} \\
\Rightarrow &a_{q_{11}} = g(\mu' \cos \theta - \sin \theta) \tag{3.13}
\end{aligned}$$

Summing moments about point G, with the clockwise direction as positive, we have

$$\begin{aligned}
\sum M_G &= J_G \alpha_c \\
&= -F_{fr} b = J_G \alpha_c \\
&= -\mu' mg b \cos \theta = J_G \alpha_c \\
\Rightarrow \alpha_c &= -\frac{\mu' g b \cos \theta}{J_G/m} \tag{3.14}
\end{aligned}$$

Then equations (3.12), (3.13) and (3.14) define the motion of a rolling sphere with  $F_{fr}$  directed toward the right.

Now, we consider the case of  $F_{fr}$  directed toward the right and  $|v| = |\omega|r$ . Summing moments about point C, with the clockwise direction as positive, we have

$$\begin{aligned}
\sum M_C &= J_C \alpha_c \\
&= -W b \sin \theta = (J_G + mb^2) \alpha_c \\
&= -mg b \sin \theta = (J_G + mb^2) \alpha_c \\
\Rightarrow \alpha_c &= -\frac{g b \sin \theta}{J_G/m + b^2} \tag{3.15}
\end{aligned}$$

Since the sphere is rolling without slipping, the following kinematic expression applies:

$$a_{q_{11}} = b \alpha_c = -\frac{g b^2 \sin \theta}{J_G/m + b^2} \tag{3.16}$$

Summing the forces in the  $\vec{c}_2$  and  $\vec{c}_1$  directions respectively, we have

$$\begin{aligned}
\sum F_{q_{22}} &= ma_{q_{22}} \\
&= N - W \cos \theta = 0 \\
&= N - mg \cos \theta = 0 \\
\Rightarrow &N = mg \cos \theta \tag{3.17}
\end{aligned}$$

and

$$\begin{aligned}
& \sum F_{q_{11}} = ma_{q_{11}} \\
= & F_{fr} - W \sin\theta = ma_{q_{11}} \\
= & F_{fr} - mg \sin\theta = -\frac{mgb^2 \sin\theta}{J_G/m + b^2} \\
\Rightarrow & F_{fr} = mg \sin\theta - \frac{mgb^2 \sin\theta}{J_G/m + b^2} \tag{3.18}
\end{aligned}$$

Then equations (3.15), (3.16), (3.17) and (3.18) define the motion of a sphere that rolls without slipping.

The model determines if the sphere is initially rolling without slipping or if the sphere is initially sliding. If the sphere is initially rolling without slipping, then the motion will continue until the sphere begins to roll down the incline. If the sphere is initially sliding, then two potential cases arise. For the first case, the sphere slides until it begins to move down the incline. For the second case, the sphere's motion will transition from sliding to rolling without slipping before rolling down the incline.

In this study we vary the sphere's density, where the principal moment of inertial can range from  $J_G = 0.1mb^2$  to  $J_G = 2/3mb^2$  for a thin spherical shell. Note the minimum value of the coefficient of static friction compatible with rolling in the incline plane will range from  $\mu_{min} = \frac{2}{7}\tan\theta$  for a solid sphere to  $\mu_{min} = \frac{2}{5}\tan\theta$  for a thin spherical shell. Hence, the equations derived above are valid if and only if  $\mu > \mu_{min}$ .

### 3.3 Rolling and Sliding Model of a Rigid Sphere on a Decline Plane

Consider the two dimensional rolling and sliding motion of a rigid sphere shown in figure 3.3. The equations of motion are written using the free-body diagram. Note the sense of the frictional force depends on whether the sphere has backspin or topspin. If the sphere has backspin, then the frictional force,  $F_{fr}$ , is directed toward the left. If the sphere has topspin, then the sense of the frictional

force depends on the relationship between  $|v|$  and  $|\omega| r$ . The different cases are summarized as follows:

- If  $|v| = |\omega| r$ , then  $F_{fr}$  is directed toward the left
- If  $|v| < |\omega| r$ , then  $F_{fr}$  is directed toward the right
- If  $|v| > |\omega| r$ , then  $F_{fr}$  is directed toward the left

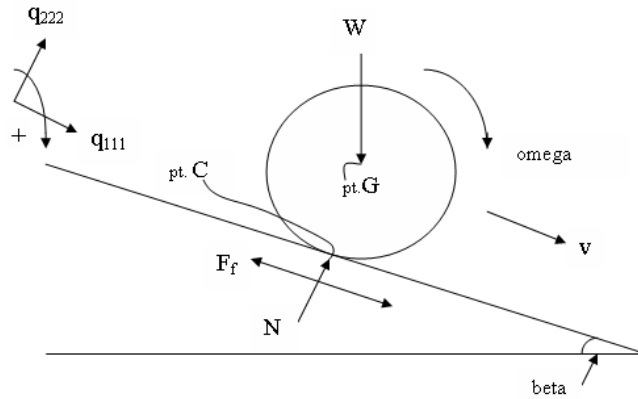


Figure 3.3: Free Body Diagram (Decline Plane)

Once the sense of the frictional force is known, the equations of motion may be defined. First, we consider the case of  $F_{fr}$  directed toward the left and  $|v| \neq |\omega| r$ . Summing the forces in the  $\vec{a}_2$  and  $\vec{a}_1$  directions respectively, we have

$$\begin{aligned}
 \sum F_{q_{222}} &= ma_{q_{222}} \\
 &= N - W \cos \beta = 0 \\
 &= N - mg \cos \beta = 0 \\
 \Rightarrow N &= mg \cos \beta
 \end{aligned} \tag{3.19}$$

and

$$\begin{aligned}
& \sum F_{q_{111}} = ma_{q_{111}} \\
= & -F_{fr} + W \sin\beta = ma_{q_{111}} \\
= & -\mu' N + mg \sin\beta = ma_{q_{111}} \\
= & -\mu' mg \cos\beta + mg \sin\beta = ma_{q_{111}} \\
\Rightarrow & a_{q_{111}} = -g(\mu' \cos\beta - \sin\beta) \tag{3.20}
\end{aligned}$$

Summing moments about point G, with the clockwise direction as positive, we have

$$\begin{aligned}
& \sum M_G = J_G \alpha_a \\
= & F_{fr} b = J_G \alpha_a \\
= & \mu' mg b \cos\beta = J_G \alpha_a \\
\Rightarrow & \alpha_a = \frac{\mu' g b \cos\beta}{J_G/m} \tag{3.21}
\end{aligned}$$

Then equations (3.19), (3.20) and (3.21) define the motion of a rolling sphere with  $F_{fr}$  directed toward the left.

Next, we consider the case of  $F_{fr}$  directed toward the right and  $|v| < |\omega| r$ . Summing the forces in the  $\vec{a}_2$  and  $\vec{a}_1$  directions respectively, we have

$$\begin{aligned}
& \sum F_{q_{222}} = ma_{q_{222}} \\
= & N - W \cos\beta = 0 \\
= & N - mg \cos\beta = 0 \\
\Rightarrow & N = mg \cos\beta \tag{3.22}
\end{aligned}$$

and

$$\begin{aligned}
& \sum F_{q_{111}} = ma_{q_{111}} \\
= & F_{fr} + W \sin\beta = ma_{q_{111}} \\
= & \mu' N + mg \sin\beta = ma_{q_{111}} \\
= & \mu' mg \cos\beta + mg \sin\beta = ma_{q_{111}} \\
\Rightarrow & a_{q_{111}} = g(\mu' \cos\beta + \sin\beta) \tag{3.23}
\end{aligned}$$

Summing moments about point G, with the clockwise direction as positive, we have

$$\begin{aligned}
& \sum M_G = J_G \alpha_a \\
= & -F_{fr} b = J_G \alpha_a \\
= & -\mu' m g b \cos \beta = J_G \alpha_a \\
\Rightarrow & \alpha_a = -\frac{\mu' g b \cos \beta}{J_G/m} \tag{3.24}
\end{aligned}$$

Then equations (3.22), (3.23) and (3.24) define the motion of a rolling sphere with  $F_{fr}$  directed toward the right.

Now, we consider the case of  $F_{fr}$  directed toward the left and  $|v| = |\omega|r$ . Summing moments about point C, with the clockwise direction as positive, we have

$$\begin{aligned}
& \sum M_C = J_C \alpha_a \\
= & W b \sin \beta = (J_G + m b^2) \alpha_a \\
= & m g b \sin \beta = (J_G + m b^2) \alpha_a \\
\Rightarrow & \alpha_a = \frac{g b \sin \beta}{J_G/m + b^2} \tag{3.25}
\end{aligned}$$

Since the sphere is rolling without slipping, the following kinematic expression applies:

$$a_{q_{111}} = b \alpha_a = \frac{g b^2 \sin \beta}{J_G/m + b^2} \tag{3.26}$$

Summing the forces in the  $\vec{a}_2$  and  $\vec{a}_1$  directions respectively, we have

$$\begin{aligned}
& \sum F_{q_{222}} = m a_{q_{222}} \\
= & N - W \cos \beta = 0 \\
= & N - m g \cos \beta = 0 \\
\Rightarrow & N = m g \cos \beta \tag{3.27}
\end{aligned}$$

and

$$\sum F_{q_{111}} = m a_{q_{111}}$$

$$\begin{aligned}
&= -F_{fr} + W \sin\beta = ma_{q_{111}} \\
&= -F_{fr} + mg \sin\beta = \frac{mgb^2 \sin\beta}{J_G/m + b^2} \\
\Rightarrow F_{fr} &= mg \sin\beta - \frac{mgb^2 \sin\beta}{J_G/m + b^2} \tag{3.28}
\end{aligned}$$

Then equations (3.25), (3.26), (3.27) and (3.28) define the motion of a sphere that rolls without slipping.

The model determines if the sphere is initially rolling without slipping or if the sphere is initially sliding. If the sphere is initially rolling without slipping, then the motion will continue until the sphere impacts the terrain. If the sphere is initially sliding, then two potential cases arise. For the first case, the sphere impacts the terrain while sliding. For the second case, the sphere's motion will transition from sliding to rolling without slipping before impacting the terrain.

In this study we vary the sphere's density, where the principal moment of inertial can range from  $J_G = 0.1mb^2$  to  $J_G = 2/3mb^2$  for a thin spherical shell. Note the minimum value of the coefficient of static friction compatible with rolling in the decline plane will range from  $\mu_{min} = \frac{2}{7}\tan\beta$  for a solid sphere to  $\mu_{min} = \frac{2}{5}\tan\beta$  for a thin spherical shell. Hence, the equations derived above are valid if and only if  $\mu > \mu_{min}$ .

# Chapter 4

## Numerical Simulation Model

### 4.1 Framework

This chapter develops the framework of a numerical model based on the dynamic models presented in previous chapters. The framework illustrates how the model can determine suitable ranges of tumbleweed design parameters required for optimal mobility. The study considers the rover's motion for arbitrary valleys, as shown in figure 4.1. Note the numerical model can generate other terrain types the tumbleweed rover may encounter, including flat planes, hills and gullies.

During a simulation the numerical model considers the rover's rolling, sliding and bouncing behaviors and the transitions between these modes of movement. The simulation also considers when the rover transitions between different terrain types.

The model requires the following parameters are specified for a defined valley:  $b$ ,  $J/m$ ,  $e$ ,  $\mu$ ,  $\mu'$ ,  $q_1$ ,  $q_2$ ,  $q_3$ ,  $u_1, \dots, u_6$  and  $g$ . Two additional assumptions supplement the model: first, we assume the rover rolls without slipping over the valley edge. This implies an initial condition of  $u_3 = -u_4/b$ . Second, we assume the rover is not experiencing any initial side spin. This assumption reduces the study from a three-dimensional to a two-dimensional analysis, and implies the following initial generalized speeds are zero:  $u_1$ ,  $u_2$  and  $u_6$ . Furthermore, equations (2.84), (2.169) and (2.255) can be ignored. The simulation is stopped once the rover rebounds or begins to roll or slide down the incline plane. Throughout the simulation the rover's motion is referenced to the  $\vec{n}$  frame. The rotation matrices given by

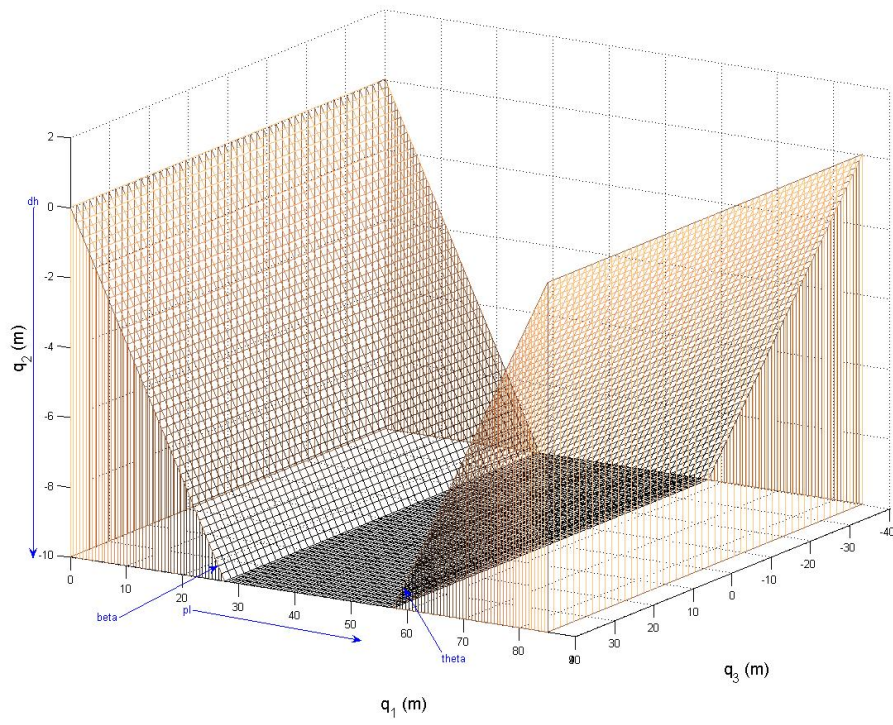


Figure 4.1: An example of an arbitrary valley encountered by a tumbleweed rover

equations (2.170) and (2.256) for the incline and decline planes respectively are used to resolve the rover's generalized speeds and position into the appropriate reference frame for computations and simulations.

Note the equations derived in the trajectory, rolling and sliding models can be solved by numerical integration methods such as the Euler or Runge-Kutta algorithms. This study implements the classic fourth-order four-stage Runge-Kutta to the models mentioned above. Instead of using adaptive Runge-Kutta methods already available in existing software, we write our own algorithms because we achieve greater control over the simulation at each time step. This approach proves beneficial when the sphere transitions between different terrain types and modes of movement as well as for numerical interpolation. See Appendix A and B for examples on the fourth-order Runge-Kutta method.

## 4.2 Numerical Simulation Example

The following example is used to define the parameters of the numerical simulation model and demonstrate the type of simulations produced. Consider figure 4.1. The parameters ( $\beta$ ,  $\theta$ ,  $dh$  and  $pl$ ) will be referred to as *terrain parameters*, where  $\beta$  and  $\theta$  are the angles of the decline and incline planes respectively,  $dh$  is the height of the decline plane and  $pl$  is the length of the horizontal plane. Note the positive sense for  $dh$  is in the upward direction. For convenience, the *terrain parameters* will be represented in the following format:  $[\beta, \theta, dh, pl]$ . The parameters ( $b$ ,  $J/m$ ,  $e$ ,  $\mu$ ,  $\mu'$ ) will be referred to as *physical parameters*, and they are defined as before. Again, for convenience the *physical parameters* will be shown as  $[b, J/m, e, \mu, \mu']$ . We define the subset of the *physical parameters*  $[b, J/m, e]$ , and refer to them as the *design parameters*. The rover's position and generalized speeds and the gravitational acceleration are the *initial conditions*. These conditions will be shown as:  $[q_1, q_2, q_3, u_1, \dots, u_6, g]$ .

In its strictest form, the numerical simulation model predicts the rover's motion for a set of parameters and initial conditions. For example, suppose the terrain and physical parameters are given by  $[\beta = 30^\circ, \theta = 30^\circ, dh = -10m, pl = 30m]$  and  $[b = 1m, J/m = 0.4m^2, e = 0.92, \mu = 1.0, \mu' = 0.8]$ . Also suppose the initial conditions are specified as  $[q_1 = 0m, q_2 = 1m, u_3 = 5rad/s,$

$u_4 = 5m/s$ ,  $g = 3.71m/s^2$ ]. Figure 4.2 shows the two-dimensional representation of the simulation, and figures 4.3 and 4.4 display the same information, but shown on a valley having three-dimensions.

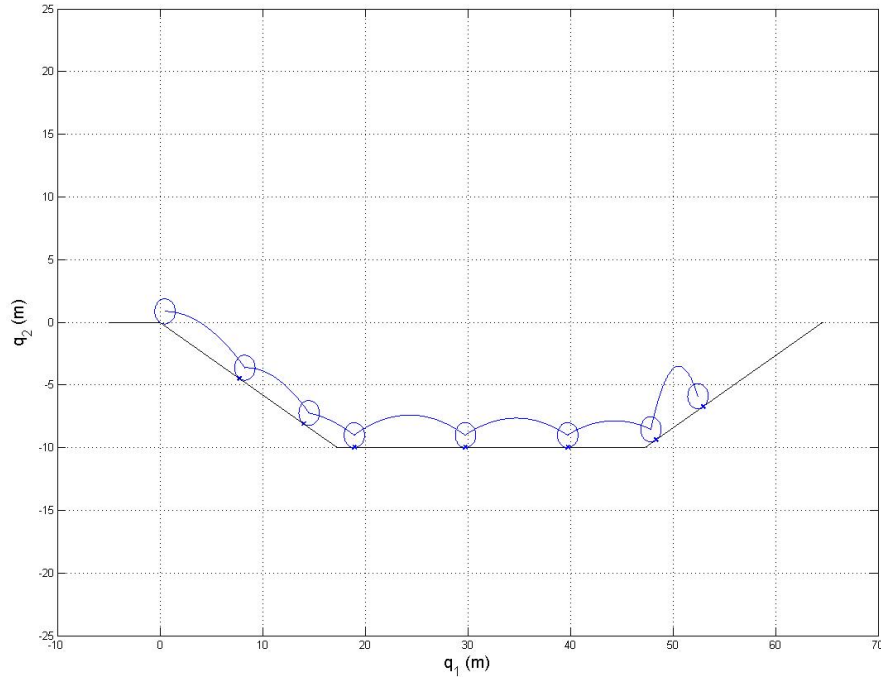


Figure 4.2: A two-dimensional simulation representation

Given this set of parameters and initial conditions we see the rover traveled 3.25 meters up from the valley's floor before rebounding off the incline plane.

### 4.3 Parametric Study Framework

To determine the tumbleweed's behavior as it engages specific valleys, parametric studies are developed, where the numerical simulation model is run for various sets of parameters and initial conditions. For all runs, we allow the design parameters to vary as follows: the radius  $b$  ranges from 1 to 6 m in increments of 1 m. The coefficient of restitution  $e$  ranges from 0.6 to 1.0 in increments of 0.01. Note

$e = 1$  represents the theoretical limit for perfectly elastic collisions. The principal moment of inertia divided by the mass  $J/m$  can take values of  $J/m = 0.1b^2$  through  $J/m = 0.6b^2$  and  $J/m = 0.67b^2$ . Note  $J/m = 0.4b^2$  and  $J/m = 0.67b^2$  correspond to a solid sphere and a thin spherical shell, respectively. Values of  $J/m < 0.4b^2$  correspond to the sphere's density being concentrated toward the sphere's geometric center. Each simulation is run over a velocity range of 2-7 m/s or 5-10 m/s in increments of 0.1 m/s. Therefore, a completed simulation has  $6 \times 41 \times 7 \times 51 = 87,822$  runs. Note for all simulations, we assume the nominal values of  $\mu = 1.0$  and  $\mu' = 0.8\mu$ . We also assume  $g = 3.71m/s^2$  on Mars,  $g = 9.81m/s^2$  on Earth and  $g = 1.60m/s^2$  on the Moon. For this study we consider parametric studies only on Mars and on Earth. Examples of parametric studies produced by the model are found in Chapter Five.

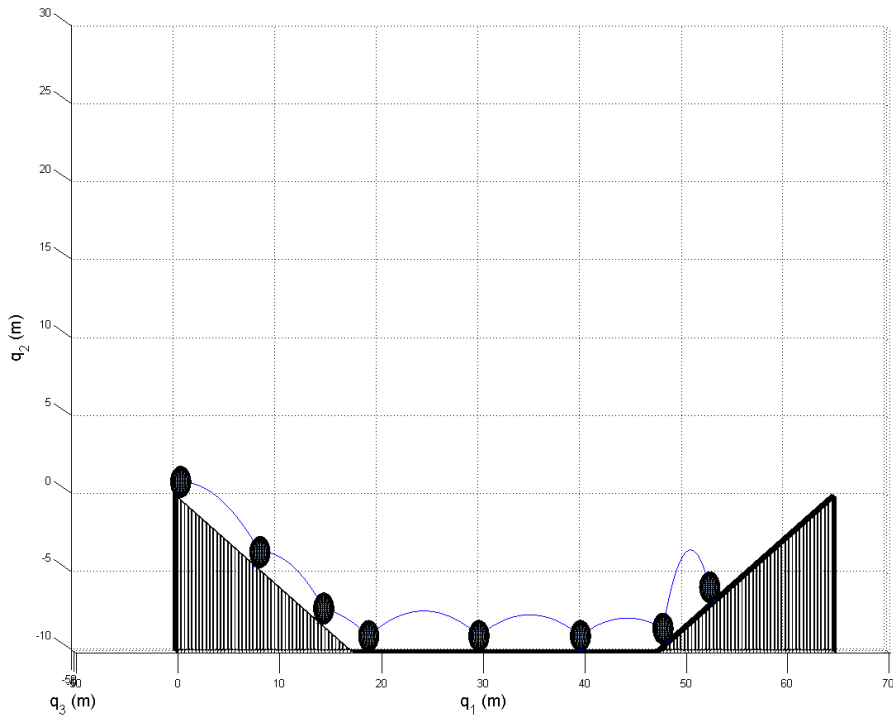


Figure 4.3: A three-dimensional simulation representation (view I)

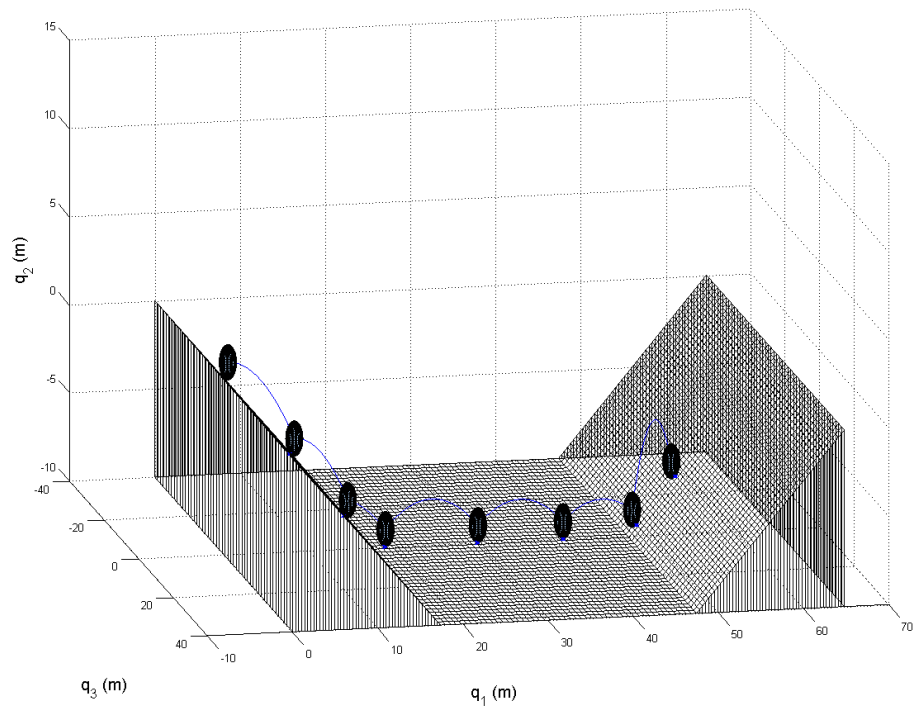


Figure 4.4: A three-dimensional simulation representation (view II)

# Chapter 5

## Parametric Studies

The parametric studies presented below demonstrate the numerical model's usefulness as an initial design tool for tumbleweed rovers encountering real terrain scenarios. The studies provide an understanding of the range of tumbleweed design parameters  $[b, J/m, e]$  essential for mobility over varied terrain. Note the parametric study figures are located at the end of the chapter.

### 5.1 Parametric Study I and II

The following studies examine the tumbleweed rover's behavior while encountering a shallow valley. Consider a valley defined by the terrain parameters  $[\beta = 15^\circ, \theta = 15^\circ, dh = -3m, pl = 9m]$ . Assume a tumbleweed rover has a velocity ranging between 2 and  $7m/s$ . Allow the design parameters to vary according to the guidelines set in Chapter 4, "Parametric Study Framework". The first parametric study is for a rover on Mars, while the second parametric study concentrates on an Earth-bound rover. Given the above conditions, the numerical model produces a series of parametric plots for various sets of design parameters, see figure 5.1 for Mars and figure 5.2 for Earth.

These plots determine the percentage crossed versus  $e$  for selected values of  $b$  and  $J/m$ . We define the percentage crossed as the average a tumbleweed rover crosses the valley for a design parameter set and velocity range.

The figures for Mars and for Earth exhibit similar trends: the percentage crossed is sensitive to values of  $e$  but remains relatively unchanged for values of  $b$  and  $J/m$ . The findings suggest the coefficient of restitution is the critical design parameter for considering the rover's ability to clear shallow valleys.

Figures 5.1 and 5.2 also reveal the percentage crossed increases monotonically for increasing values of  $e$  before leveling off. We define the value of  $e$  at this transition point as  $e_{crit}$ , and values of  $e$  satisfying the inequality

$$e \geq e_{crit} \tag{5.1}$$

maximize the rover's chance to cross the valley for any mission statement.

## 5.2 Parametric Study III and IV

The following studies examine the tumbleweed rover's behavior while encountering a deep valley. Consider a valley defined by the terrain parameters [ $\beta = 25^\circ$ ,  $\theta = 25^\circ$ ,  $dh = -30m$ ,  $pl = 90m$ ]. Assume the tumbleweed rover has a velocity ranging between 5 and 10m/s. Also, assume an area of interest on the valley's adjacent wall is at a height of  $-15m$  and above. Allow the design parameters to vary according to the guidelines set in Chapter 4, "Parametric Study Framework". The third parametric study is for a Mars-bound rover, while the fourth parametric study is for a rover on Earth. Given the above conditions, the numerical model produces a series of parametric plots for various sets of design parameters, see figures 5.3 through 5.17 for Mars and figures 5.18 through 5.32 for Earth.

These plots determine the average tumbleweed height versus  $e$  for selected values of  $b$  and  $J/m$ . Note the average height is determined for each design parameter set and velocity range. The vertical error bars on the plots represent the standard deviation or the variability of the height values from the mean height.

The figures for Mars and for Earth exhibit similar trends: the average height is nearly level for initial values of  $e$  (region I), then increases monotonically for increasing  $e$  (region II) before leveling off (region III). This result suggests a critical value of  $e$  exists, namely  $e_{crit}$ , where the average height stops to strictly increase.

For  $e \geq e_{crit}$  (region III), the rover will approximately attain its maximum height traveling up the valley. Generally, we see the error bars are larger in region II, while they show the smallest variability in region III.

Figures 5.11 through 5.17 and figures 5.26 through 5.32 for Mars and Earth respectively, superimpose the rover's height for specific velocities. The figures show for  $e \geq e_{crit}$ , the rover's height for varying velocities is more likely to be bounded within the error bars associated with the average height. Consequently, the plots confirm the rover's maximum height traveling up the valley occurs for  $e \geq e_{crit}$ .

Notice from the figures, different values of  $b$  produce relatively minor changes in the average height. This is not the case, however, for values of  $J/m$ , see figures 5.10 and 5.25 for Mars and Earth respectively. For clarity, the error bars have been omitted. Initially, the average height drops off for increasing values of  $J/m$  before leveling off. Moreover, larger values of  $J/m$  show the greatest variability in the rover's height. Thus, for optimal performance the tendency for a bigger rover with its density concentrated at its center exists on both planets.

### 5.3 Parametric Study Figures

Below are the parametric study figures.

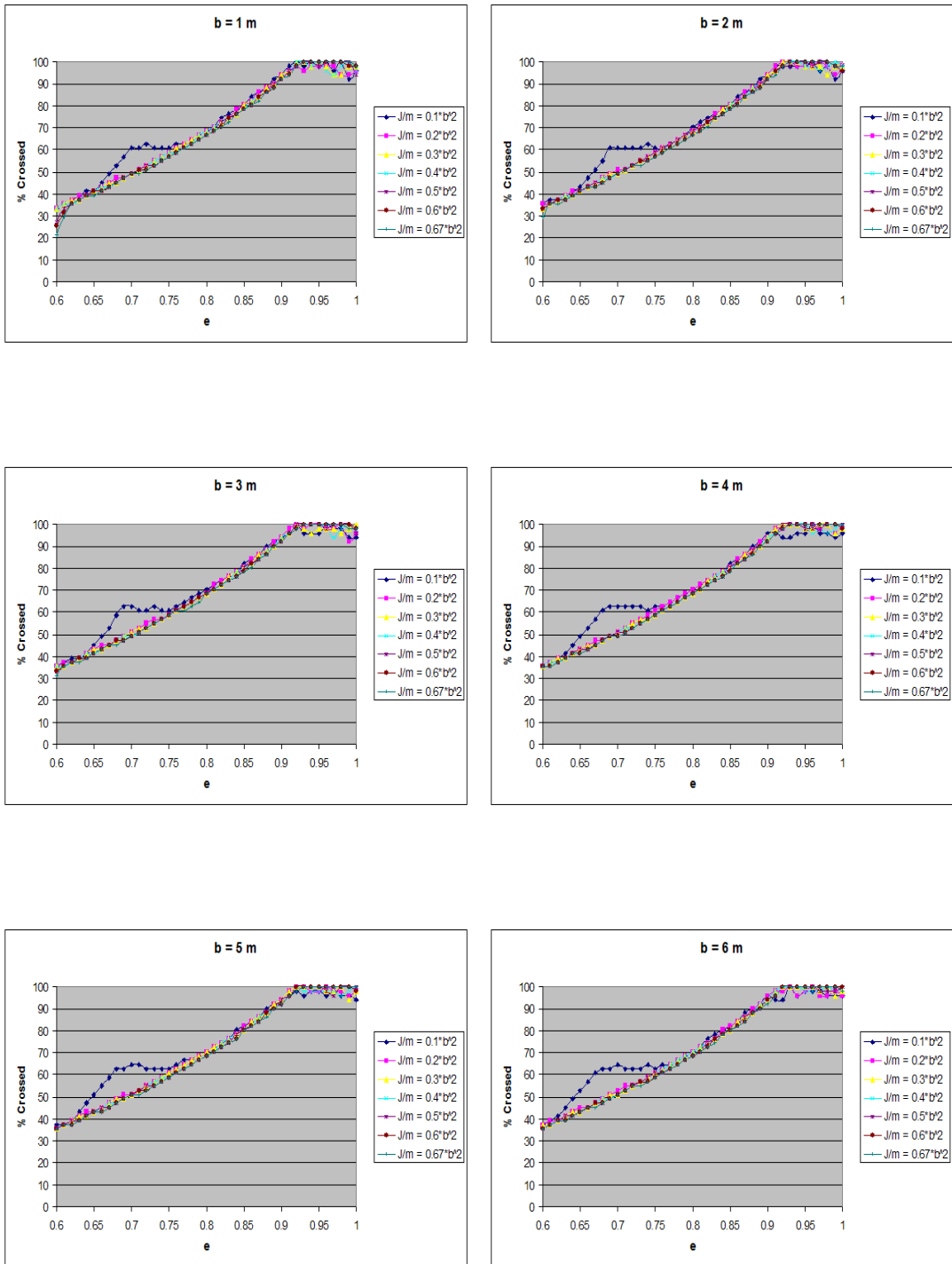


Figure 5.1: Percentage crossed for varying design parameter sets and velocity range ( $2 - 7m/s$ ) on Mars.

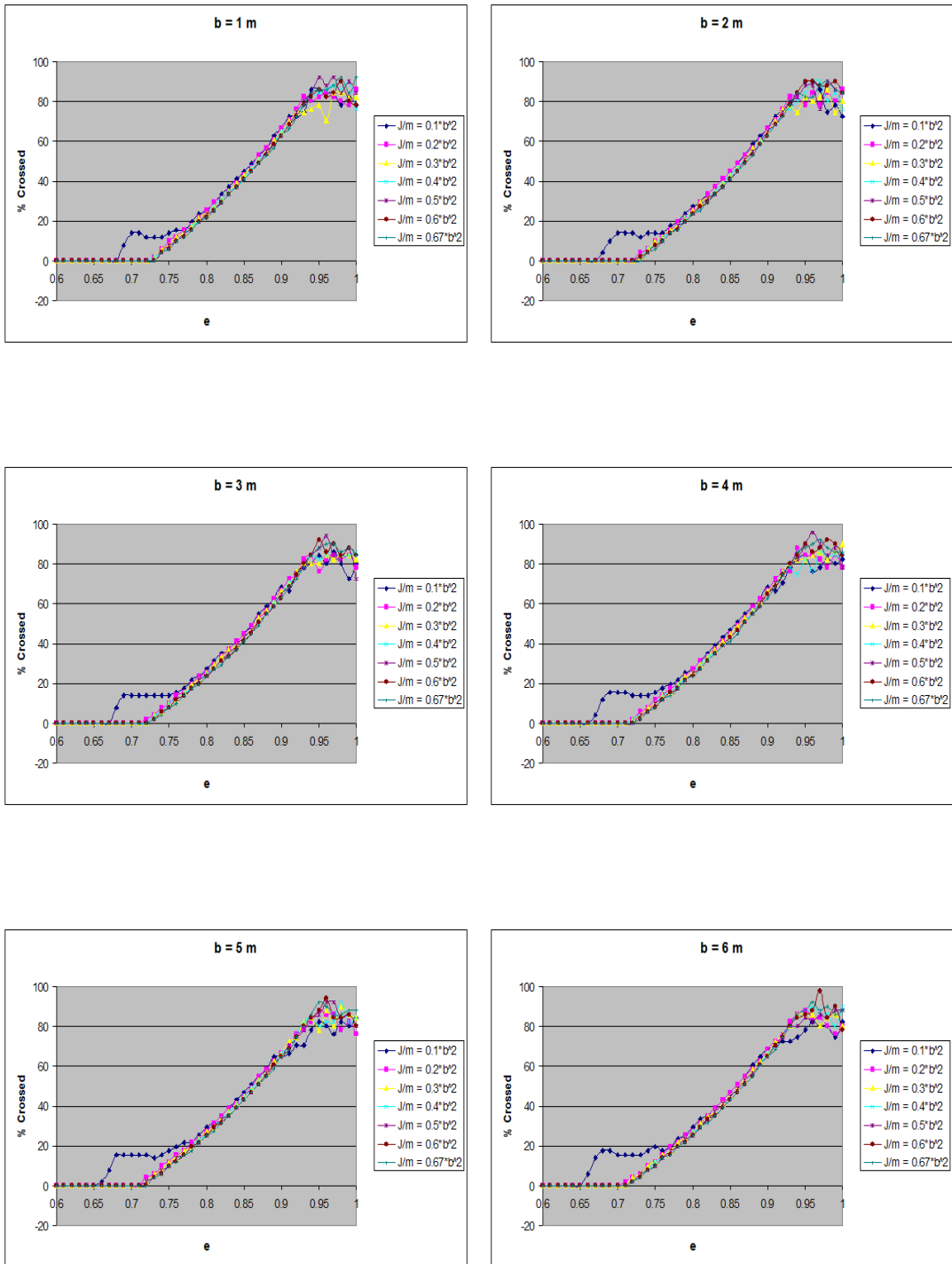


Figure 5.2: Percentage crossed for varying design parameter sets and velocity range ( $2 - 7m/s$ ) on Earth.

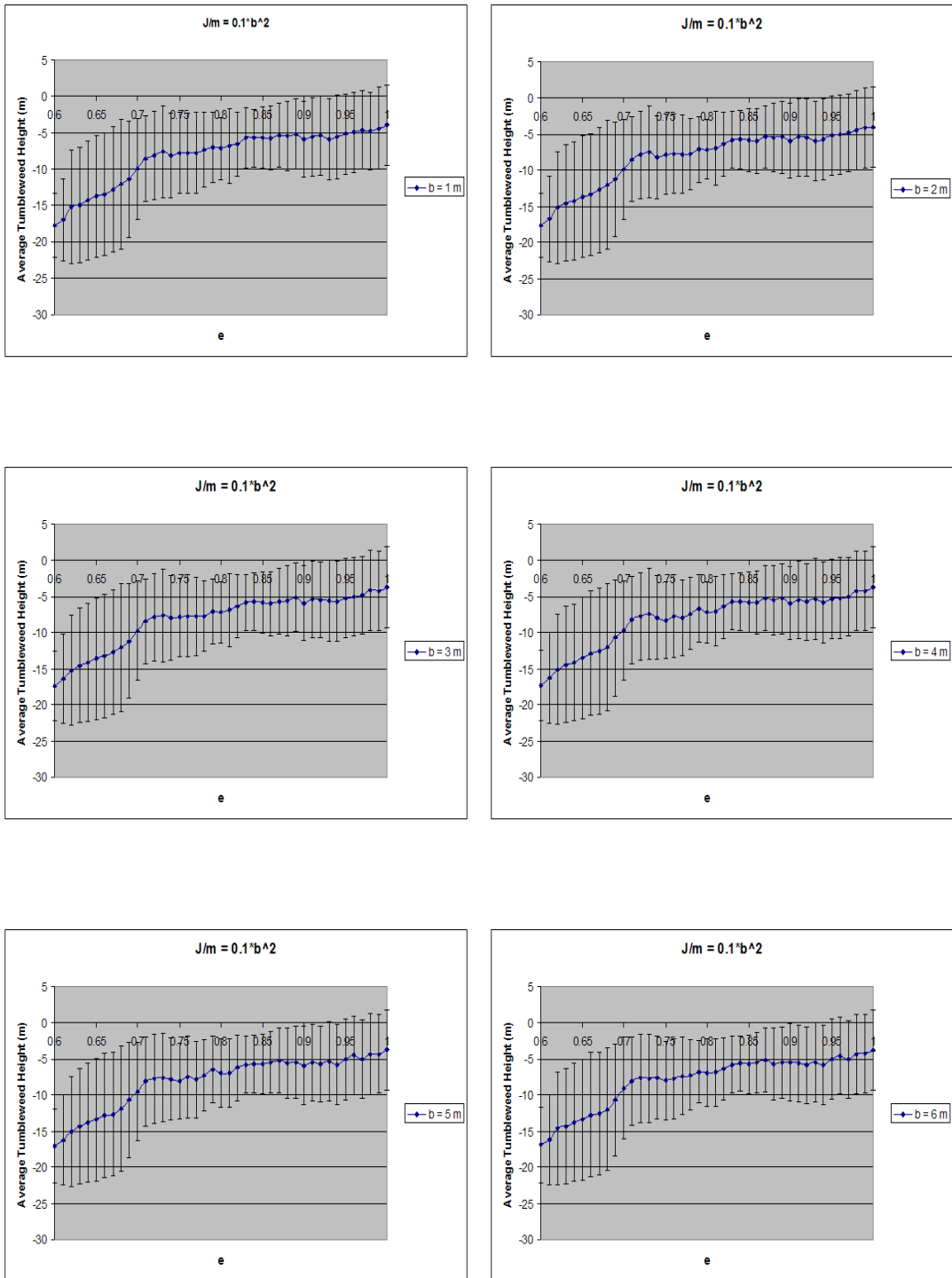


Figure 5.3: Average tumbleweed height for varying design parameter sets and velocity range (5 – 10m/s) on Mars. Note  $J/m = 0.1b^2$ .

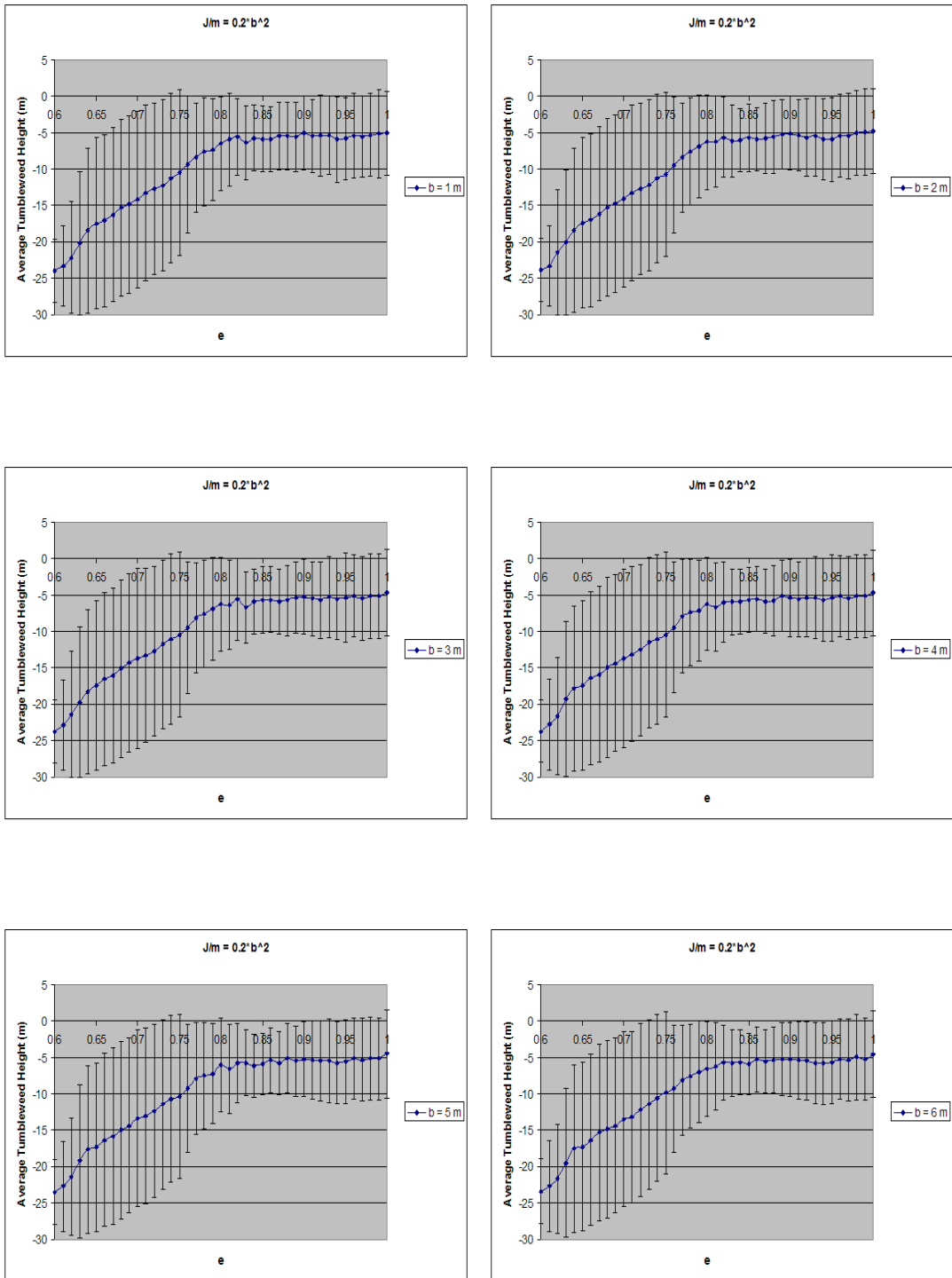


Figure 5.4: Average tumbleweed height for varying design parameter sets and velocity range (5 – 10m/s) on Mars. Note  $J/m = 0.2b^2$ .

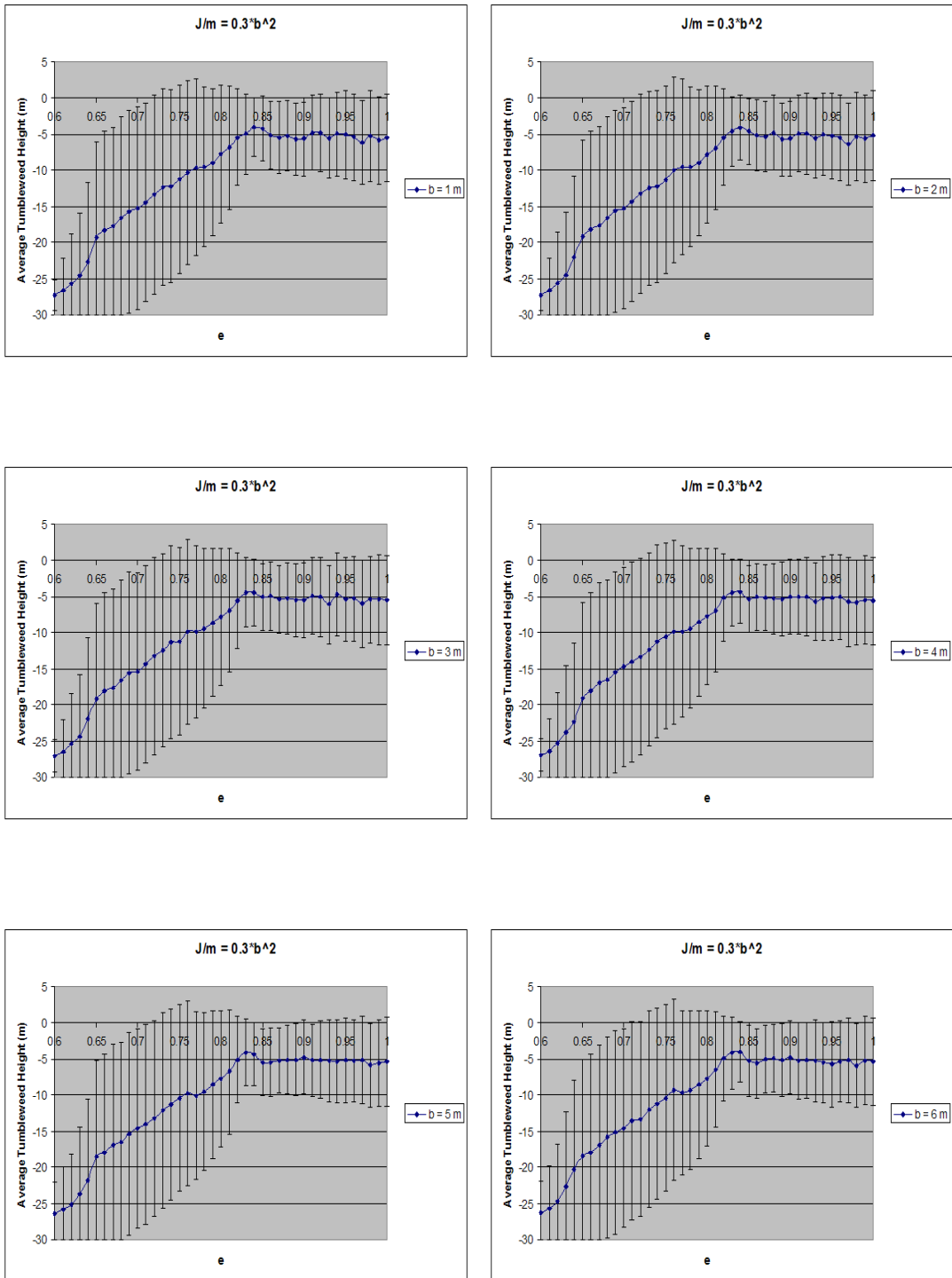


Figure 5.5: Average tumbleweed height for varying design parameter sets and velocity range (5 – 10m/s) on Mars. Note  $J/m = 0.3b^2$ .

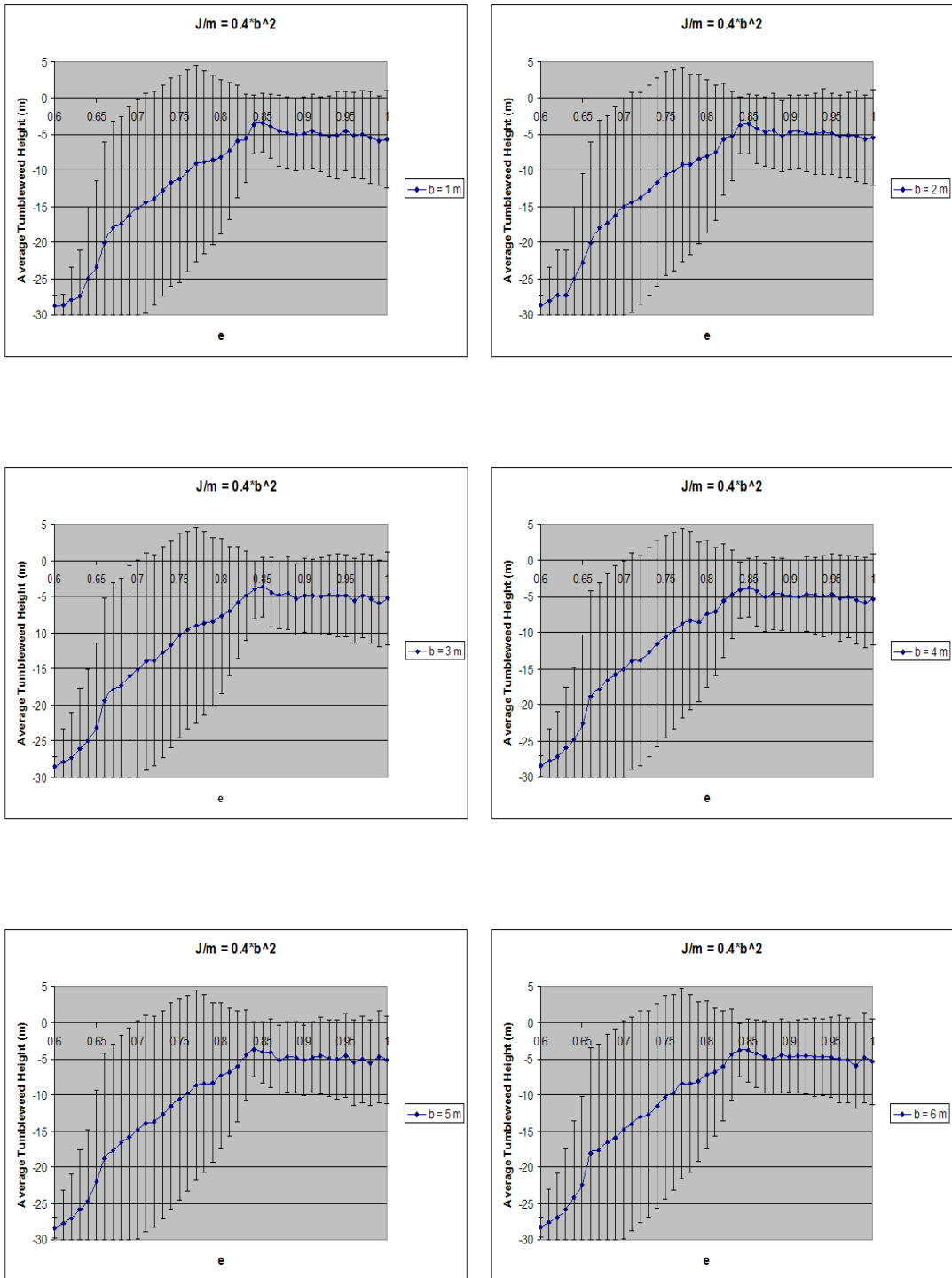


Figure 5.6: Average tumbleweed height for varying design parameter sets and velocity range (5 – 10m/s) on Mars. Note  $J/m = 0.4b^2$ .

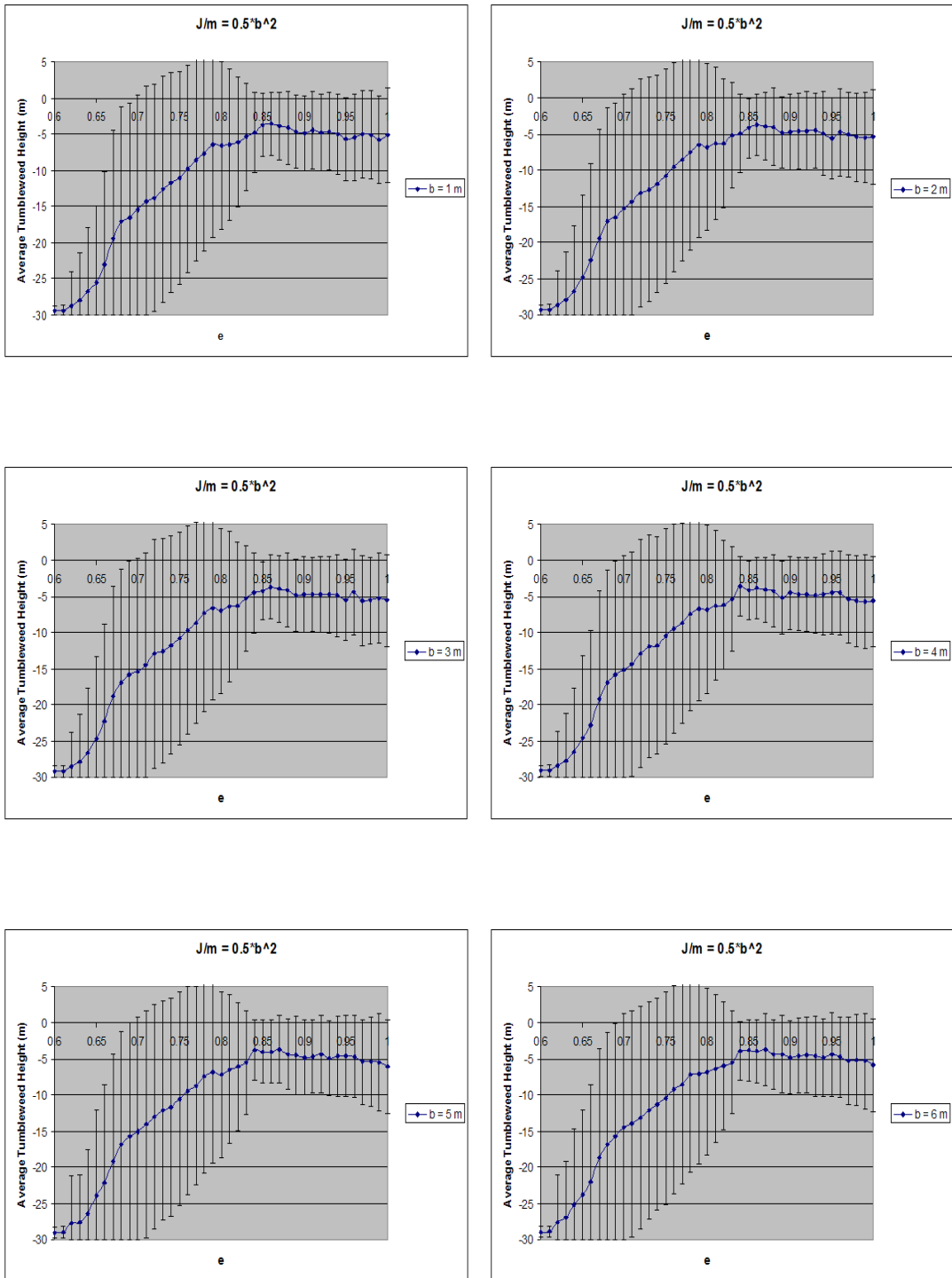


Figure 5.7: Average tumbleweed height for varying design parameter sets and velocity range (5 – 10m/s) on Mars. Note  $J/m = 0.5b^2$ .

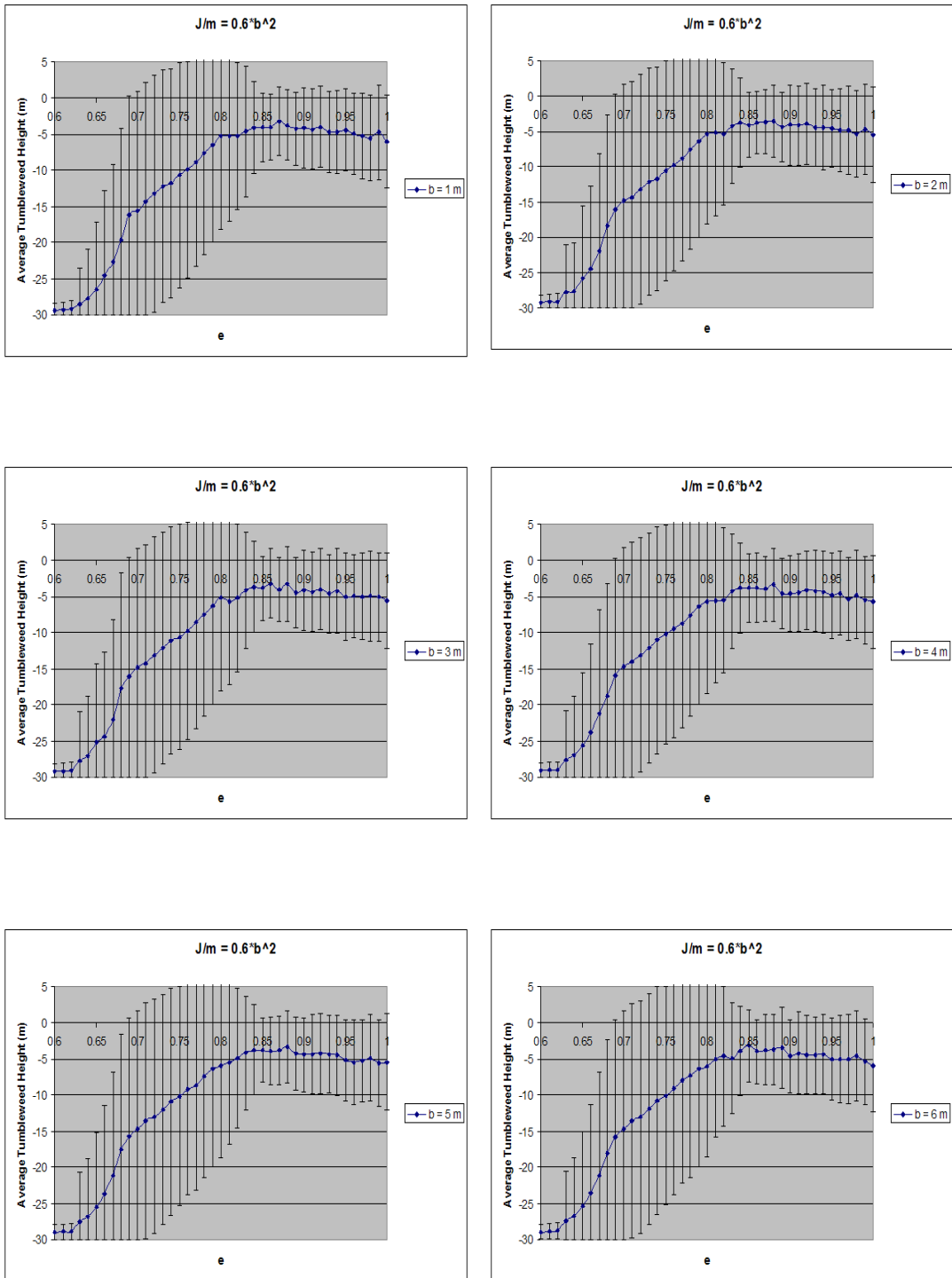


Figure 5.8: Average tumbleweed height for varying design parameter sets and velocity range (5 – 10m/s) on Mars. Note  $J/m = 0.6b^2$ .

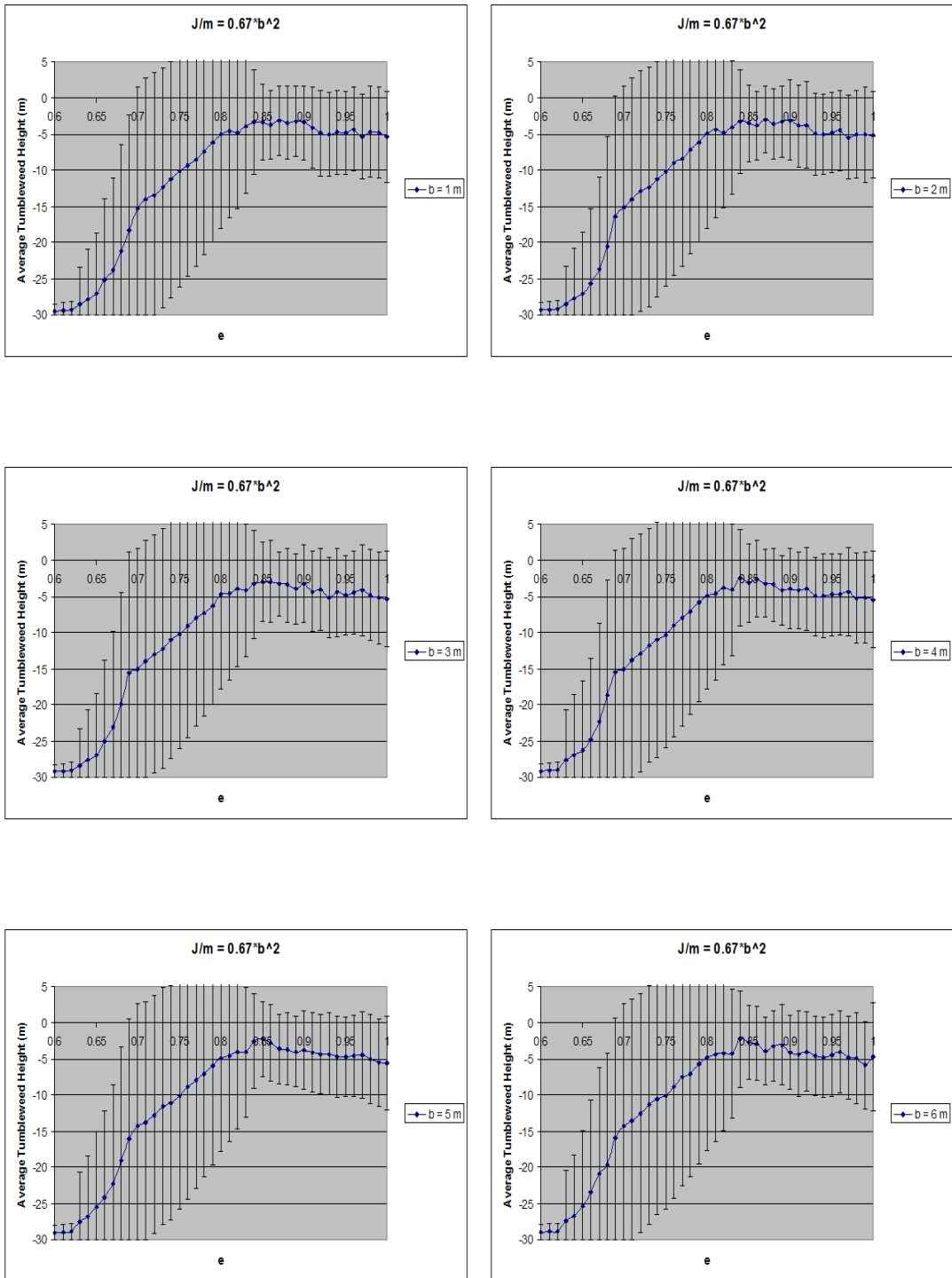


Figure 5.9: Average tumbleweed height for varying design parameter sets and velocity range (5 – 10m/s) on Mars. Note  $J/m = 0.67b^2$ .

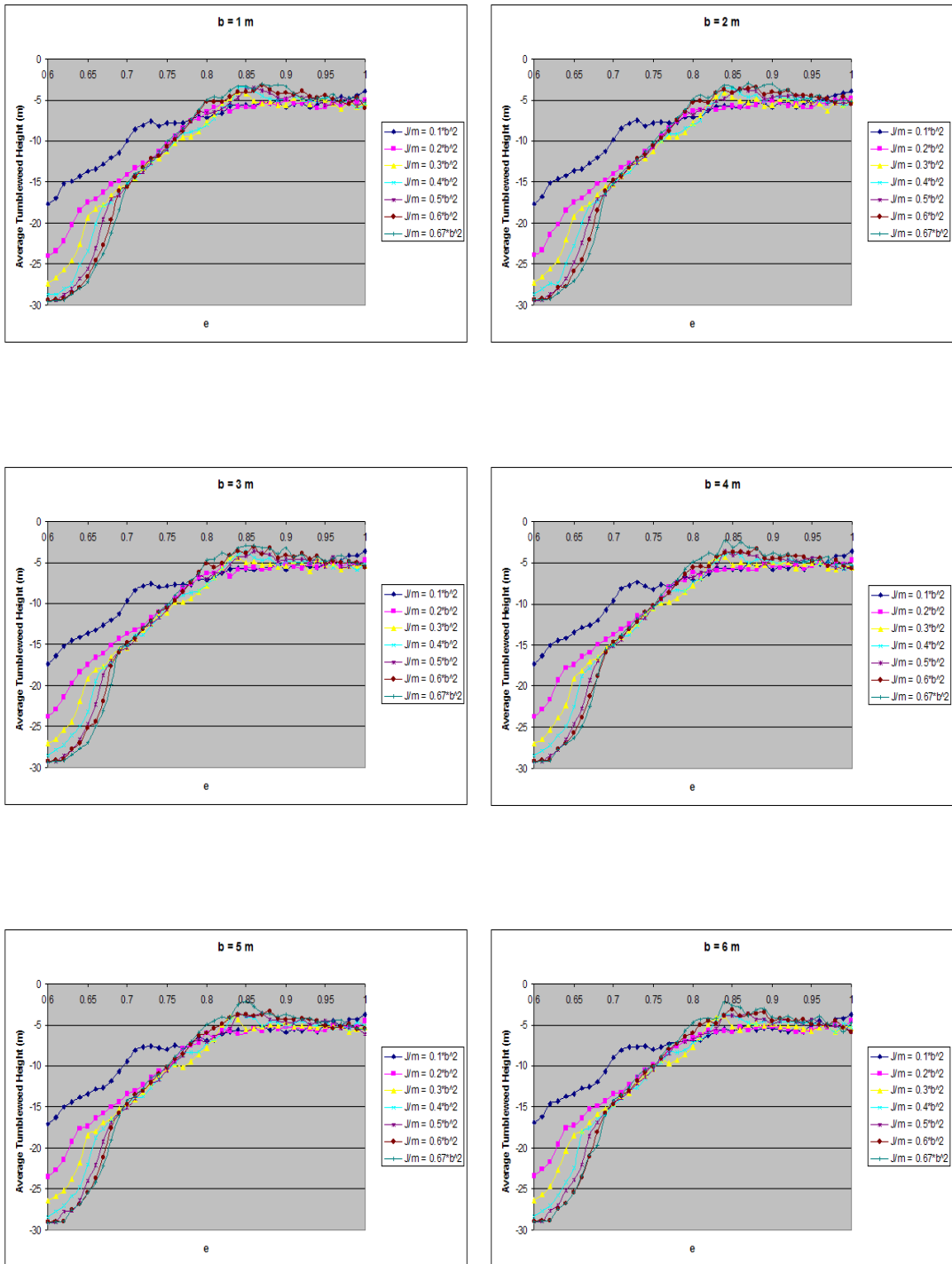


Figure 5.10: Average tumbleweed height for varying design parameter sets and velocity range (5 – 10m/s) on Mars.

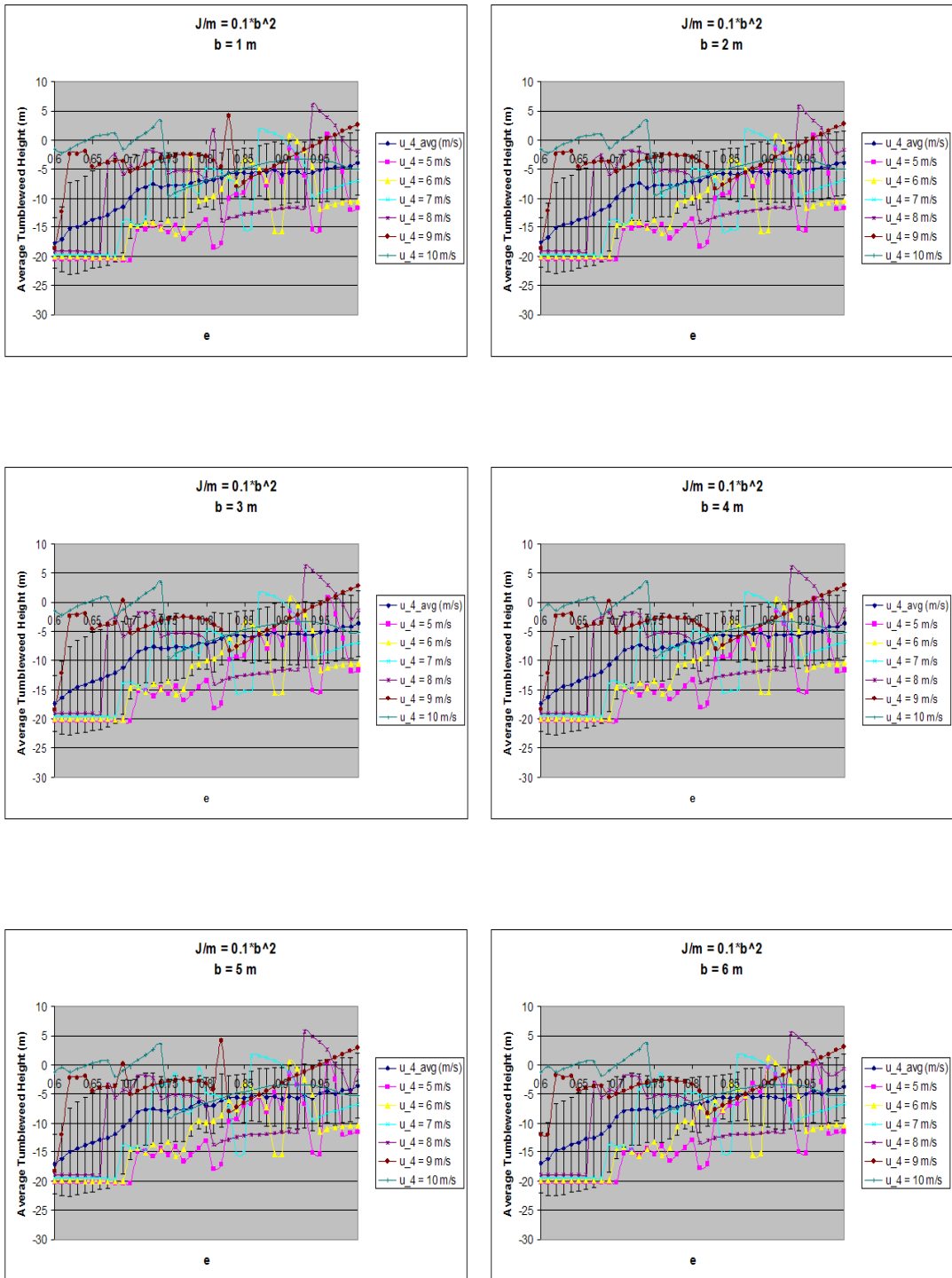


Figure 5.11: Tumbleweed height for varying design parameter sets and velocity profiles (5 – 10m/s) on Mars. Note  $J/m = 0.1b^2$ .

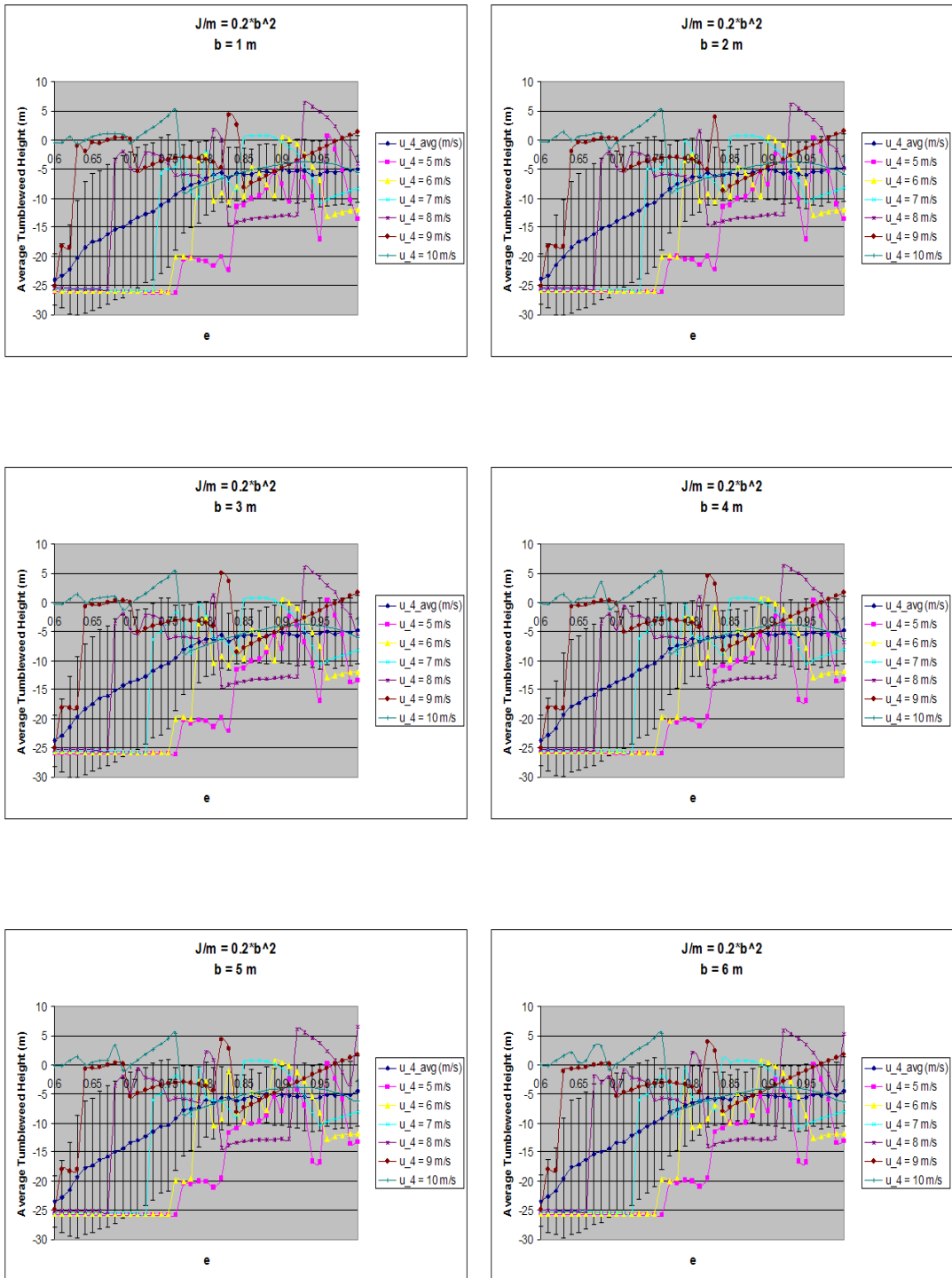


Figure 5.12: Tumbleweed height for varying design parameter sets and velocity profiles (5 – 10m/s) on Mars. Note  $J/m = 0.2b^2$ .

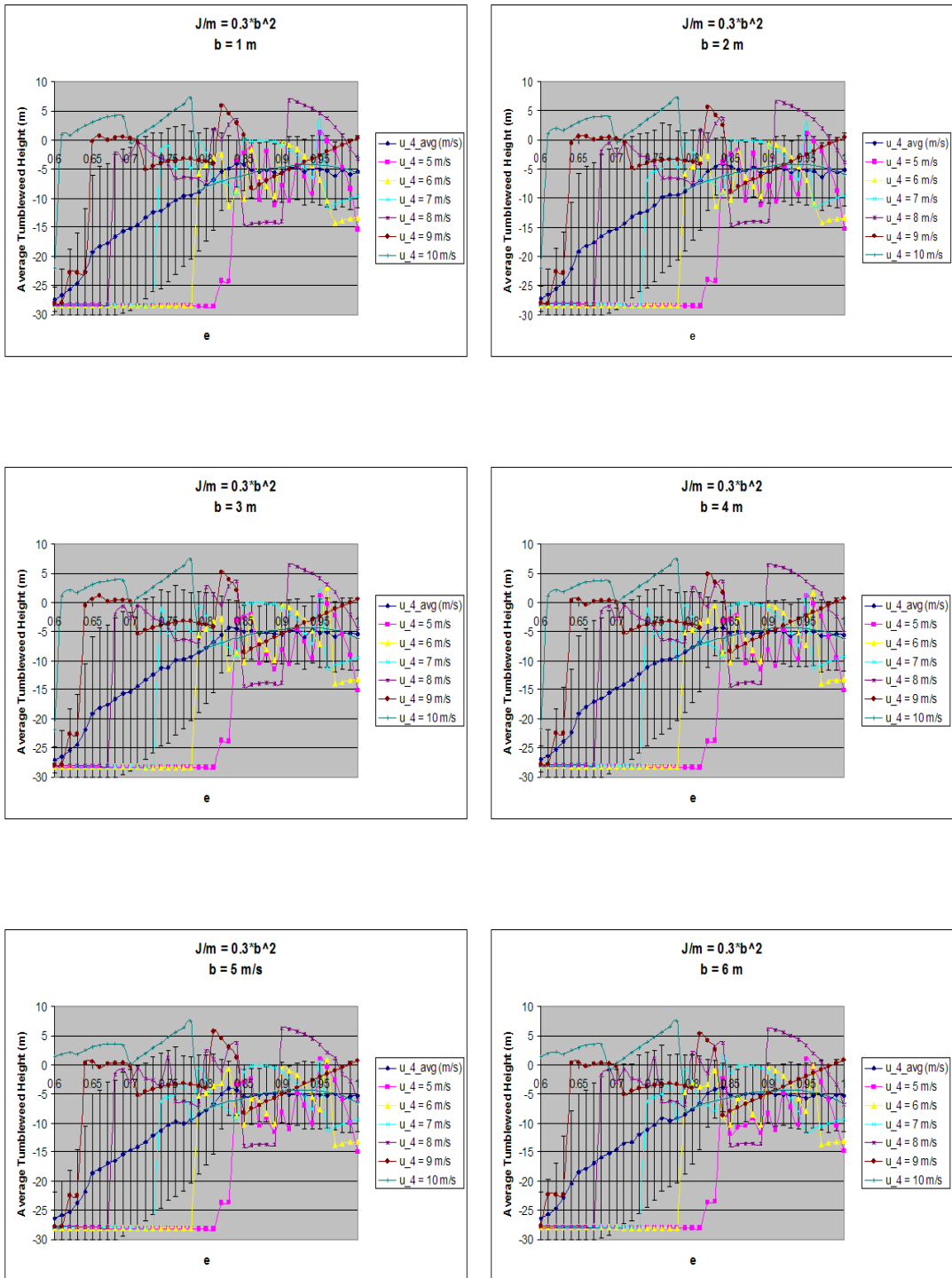


Figure 5.13: Tumbleweed height for varying design parameter sets and velocity profiles (5 – 10m/s) on Mars. Note  $J/m = 0.3b^2$ .

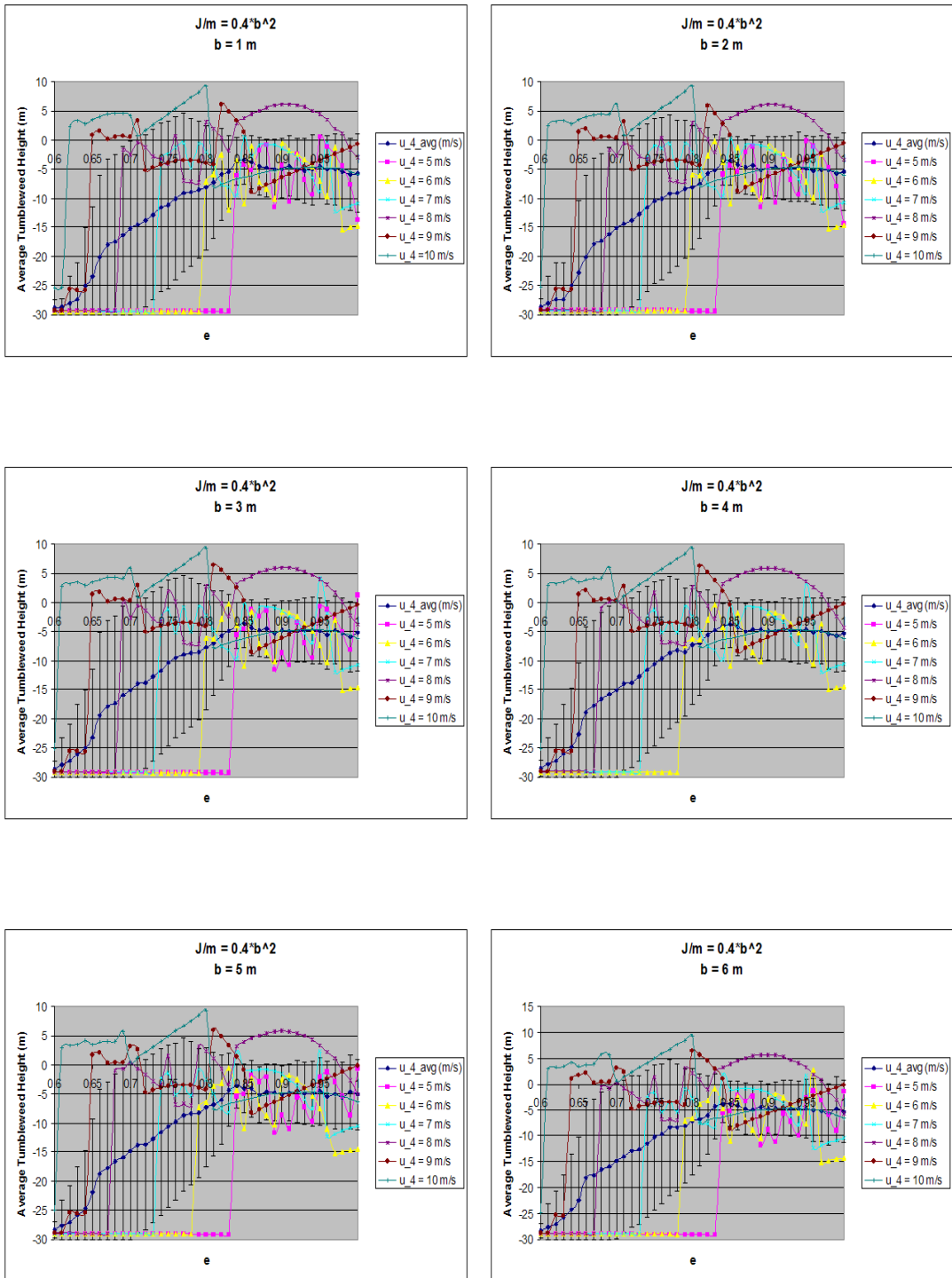


Figure 5.14: Tumbleweed height for varying design parameter sets and velocity profiles (5 – 10m/s) on Mars. Note  $J/m = 0.4b^2$ .

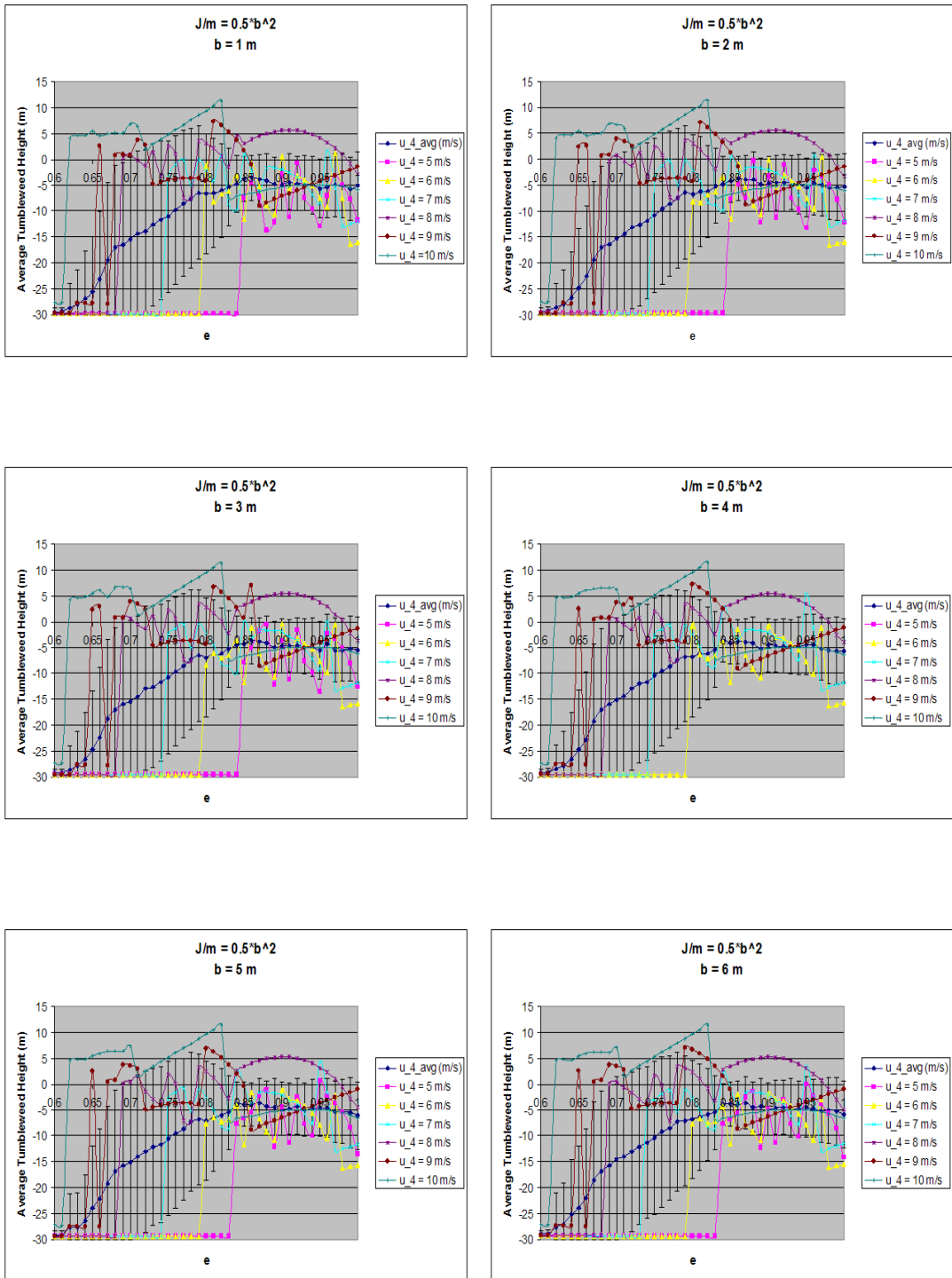


Figure 5.15: Tumbleweed height for varying design parameter sets and velocity profiles (5 – 10m/s) on Mars. Note  $J/m = 0.5b^2$ .

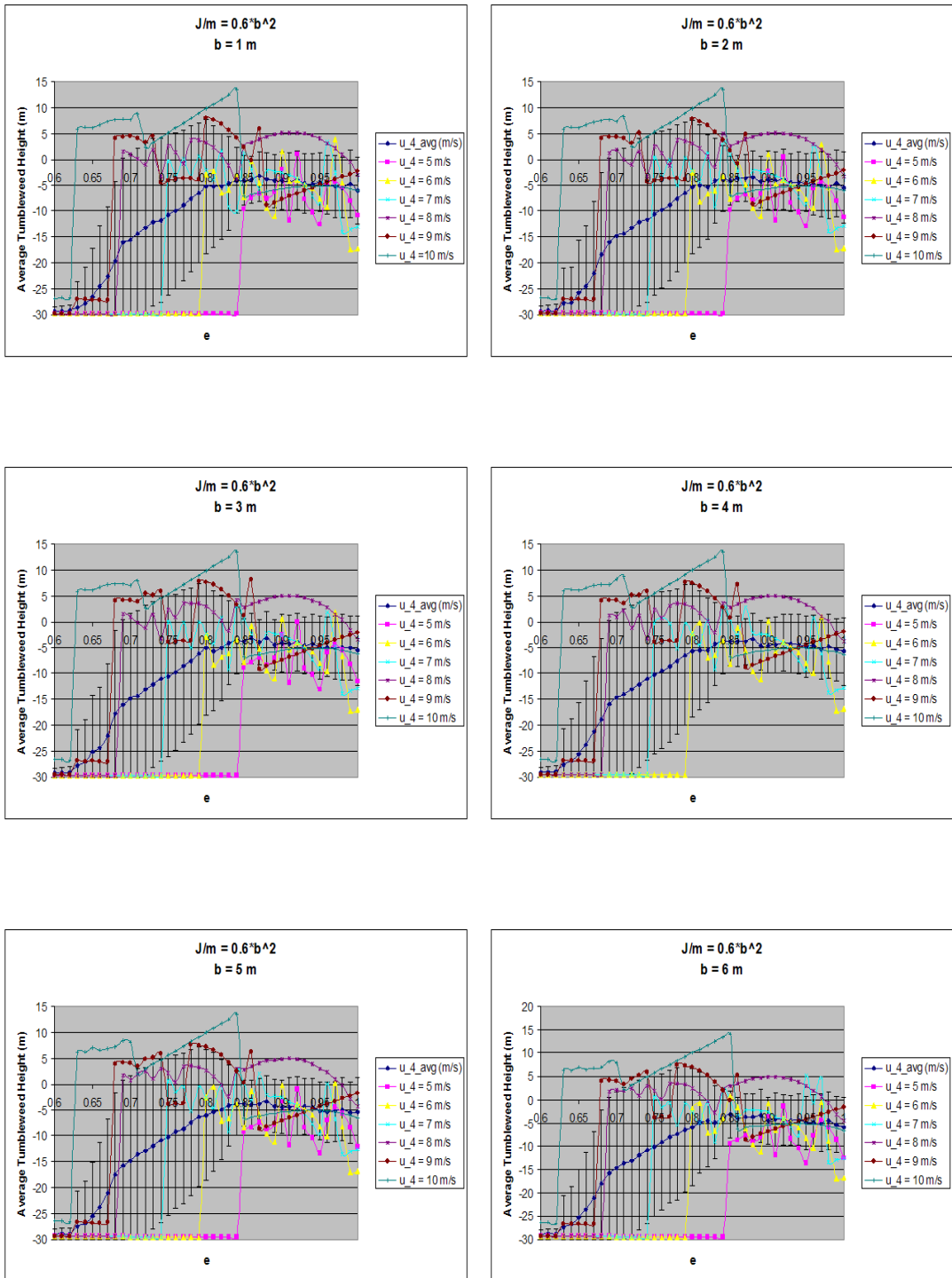


Figure 5.16: Tumbleweed height for varying design parameter sets and velocity profiles (5 – 10 m/s) on Mars. Note  $J/m = 0.6b^2$ .

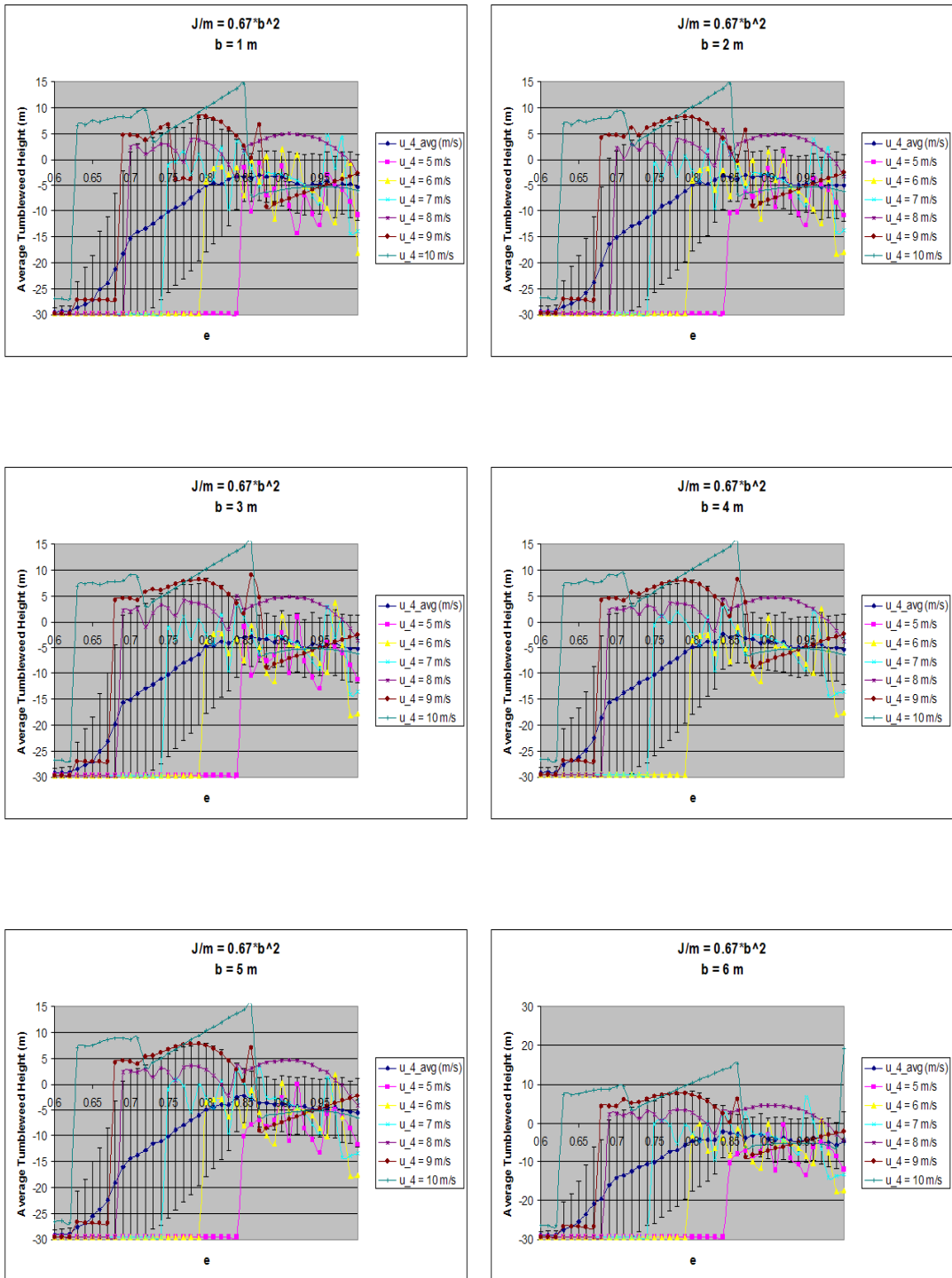


Figure 5.17: Tumbleweed height for varying design parameter sets and velocity profiles (5 – 10m/s) on Mars. Note  $J/m = 0.67b^2$ .

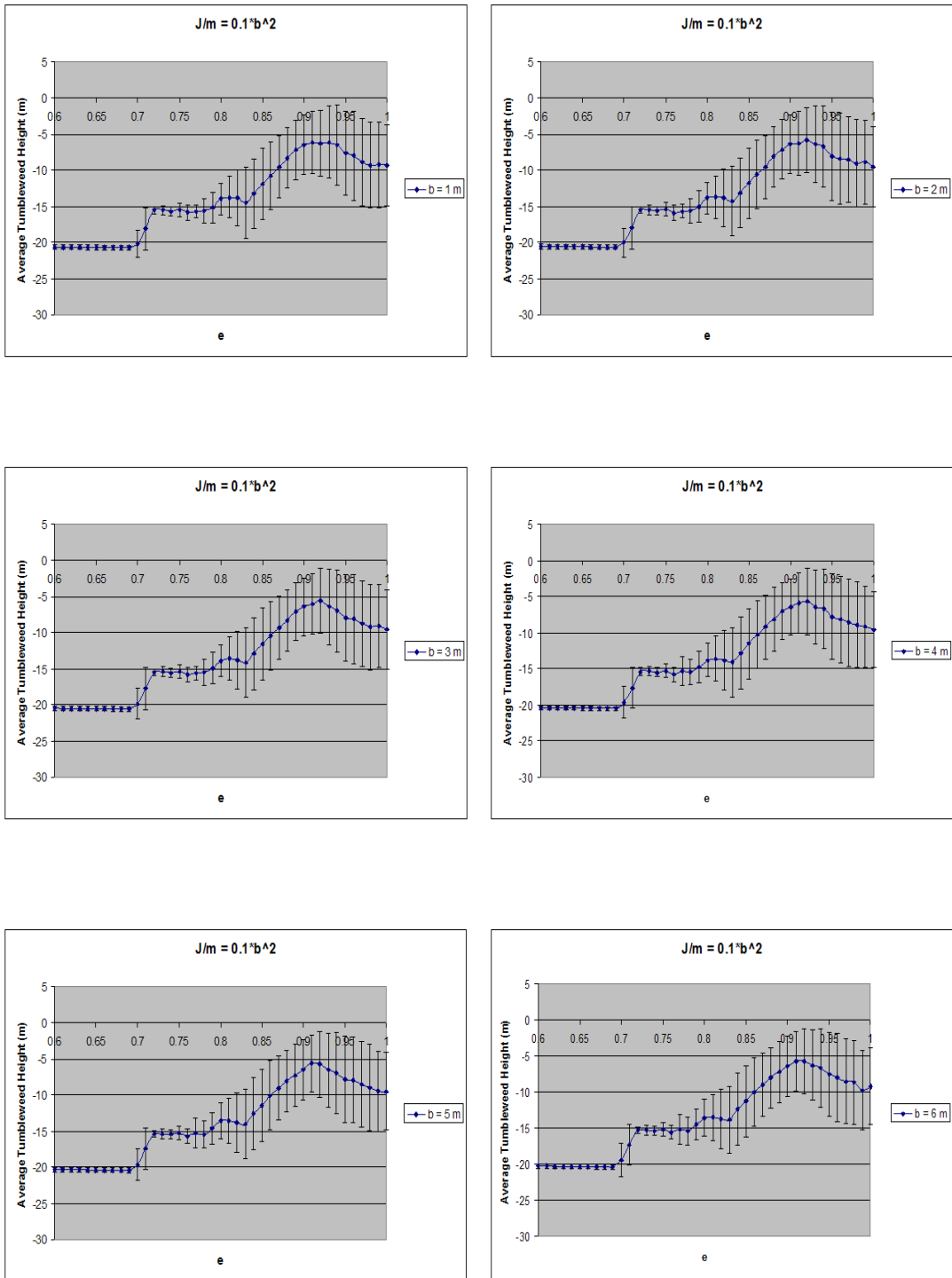


Figure 5.18: Average tumbleweed height for varying design parameter sets and velocity range (5 – 10m/s) on Earth. Note  $J/m = 0.1b^2$ .

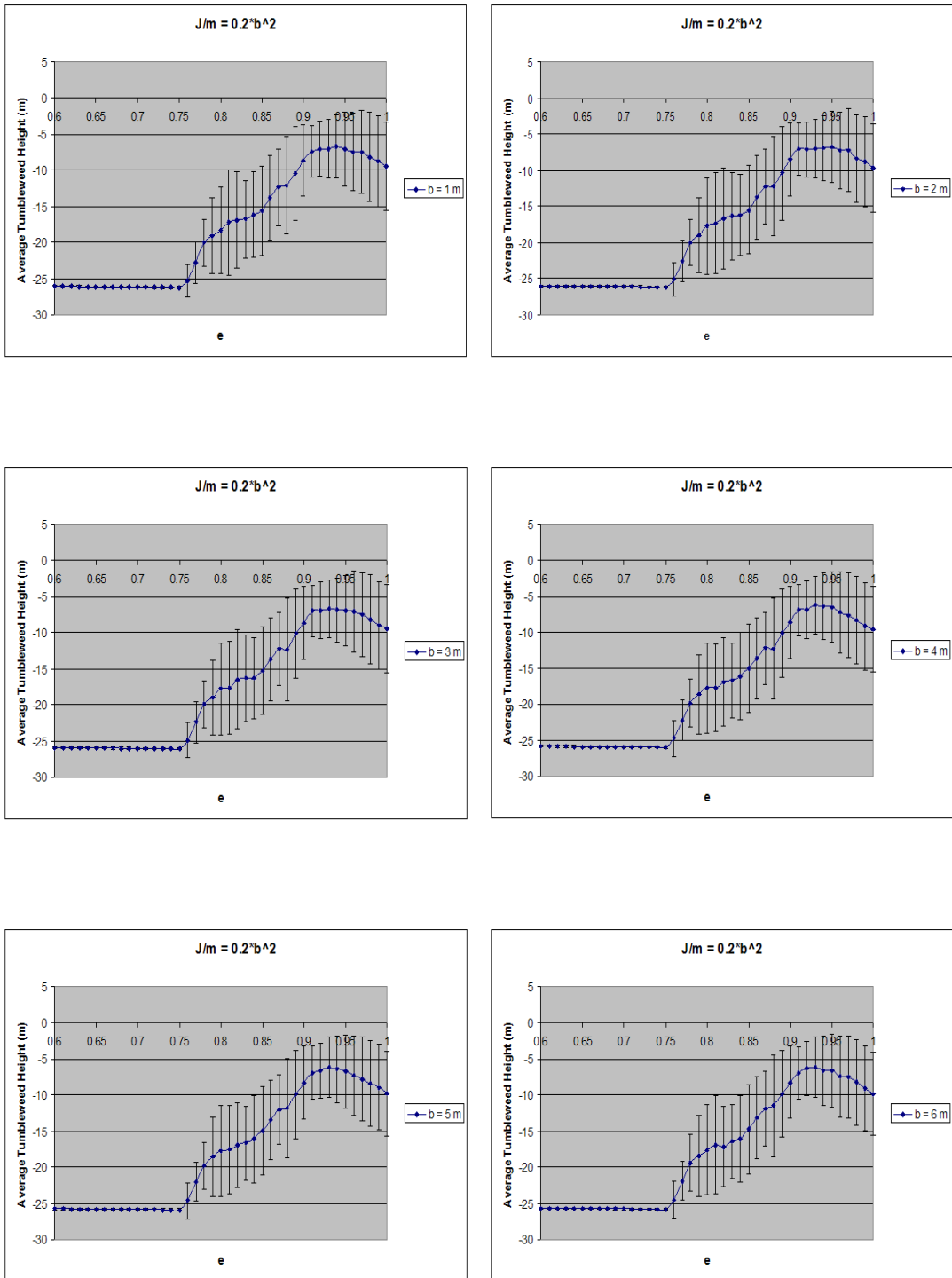


Figure 5.19: Average tumbleweed height for varying design parameter sets and velocity range (5 – 10m/s) on Earth. Note  $J/m = 0.2b^2$ .

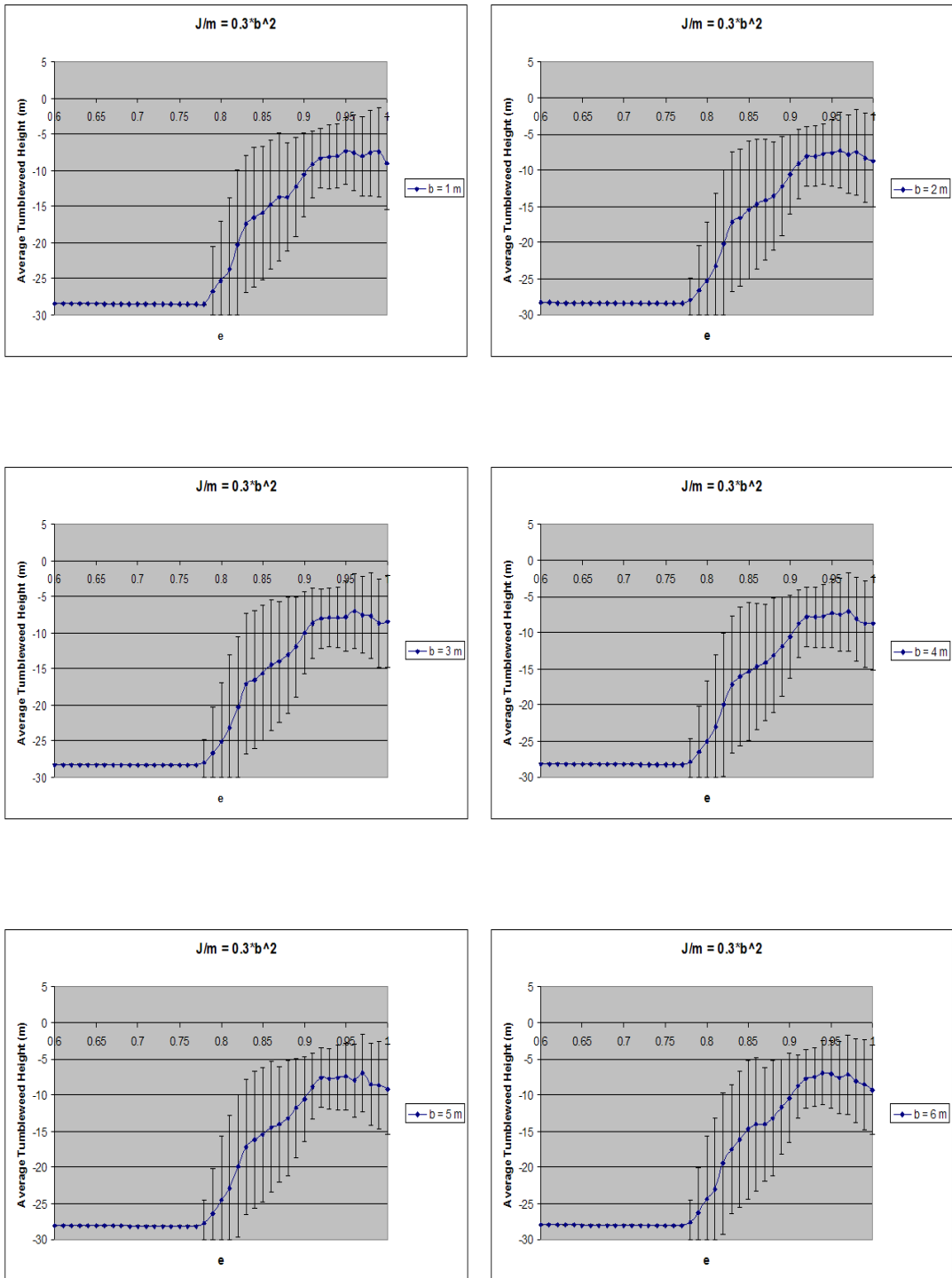


Figure 5.20: Average tumbleweed height for varying design parameter sets and velocity range (5 – 10m/s) on Earth. Note  $J/m = 0.3b^2$ .

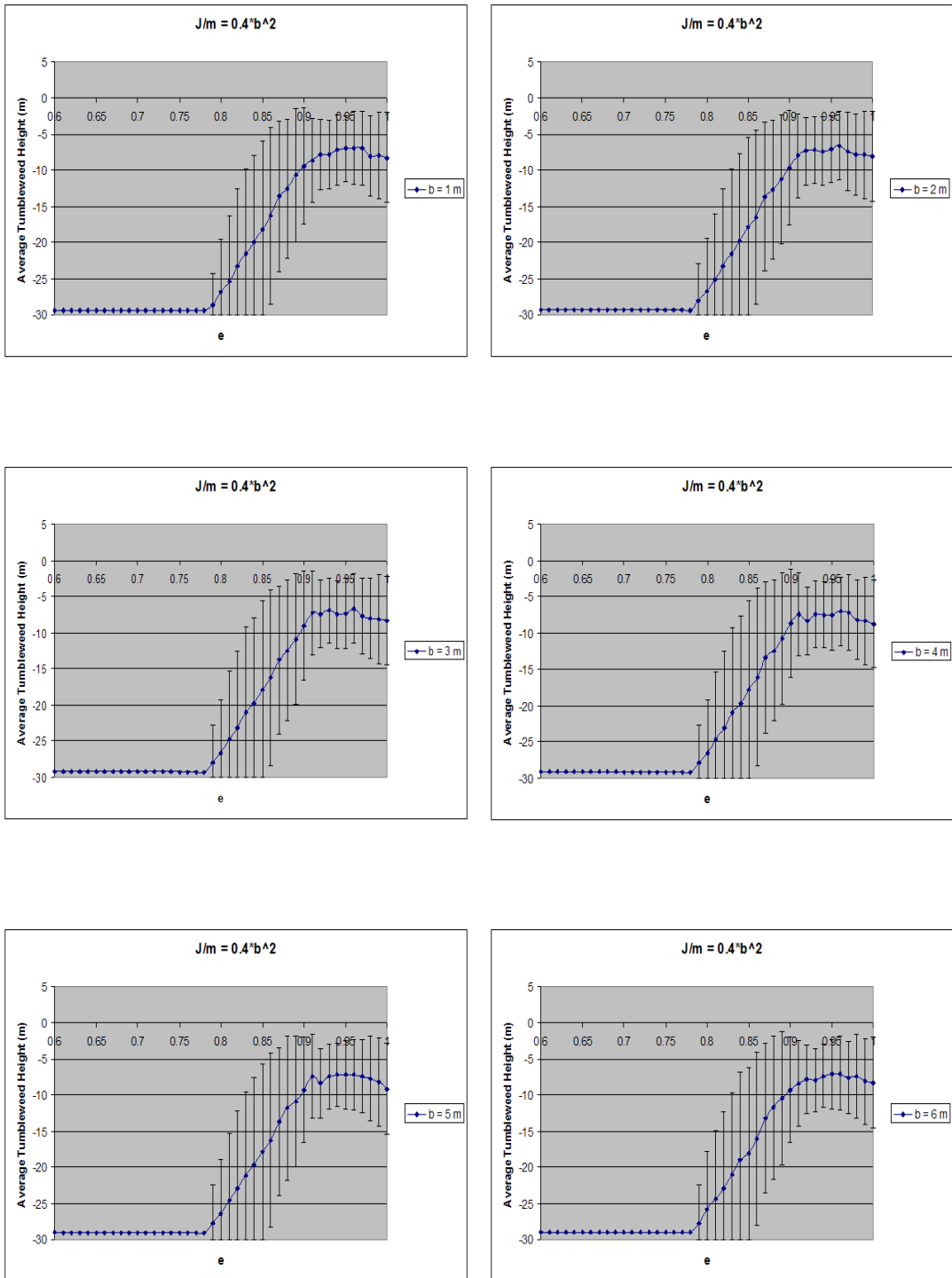


Figure 5.21: Average tumbleweed height for varying design parameter sets and velocity range (5 – 10m/s) on Earth. Note  $J/m = 0.4b^2$ .

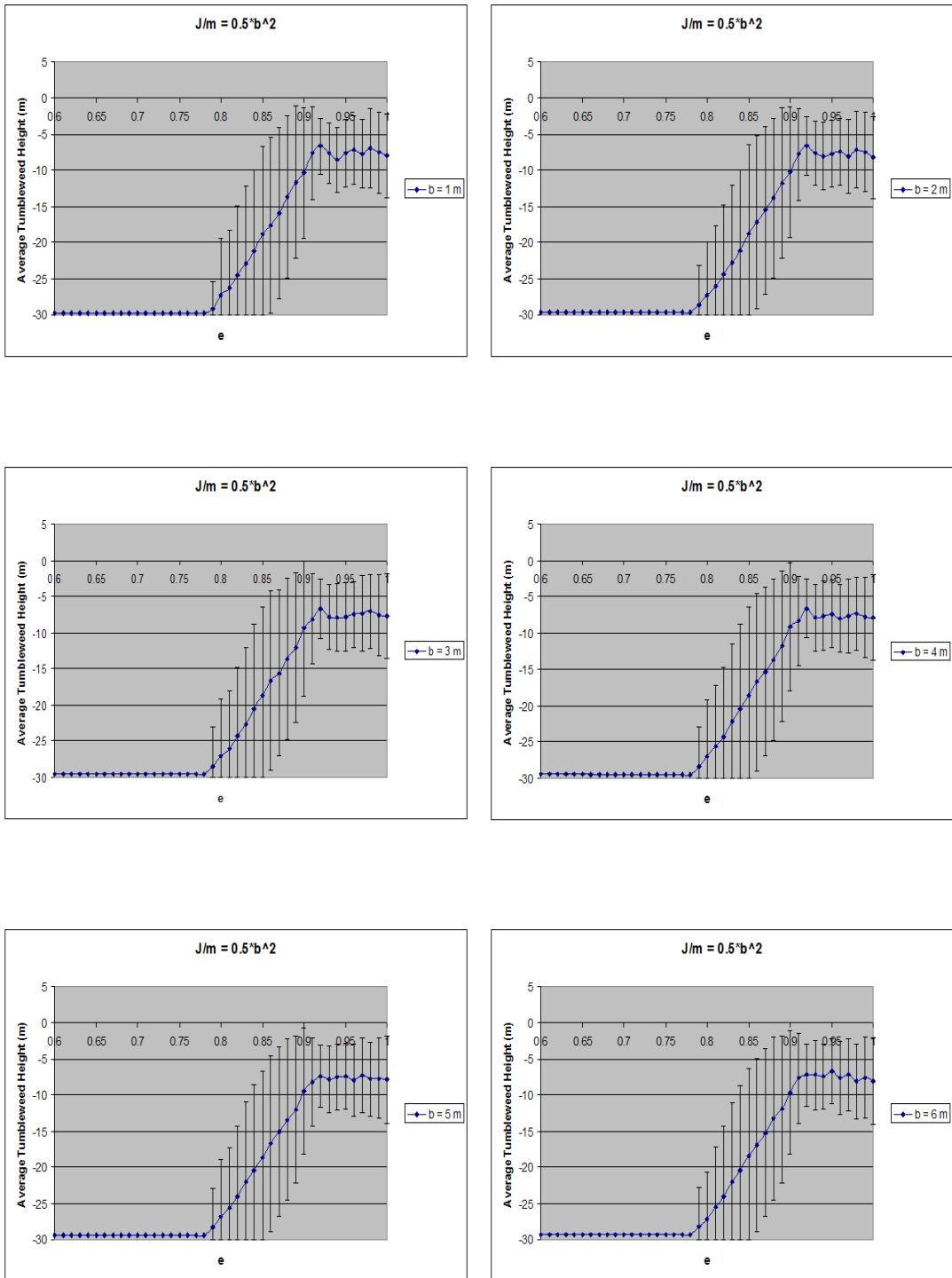


Figure 5.22: Average tumbleweed height for varying design parameter sets and velocity range (5 – 10m/s) on Earth. Note  $J/m = 0.5b^2$ .

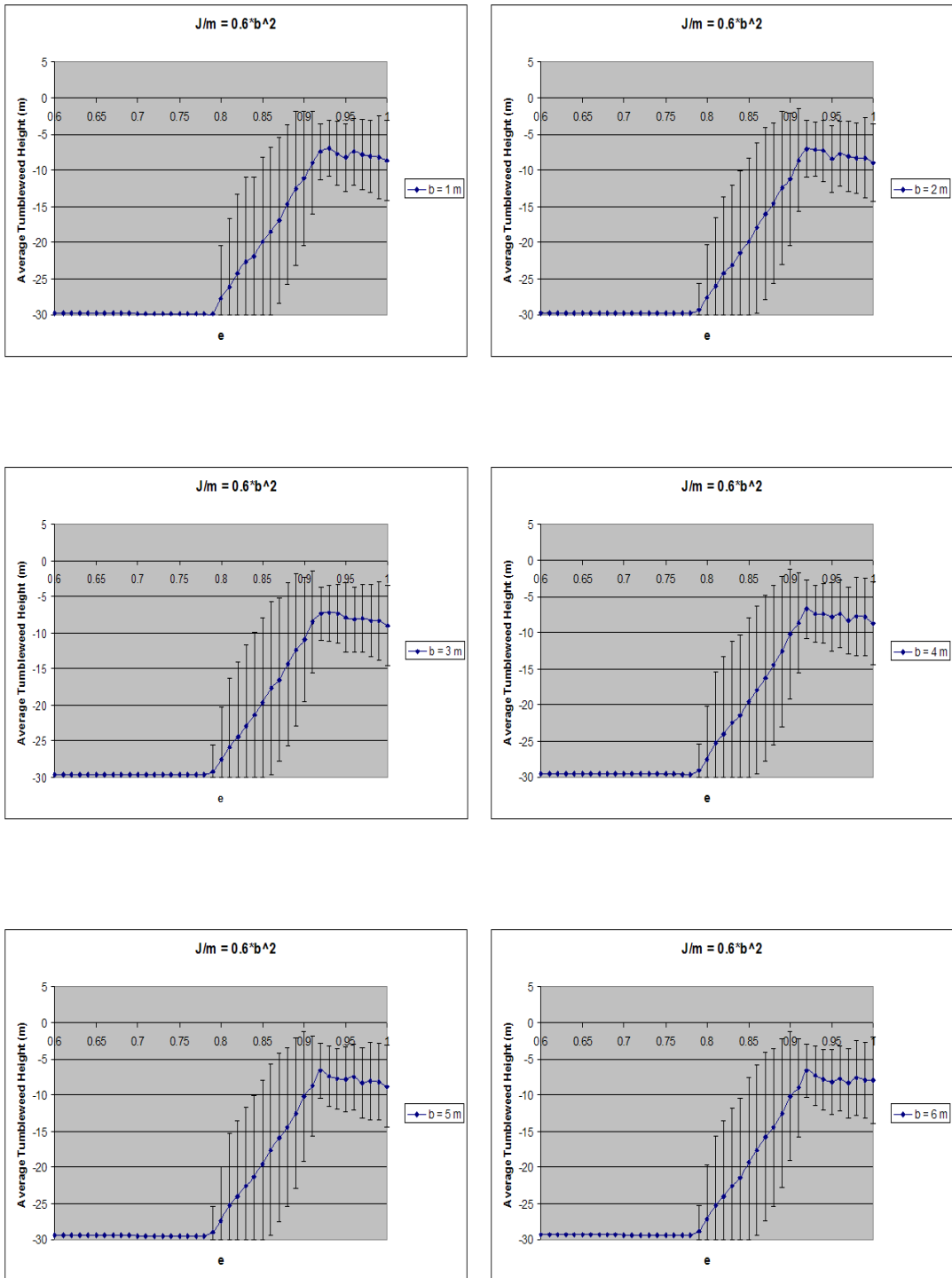


Figure 5.23: Average tumbleweed height for varying design parameter sets and velocity range (5 – 10m/s) on Earth. Note  $J/m = 0.6b^2$ .

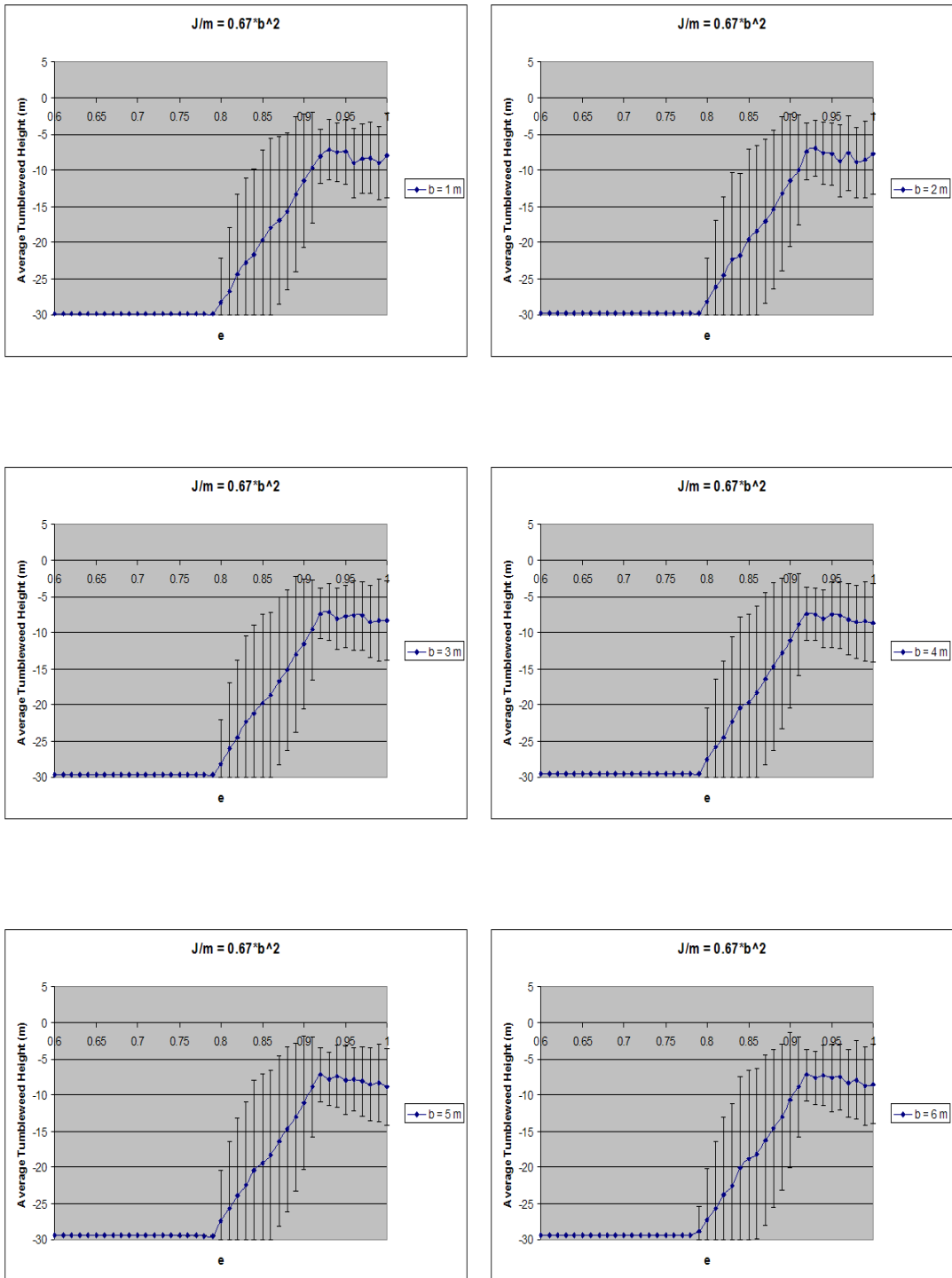


Figure 5.24: Average tumbleweed height for varying design parameter sets and velocity range (5 – 10m/s) on Earth. Note  $J/m = 0.67b^2$ .

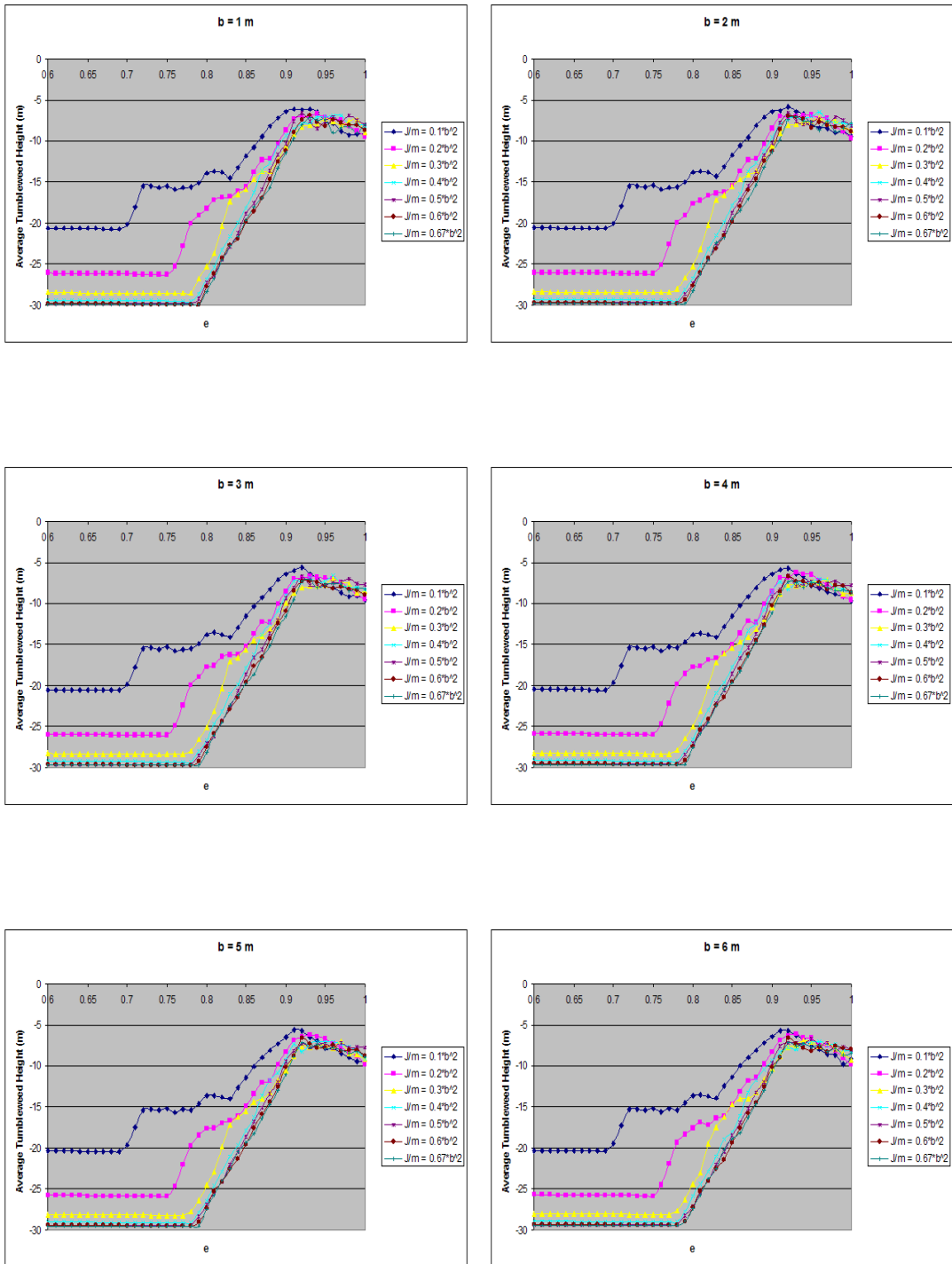


Figure 5.25: Average tumbleweed height for varying design parameter sets and velocity range (5 – 10m/s) on Earth.

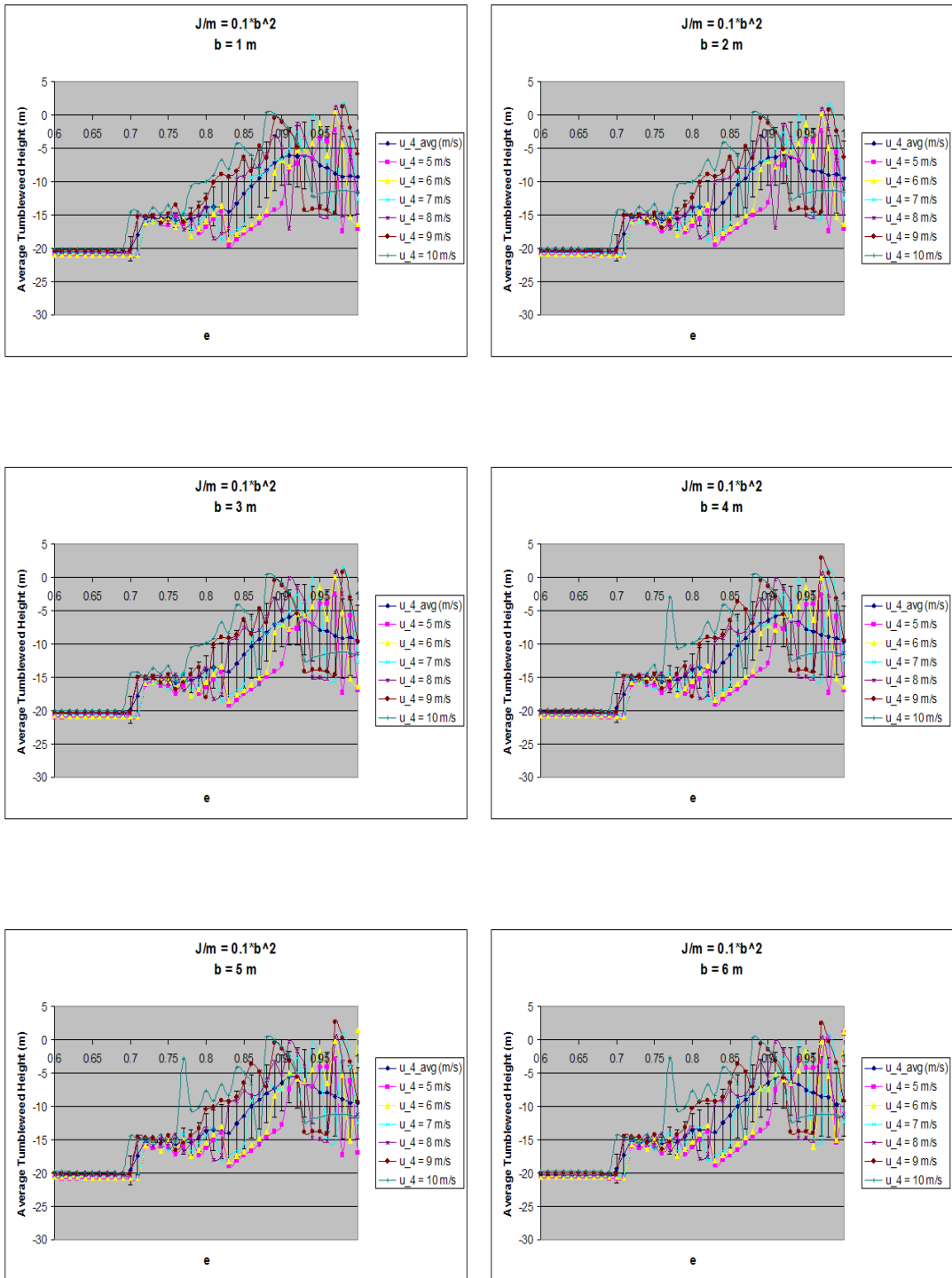


Figure 5.26: Tumbleweed height for varying design parameter sets and velocity profiles (5 – 10 m/s) on Earth. Note  $J/m = 0.1b^2$ .

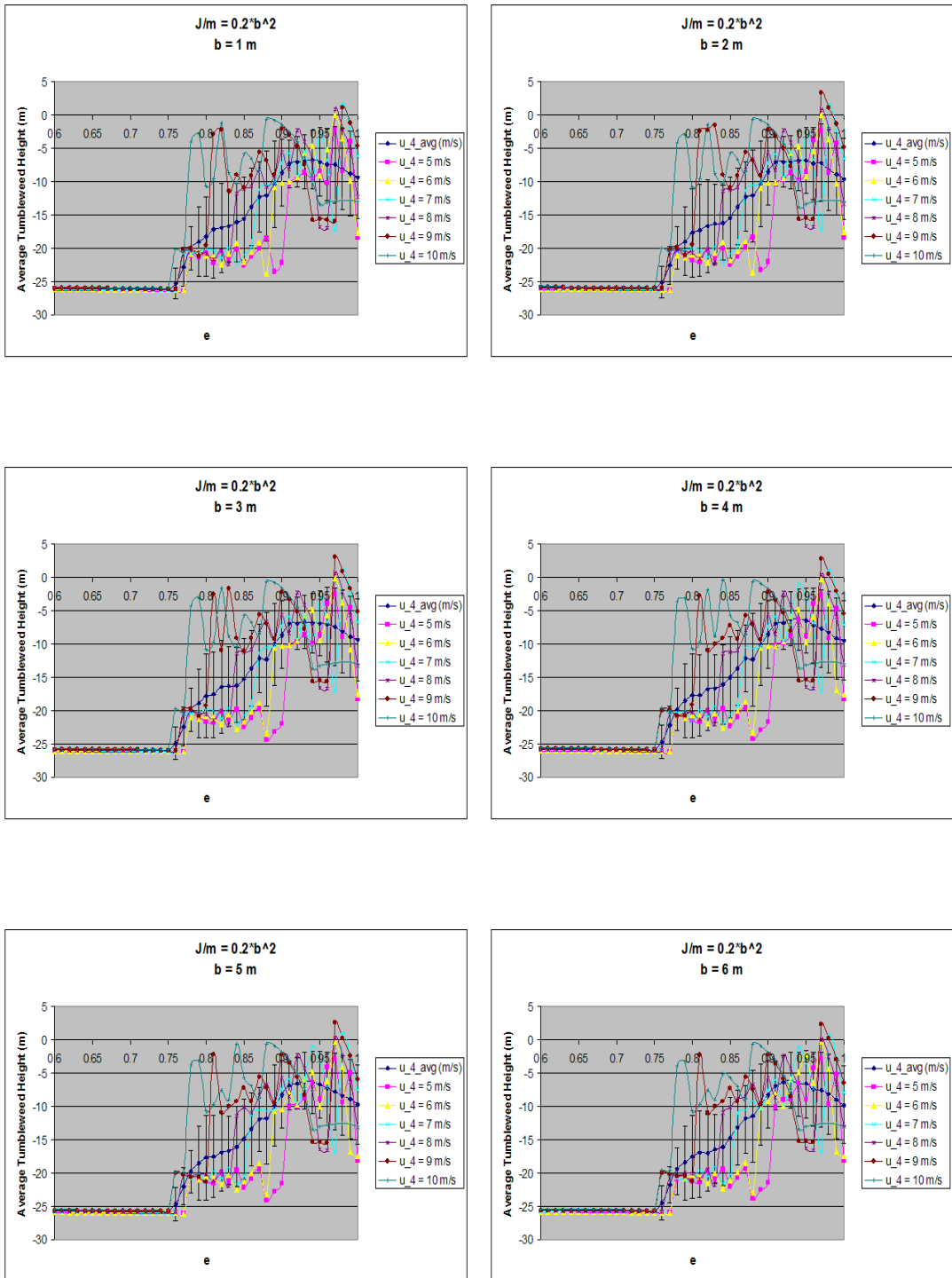


Figure 5.27: Tumbleweed height for varying design parameter sets and velocity profiles (5 – 10 m/s) on Earth. Note  $J/m = 0.2b^2$ .

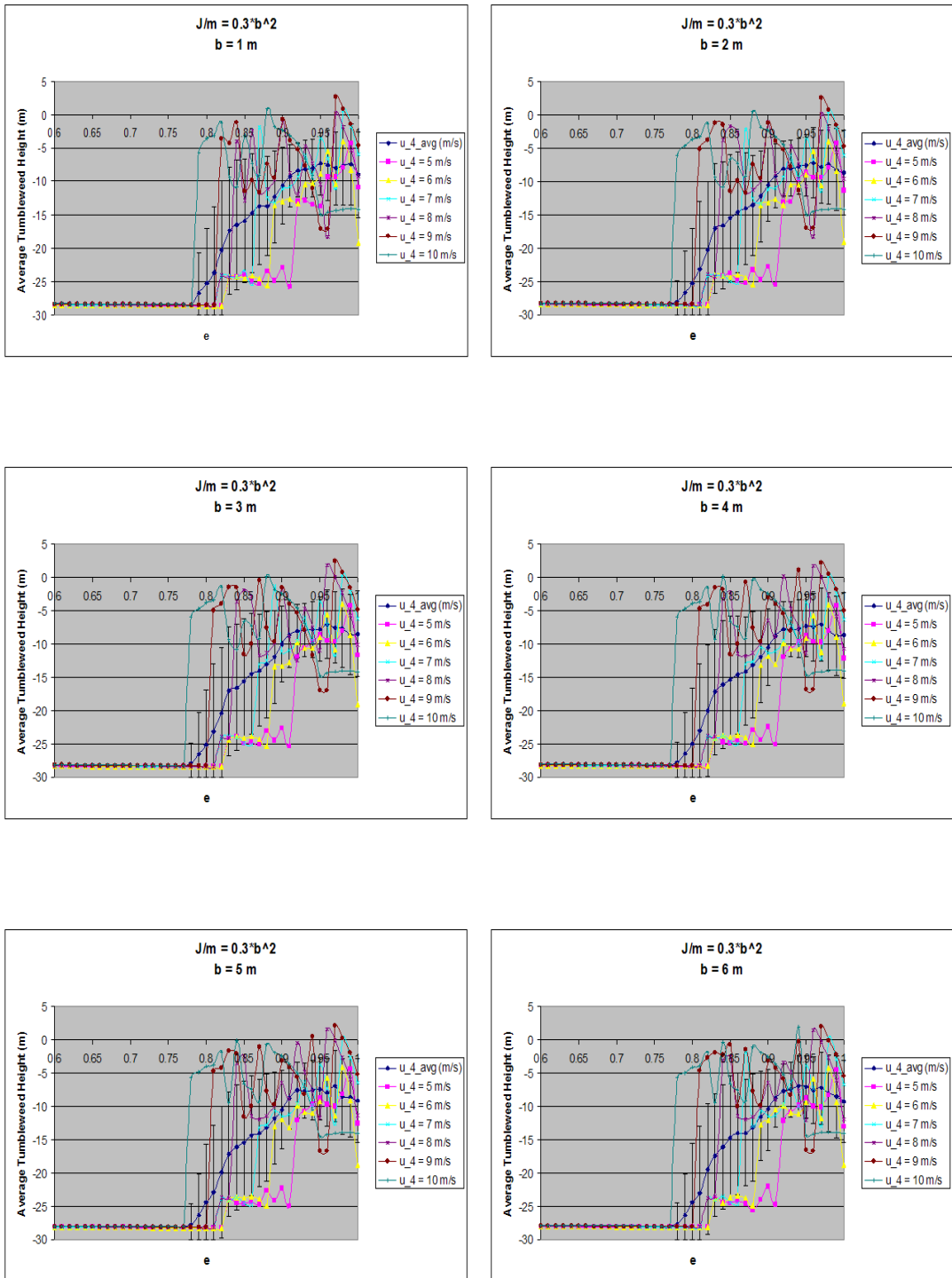


Figure 5.28: Tumbleweed height for varying design parameter sets and velocity profiles (5 – 10m/s) on Earth. Note  $J/m = 0.3b^2$ .

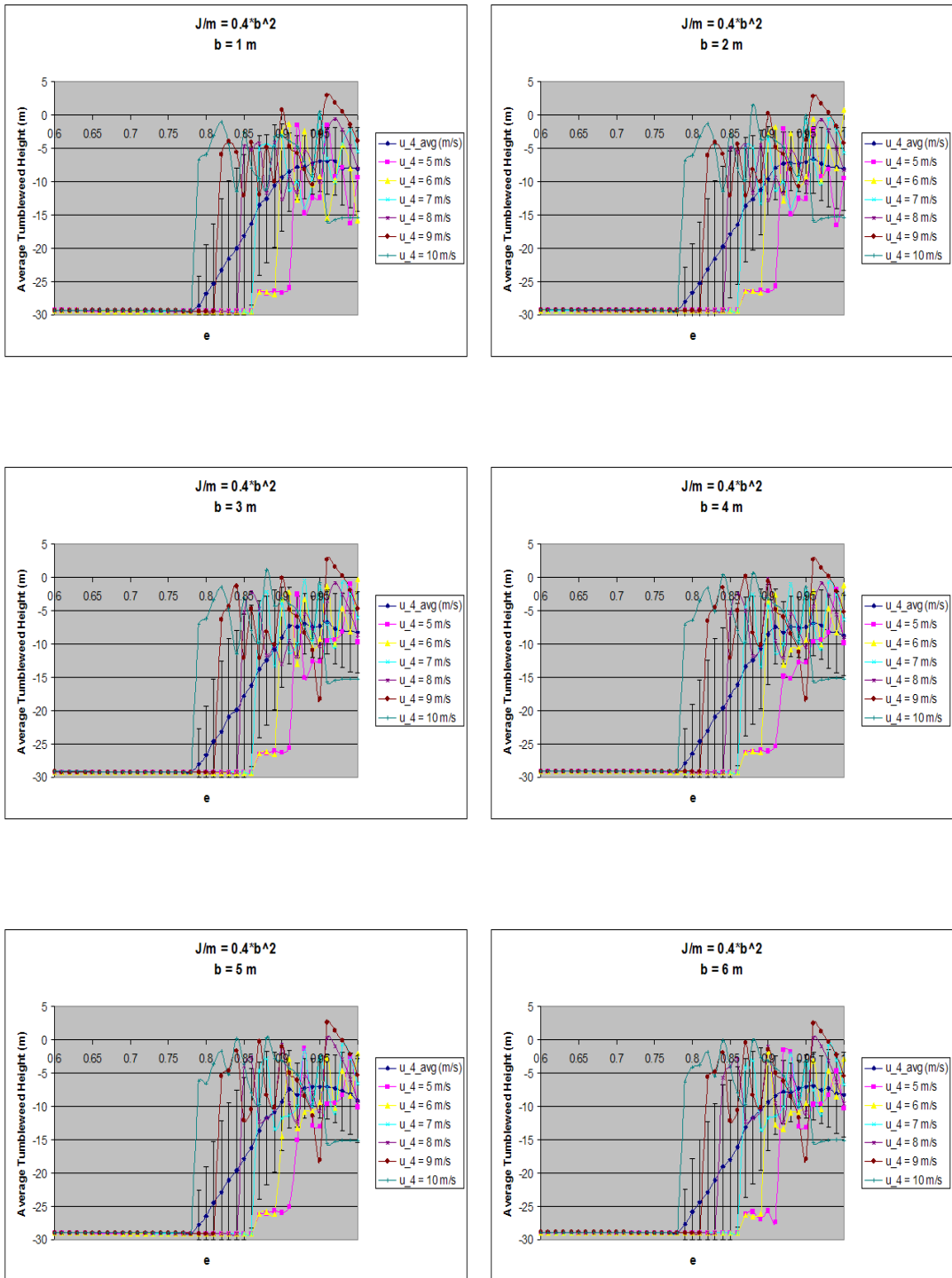


Figure 5.29: Tumbleweed height for varying design parameter sets and velocity profiles (5 – 10m/s) on Earth. Note  $J/m = 0.4b^2$ .

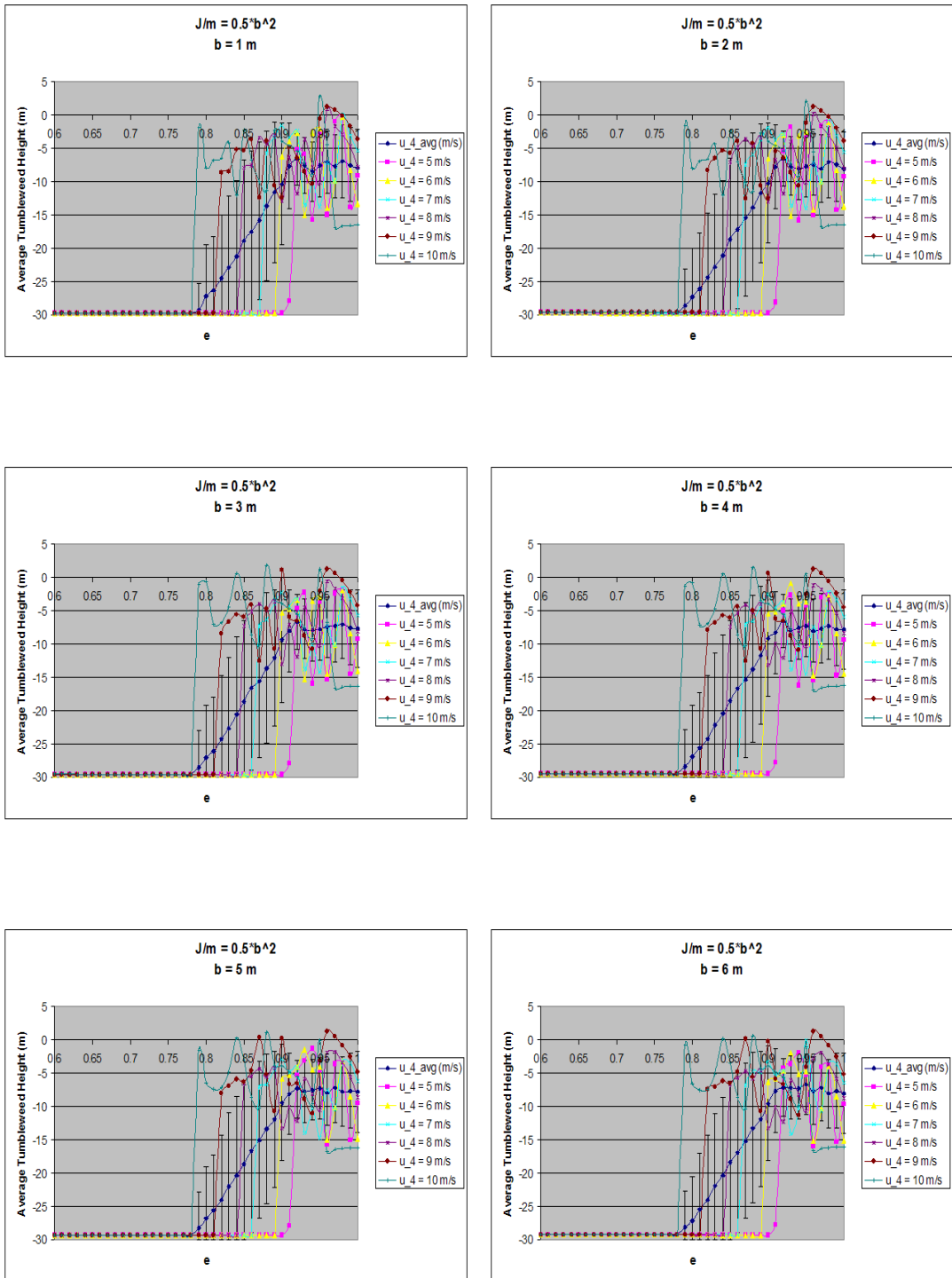


Figure 5.30: Tumbleweed height for varying design parameter sets and velocity profiles (5 – 10 m/s) on Earth. Note  $J/m = 0.5b^2$ .

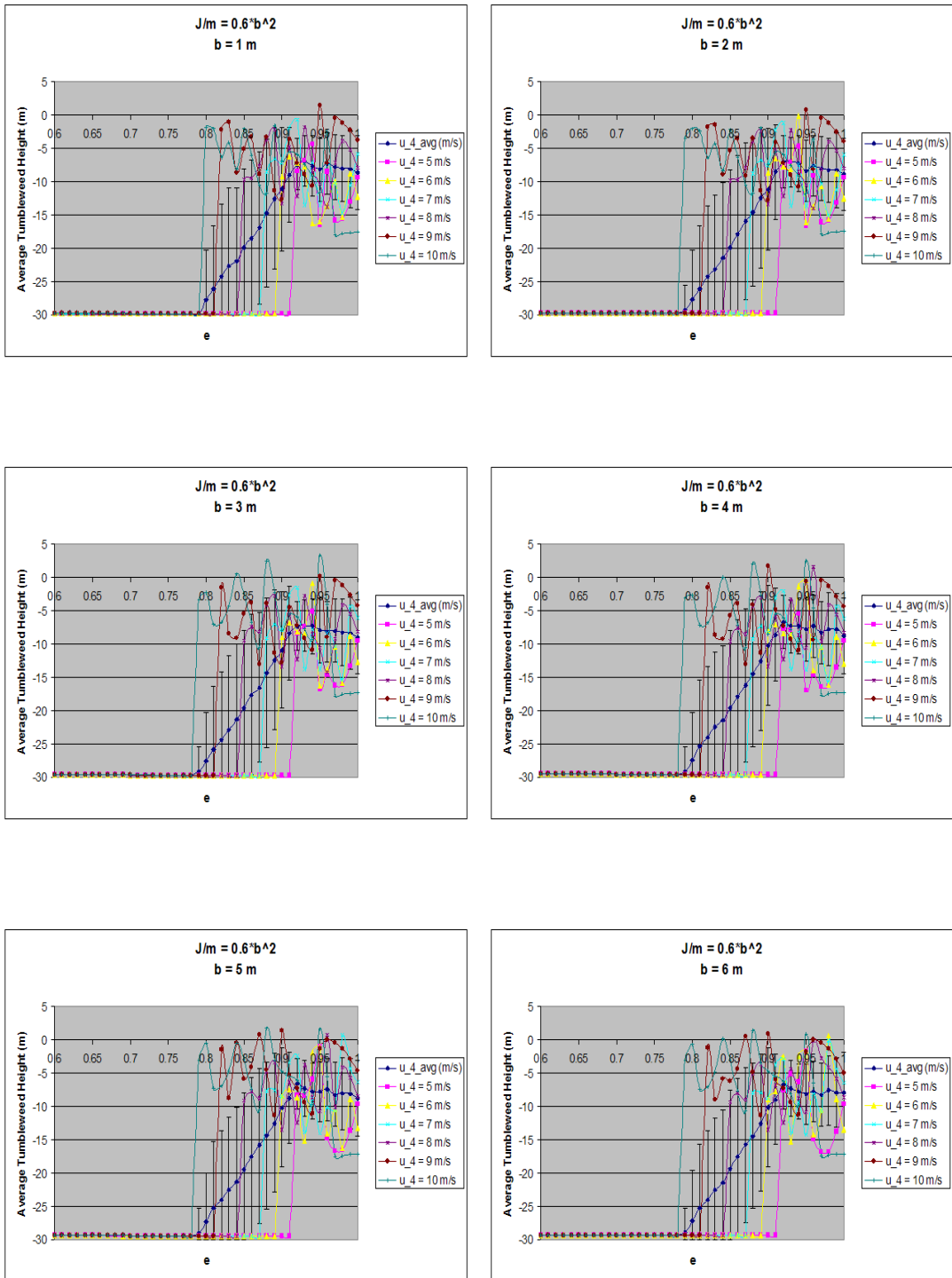


Figure 5.31: Tumbleweed height for varying design parameter sets and velocity profiles (5 – 10m/s) on Earth. Note  $J/m = 0.6b^2$ .

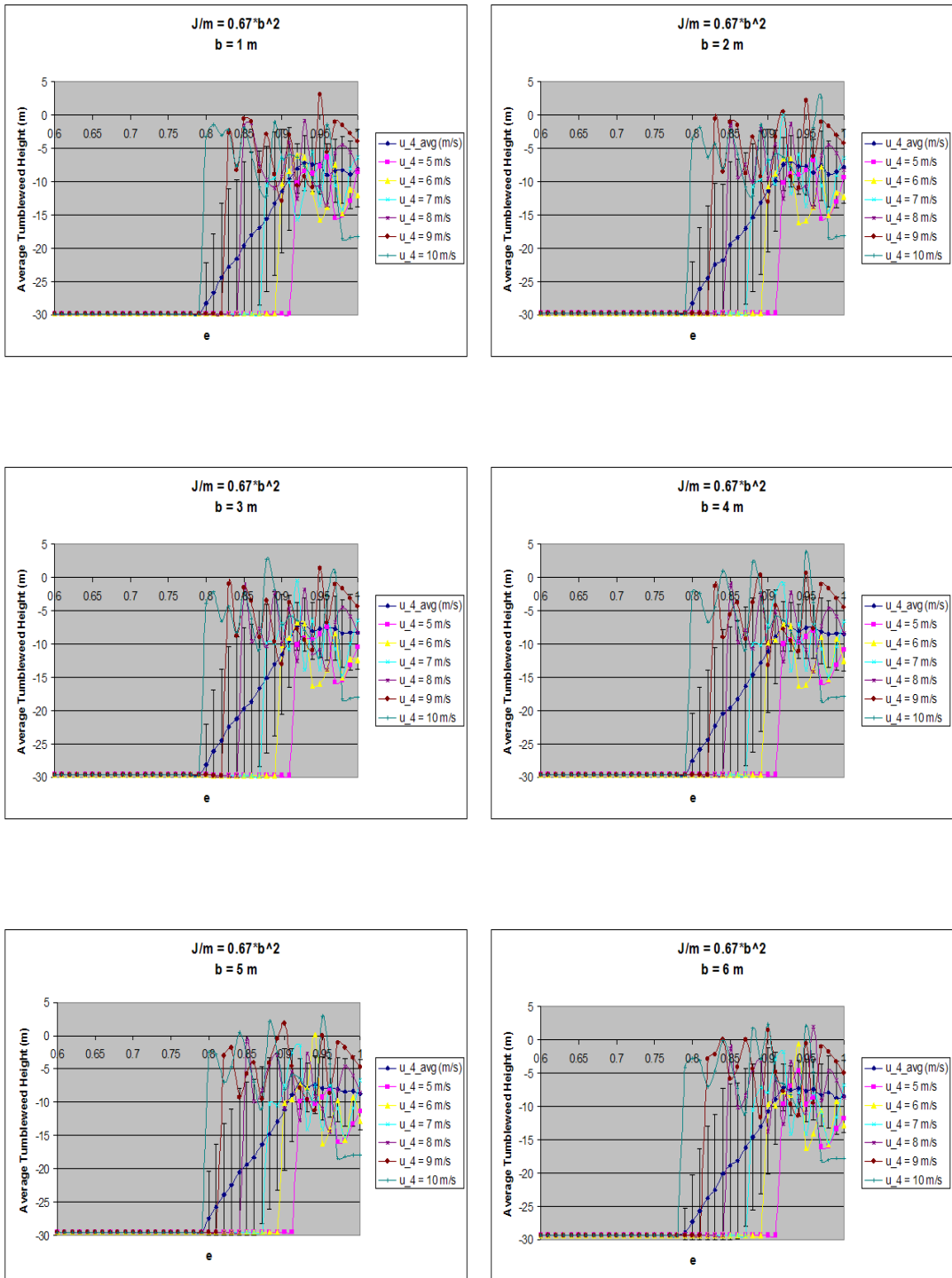


Figure 5.32: Tumbleweed height for varying design parameter sets and velocity profiles (5 – 10m/s) on Earth. Note  $J/m = 0.67b^2$ .

# Chapter 6

## Case Studies

The case studies presented below determine the optimal tumbleweed design parameters  $[b, J/m, e]$  essential for mobility for several terrain scenarios, and spotlights the principal results developed in this study.

### 6.1 Case Study I

Landing on Mars is hazardous because the planet is filled with rough terrain, steep slopes and rocks that could damage the rover. Landing constraints imposed by (1) spacecraft and rover designs, (2) entry, descent and landing, (3) scientific potential at various sites and (4) safety are important considerations in landing site selection. Landing requires smooth, flat (low slope) areas with low-to-moderate rock distributions. (19). Consequently, regions of scientific interest are far away from the landing sites, requiring tumbleweed rovers to travel substantial distances across varied terrain. During the tumbleweed's expedition, the rover is likely to encounter shallow valleys. This case study determines the optimal range of tumbleweed design parameters required for the rover to cross such areas.

Picture a tumbleweed rover deployed on the Martian surface, where the terrain is flat except for areas populated with shallow valleys. Assume a characteristic valley is defined by the terrain parameters  $[\beta = 15^\circ, \theta = 15^\circ, dh = -3m, pl = 9m]$ . Also, assume the tumbleweed has a velocity ranging between 2 and 7m/s. This velocity range is consistent with typical surface wind speeds during

a Martian summer. Given the above conditions, the numerical model produces parametric plots for various sets of design parameters, see figure 5.1. These plots determine the percentage crossed versus  $e$  for selected values of  $b$  and  $J/m$ . We define the percentage crossed as the average a tumbleweed rover crosses the valley for a design parameter set and velocity range.

Suppose a mission is considered successful if the rover crosses the valley 80 percent of the time for a velocity range defined as before. Also, suppose the dimensions of the instrument payload dictates a rover with  $b = 2m$  and  $J/m = 0.3b^2$ . Figure 5.1 reveals  $e \geq 0.85$  results in mission success. The figure also shows  $e_{crit} = 0.92$ , indicating values of  $e$  ranging from 0.92 to 1 maximizes the rover's ability to cross the valley for any mission. Financial and material constraints, however, often favor rovers with lower  $e$  values. Based on this information, suppose a mission planner selects a material with  $e = 0.85$  for the construction of the rover. Then, a possible design parameter set satisfying conditions of the mission is  $[b = 2m, J/m = 0.3b^2, e = 0.85]$ .

## 6.2 Case Study II

Case Study II is similar to the first case study, with exception to setting  $g = 9.81m/s^2$ . This case study demonstrates the variability in the range of tumbleweed design parameters for a mission performed on Earth versus a Mars mission. Again, the numerical model produces a series of parametric plots for various sets of design parameters, see figure 5.2. These plots determine the percentage crossed versus  $e$  for selected values of  $b$  and  $J/m$ .

Suppose a mission is deemed successful if the rover crosses the valley 80 percent of the time for a velocity range defined as before. Also, suppose  $b = 2m$  and  $J/m = 0.3b^2$ . For these conditions we notice  $e > 0.95$  results in mission success. We also see  $e_{crit} = 0.95$ , indicating values of  $e$  ranging from 0.95 to 1 maximizes the rover's ability to cross the valley for most missions. Suppose a mission planner selects  $e = 0.95$ . Then a possible design parameter set satisfying conditions of the mission is  $[b = 2m, J/m = 0.3b^2, e = 0.95]$ .

Comparing Case Studies I and II (and figures 5.1 and 5.2), we notice design considerations must account for the gravitational force, which effects the percent-

age crossed, the value range of  $e$  for mission success and the location of  $e_{crit}$ . The findings suggest possible sizes and material options ruled out for the construction of a rover on Earth may still be a viable option for successful Mars missions.

### 6.3 Case Study III

On Mars, science considerations on Martian climate and geology favor sites at the mouths of outflow channels, highland sites and areas covered with dark unoxidized materials. Science considerations also favor sites suspected of housing underground water sources. Regions exhibiting scientific potential include Ares Vallis, Tritonis Lacus and Isidis (19) – (21). These regions are valleys possibly carved by large water flows billions of years ago. Tumbleweed rovers, equipped with a package of scientific instruments, are designed to explore such areas, and future missions will require these rovers to examine specific regions within the valleys. This case study determines the optimal range of tumbleweed design parameters required for the rover to reach a specified height in a deep valley.

Consider a tumbleweed rover encountering a deep valley on the Martian surface. Assume the valley is defined by the terrain parameters [ $\beta = 25^\circ$ ,  $\theta = 25^\circ$ ,  $dh = -30m$ ,  $pl = 90m$ ]. Also, assume the tumbleweed has a velocity ranging between 5 and 10m/s. This velocity range is consistent with typical surface wind speeds during a Martian fall. Suppose the tumbleweed rover identifies an area of interest on the valley's adjacent wall at a height of  $-15m$  and above. Given the above conditions, the numerical model produces a series of parametric plots for various sets of design parameters, see figures 5.3 through 5.17. These plots determine the average tumbleweed height versus  $e$  for selected values of  $b$  and  $J/m$ , where the average height is determined for each design parameter set and velocity range.

The figures suggest to maximize the average height while minimizing the variability in the height range, the rover should be constructed with its density concentrated toward its center. Hence, we select  $J/m = 0.1b^2$ . From figure 5.3 different values of  $b$  produce relatively minor changes in the average height and size of the error bars. Tumbleweed rovers are designed to be large, so suppose a rover with a radius of  $2m$  is chosen. For this radius figure 5.3 shows  $e$  ranging

from  $0.71 - 1$  provides an average height greater than  $-15m$ , while minimizing the length of the error bars. For this  $e$  range, the average height and its corresponding error bars are above  $-15m$ . Figure 5.11 also shows for  $e \geq e_{crit}$ , the tumbleweed height for different velocities is more likely to be bounded within the error bars associated with the average height. Financial and material constraints, however, are inclined toward rovers with lower  $e$  values. Then based on figures 5.3 and 5.11, we select  $e = 0.71$ . A possible design parameter set to satisfy conditions of the mission is  $[b = 2m, J/m = 0.1b^2, e = 0.71]$ .

To demonstrate the selected design parameter set accomplishes the mission for a defined velocity range, the numerical simulation model is run for an arbitrary velocity of  $6.4m/s$ . Figure 6.1 shows the simulation, where the rover reaches a height of  $-14.69m$  (or  $15.31m$  up from the valley's floor) and it confirms our choice for the design parameter set.

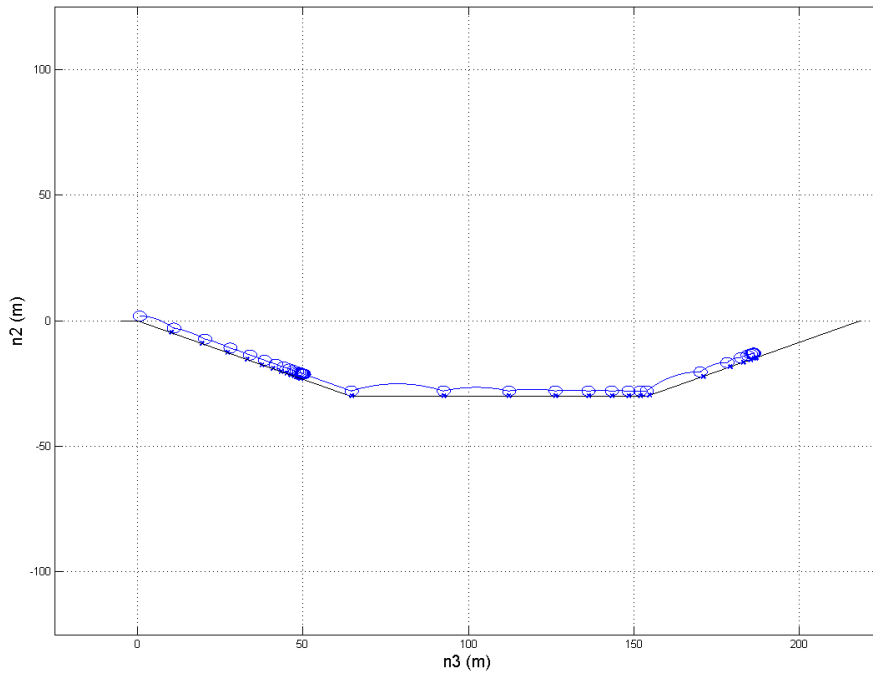


Figure 6.1: A two-dimensional simulation representation on Mars.

## 6.4 Case Study IV

Field studies performed at the South Pole by JPL in 2004, confirmed the tumbleweed rover's ability to roll using the wind and the vehicle ultimately demonstrated its long-term durability in an extreme environment. Plans to construct the next generation tumbleweed rovers are underway at JPL and LaRC, and future tests will attempt to mimic the conditions on Mars with a plan to use these rovers to explore the Martian polar caps for terrain and ice surveys (22). Case Study IV replicates the third case study only this time on Earth. The numerical model produces a series of parametric plots for various sets of design parameters on Earth, see figures 5.18 through 5.32. These plots determine the average tumbleweed height versus  $e$  for selected values of  $b$  and  $J/m$ , where the average height is determined for each design parameter set and velocity range.

The field studies performed at the South Pole used a two-meter diameter rover, and suppose  $J/m$  and  $e$  were allowed to vary. The figures indicate to maximize the average height while minimizing the variability in the height range, the rover should be constructed with its density concentrated toward its center. Hence, we select  $J/m = 0.1b^2$ . For these parameters figure 5.18 shows  $e$  ranging from  $0.87 - 1$  provides an average height greater than  $-15m$ . For this  $e$  range, the average height and its corresponding error bars are above  $-15m$ . Figure 5.26 shows for  $e \geq e_{crit}$ , the tumbleweed height for different velocities is more likely to be bounded within the error bars associated with the average height. Based on figures 5.18 and 5.26, we select  $e = 0.87$ . Thus, a possible design parameter set to satisfy conditions of the mission is  $[b = 1m, J/m = 0.1b^2, e = 0.87]$ .

To demonstrate the selected design parameter set accomplishes the mission for a defined velocity range, the numerical simulation model is run for an arbitrary velocity of  $8.3m/s$ . Figure 6.2 shows the simulation, where the rover reaches a height of  $-7.28m$  (or  $22.72m$  up from the valley's floor) and it confirms our choice for the design parameter set.

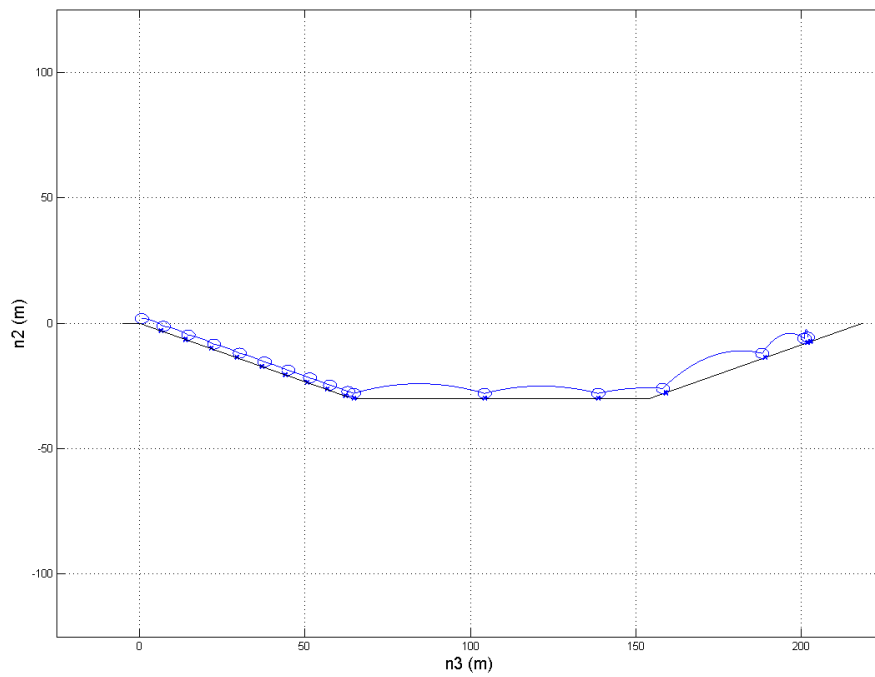


Figure 6.2: A two-dimensional simulation representation on Earth.

# Chapter 7

## Conclusions

The main results of this thesis can be summarized as follows:

- A collision model based on Kane's method of dynamics is used to study the impact between the tumbleweed rover and flat terrain. We extend the model by considering collisions on the incline and decline planes, and ultimately establish a trajectory model tracking the rover's motion between bounces.
- A rolling and sliding model for a rover in motion is created for flat, incline and decline planes.
- A numerical simulation model covering the tumbleweed's rolling, sliding and bouncing behaviors and the transitions between these modes of movement is developed. The model also tracks the rover's movement and transition between different terrain types. In its strictest form, the numerical simulation model predicts the tumbleweed's motion for a set of parameters and initial conditions. Parametric studies are established, where the rover's behavior as it engages specific terrains is determined.
- A set of presented case studies show the numerical model's utility as an initial design tool for tumbleweed rovers encountering real terrain scenarios. The case studies provide an understanding of the range of tumbleweed design parameters  $[b, J/m, e]$  essential for mobility over (shallow and deep) valleys.

# References

- [1] NASA, "Having a Ball on Mars," <http://spacescience.com/headlines/y2001/ast17aug1.htm>. Accessed 06/10/2006.  
vi, 2
- [2] Antol, J., Calhoun, P., Flick, J., Hajos, G., Kolancinski, R., Minton, D., Owens, R., and Parker, J., "Low Cost Mars Surface Exploration: The Mars Tumbleweed," NASA TM-2003-212411, August 2003. 3
- [3] Flick, J. and Toniolo, M.: "Preliminary Dynamic Feasibility and Analysis of a Spherical, Wind Driven (Tumbleweed) Martian Rover" AIAA-2005-0250, 43rd AIAA Aerospace Sciences Meeting and Exhibit, Reno, NV, January 10-13, 2005. 3
- [4] Antol, J., Chattin, R. L., Copeland, B. M., and Krizan, S. A., "The NASA Langley Mars Tumbleweed Rover Prototype," Proceedings of the 44th AIAA Aerospace Sciences Meeting, Reno, Nevada, USA, January, 9-12 2005, No. 2006-0064.
- [5] Hajos, G., Jones, J., Behar A., Dodd, M., "An Overview of Wind-Driven Rovers for Planetary Exploration," 43rd AIAA Aerospace Sciences Meeting and Exhibit, Reno, NV, January 10-13, 2005.
- [6] Antol, J., Calhoun, P., Flick, J., Hajos, G., Keyes, J., Stillwagen, F., Krizan, S., Strickland, C., Owens, R., and Wisniewski, M.: "Mars Tumbleweed: FY2003 Conceptual Design Assessment" NASA TM-2005-213527, August 2005.

- [7] Antol, J., "A New Vehicle for Planetary Surface Exploration: The Mars Tumbleweed," 1st Space Exploration Conference: Continuing the Voyage of Discovery , Orlando, 31 January - 1 February 2005.
- [8] Janes, D. M.: "The Mars Ball: A Prototype Martian Rover," AAS 87-272, The Case For Mars III, Part II - Volume 75, AAS Science and Technology Series, Eds. Carol R. Stoker, pp. 569-574, 1989.
- [9] Antol, J., Harris, S. B., Hajos, G. A., and Strickland, C. V., "Wind Tunnel Tests of Evolved Mars Tumbleweed Concepts," Proceedings of the 44th AIAA Aerospace Sciences Meeting, Reno, Nevada, USA, January, 9-12 2005, No. 2006-0069.
- [10] Claycomb, J. S., DeJarnette, F. R., and Mazzoleni, A. P., "Development and Construction of a Prototype Mars Tumbleweed Rover," Proceedings of the 44th AIAA Aerospace Sciences Meeting, Reno, Nevada, USA, January, 9-12 2005, No. 2006-66. [3](#)
- [11] Rose, S., Moody, C., James, D. L., and Barhorst, A. A., "Drag Measurement and Dynamic Simulation of Martian Wind Driven Sensor Platform Concepts," Proceedings of the 43rd AIAA Aerospace Sciences Meeting, Reno, Nevada, USA, January, 10-13 2005, No. 2005-249. [3](#)
- [12] Rose, S. E., Moody, C. B., James, D. L., and Barhorst, A. A., "Drag Measurement and Dynamic Simulation of Martian Wind Driven Sensor Platform Concepts," Journal of Fluids and Structures, Vol. 21, No. 7, 2005. [3](#)
- [13] Barhorst, A. A. and James D. L., "Elasto-dynamic Model of a Segmented Martian Tumbleweed Concept," Proceedings of the 44th AIAA Aerospace Sciences Meeting, Reno, Nevada, USA, January, 9-12 2005, No. 2006-68.
- [14] Ylikorpi, T., Halme, A., and Suomela, J., "Comparison Between Wind-Propelled Thistle and Motor-Driven Un-Balanced Thistle," Proceedings of the 44th AIAA Aerospace Sciences Meeting, Reno, Nevada, USA, January, 9-12 2005, No. 2006-67.

- [15] Kolacinski, R.M., and Quinn, R.D., "Numerical Simulation of a Bouncing, Rolling and Sliding Tumbleweed Rover," AIAA-2005-0251, 43rd AIAA Aerospace Sciences Meeting and Exhibit, Reno, NV, January 10-13, 2005. 3
- [16] Calhoun, P., Harris, S., Raiszadeh, B., Zaleski, K.: "Conceptual Design and Dynamics Testing and Modeling of a Mars Tumbleweed Rover," AIAA-2005-0247, 43rd AIAA Aerospace Sciences Meeting and Exhibit, Reno, NV, January 10-13, 2005.
- [17] Wang, H., Yang, B., and Jones, J.A., "Mobility Analysis of an Inflated Tumbleweed Ball under Wind Loads," AIAA-2002-1556, 43rd AIAA Structures, Structural Dynamics, and Materials Conference, Denver, Colorado, April 22-25, 2002. 3
- [18] Kane, T.R. and Levinson, D.A., *Dynamics: Theory and Applications*, McGraw-Hill, New York, 1985. 5, 7, 19, 32
- [19] Golombek, M.P., Cook, R.A., Moore, H.J., and Parker, T.J., "Selection of the Mars Pathfinder landing site," *Journal of Geophysical Research*, Vol. 103, No. E2, 1997. 97, 99
- [20] Hoeg, T., Southard, L., Boxerbaum, A., Reis, L., Antol, J., Heldmann, J., and Quinn, R., "Tumbleweed Rover Science Mission to Dao Vallis," *Proceedings of the 44th AIAA Aerospace Sciences Meeting*, Reno, Nevada, USA, January, 9-12 2005, No. 2006-70.
- [21] Antol, J. and Heldmann, J.: "Using Wind Driven Tumbleweed Rovers to Explore Martian Gully Features" AIAA-2005-0245, 43rd AIAA Aerospace Sciences Meeting and Exhibit, Reno, NV, January 10-13, 2005. 99
- [22] Universe Today, "Tumbleweed Rover Rolls in Antarctica," <http://www.universetoday.com/am/exec/view.cgi/1/1141>. Accessed 06/20/2006.  
101
- [23] Hibbeler, R.C., *Engineering Mechanics: Dynamics*, Pearson Prentice Hall, New Jersey, 2004.

- [24] Boyce, W.E., and DiPrima, R.C., *Elementary Differential Equations and Boundary Value Problems*, Wiley, New Jersey, 2003. [109](#)
- [25] Matlab, The Language of Technical Computing, Software Package, Ver, 6.5.0 Release 13, The MathWorks Inc., Natick, MA, 2002.

# Appendix

# Appendix A

## Example Of The Runge-Kutta Method

Consider the initial value problem

$$y' = f(t, y) \quad y(t_0) = y_0 \quad (\text{A.1})$$

The fourth-order Runge-Kutta method involves a weighted average of values of  $f(t, y)$  at different points in the interval  $t_n \leq t \leq t_{n+1}$ . It is given by

$$y_{n+1} = y_n + \frac{1}{6}(k_1 + 2k_2 + 2k_3 + k_4) \quad (\text{A.2})$$

where

$$k_1 = hf(t_n, y_n) \quad (\text{A.3})$$

$$k_2 = hf\left(t_n + \frac{h}{2}, y_n + \frac{1}{2}k_{n1}\right) \quad (\text{A.4})$$

$$k_3 = hf\left(t_n + \frac{h}{2}, y_n + \frac{1}{2}k_{n2}\right) \quad (\text{A.5})$$

$$k_4 = hf(t_{n+1}, y_n + k_{n3}) \quad (\text{A.6})$$

Note that the effective slope used is a weighted average of the slopes at the four points  $(t_n, y_n)$ ,  $(t_n + \frac{h}{2}, y_n + \frac{1}{2}k_{n1})$ ,  $(t_n + \frac{h}{2}, y_n + \frac{1}{2}k_{n2})$  and  $(t_{n+1}, y_n + k_{n3})$  in the  $t, y$  plane, an average because the sum of the coefficients  $1/6, 2/6, 2/6, 1/6$  that multiply the  $k$ 's is 1 (24).

# Appendix B

## Application Of The Runge-Kutta Method

This appendix illustrates the application of the Runge-Kutta method to the equations of motion derived for the trajectory and the rolling and sliding models for the horizontal, incline and decline planes.

### B.1 Numerical Models on the Horizontal Plane

Applying the Runge-Kutta method to equations (2.82) and (2.83) yields expressions that determine the sphere's position and velocity between bounces in the  $\vec{n}_1$  and  $\vec{n}_2$  directions respectively. Assuming a time step of  $h$ , we have in the  $\vec{n}_1$  direction:

$$q_1(i + 1) = q_1(i) + 1/6 * (k_1 + 2 * k_2 + 2 * k_3 + k_4) \quad (\text{B.1})$$

$$u_4(i + 1) = u_4(i) + 1/6 * (l_1 + 2 * l_2 + 2 * l_3 + l_4) \quad (\text{B.2})$$

where

$$k_1 = h * u_4(i) \quad (\text{B.3})$$

$$l_1 = 0 \quad (\text{B.4})$$

$$k2 = h * (u4(i) + 0.5 * l1) \quad (\text{B.5})$$

$$l2 = 0 \quad (\text{B.6})$$

$$k3 = h * (u4(i) + 0.5 * l2) \quad (\text{B.7})$$

$$l3 = 0 \quad (\text{B.8})$$

$$k4 = h * (u4(i) + l3) \quad (\text{B.9})$$

$$l4 = 0 \quad (\text{B.10})$$

For the  $\vec{n}_2$  direction, we have:

$$q_2(i + 1) = q_2(i) + 1/6 * (k1 + 2 * k2 + 2 * k3 + k4) \quad (\text{B.11})$$

$$u_5(i + 1) = u_5(i) + 1/6 * (l1 + 2 * l2 + 2 * l3 + l4) \quad (\text{B.12})$$

where

$$k1 = h * u_5(i) \quad (\text{B.13})$$

$$l1 = -h * g \quad (\text{B.14})$$

$$k2 = h * (u_5(i) + 0.5 * l1) \quad (\text{B.15})$$

$$l2 = -h * g \quad (\text{B.16})$$

$$k3 = h * (u_5(i) + 0.5 * l2) \quad (\text{B.17})$$

$$l3 = -h * g \quad (\text{B.18})$$

$$k4 = h * (u_5(i) + l3) \quad (\text{B.19})$$

$$l4 = -h * g \quad (\text{B.20})$$

Next, we apply the Runge-Kutta method to the rolling model previously developed. We list the expressions that determine the sphere's position and translational velocity in the  $\vec{n}_1, \vec{n}_2$  directions and the angular velocity in the  $\vec{n}_3$  direction respectively. Again, we must take into account the relationship between  $|v|$  and  $|\omega| r$ . For  $|v| > |\omega| r$  and considering equations (3.2) and (3.3), we have:

$$q_2(i + 1) = q_2(i) \quad (\text{B.21})$$

$$q_1(i + 1) = q_1(i) + 1/6 * (k1 + 2 * k2 + 2 * k3 + k4) \quad (\text{B.22})$$

$$u_4(i + 1) = u_4(i) + 1/6 * (l1 + 2 * l2 + 2 * l3 + l4) \quad (\text{B.23})$$

where

$$k1 = h * u4(i) \quad (B.24)$$

$$l1 = -h * \mu' * g \quad (B.25)$$

$$k2 = h * (u4(i) + 0.5 * l1) \quad (B.26)$$

$$l2 = -h * \mu' * g \quad (B.27)$$

$$k3 = h * (u4(i) + 0.5 * l2) \quad (B.28)$$

$$l3 = -h * \mu' * g \quad (B.29)$$

$$k4 = h * (u4(i) + l3) \quad (B.30)$$

$$l4 = -h * \mu' * g \quad (B.31)$$

and

$$u3(i + 1) = u3(i) + 1/6 * (l1 + 2 * l2 + 2 * l3 + l4) \quad (B.32)$$

where

$$k1 = h * u3(i) \quad (B.33)$$

$$l1 = h * b * \mu' * g / J_G / m \quad (B.34)$$

$$k2 = h * (u3(i) + 0.5 * l1) \quad (B.35)$$

$$l2 = h * b * \mu' * g / J_G / m \quad (B.36)$$

$$k3 = h * (u3(i) + 0.5 * l2) \quad (B.37)$$

$$l3 = h * b * \mu' * g / J_G / m \quad (B.38)$$

$$k4 = h * (u3(i) + l3) \quad (B.39)$$

$$l4 = h * b * \mu' * g / J_G / m \quad (B.40)$$

For  $|v| < |\omega| r$  and considering equations (3.5) and (3.6), we have:

$$q2(i + 1) = q2(i) \quad (B.41)$$

$$q1(i + 1) = q1(i) + 1/6 * (k1 + 2 * k2 + 2 * k3 + k4) \quad (B.42)$$

$$u4(i + 1) = u4(i) + 1/6 * (l1 + 2 * l2 + 2 * l3 + l4) \quad (B.43)$$

where

$$k1 = h * u4(i) \quad (B.44)$$

$$l1 = h * \mu' * g \quad (B.45)$$

$$k2 = h * (u4(i) + 0.5 * l1) \quad (B.46)$$

$$l2 = h * \mu' * g \quad (B.47)$$

$$k3 = h * (u4(i) + 0.5 * l2) \quad (B.48)$$

$$l3 = h * \mu' * g \quad (B.49)$$

$$k4 = h * (u4(i) + l3) \quad (B.50)$$

$$l4 = h * \mu' * g \quad (B.51)$$

and

$$u3(i + 1) = u3(i) + 1/6 * (l1 + 2 * l2 + 2 * l3 + l4) \quad (B.52)$$

where

$$k1 = h * u3(i) \quad (B.53)$$

$$l1 = -h * b * \mu' * g / J_G / m \quad (B.54)$$

$$k2 = h * (u3(i) + 0.5 * l1) \quad (B.55)$$

$$l2 = -h * b * \mu' * g / J_G / m \quad (B.56)$$

$$k3 = h * (u3(i) + 0.5 * l2) \quad (B.57)$$

$$l3 = -h * b * \mu' * g / J_G / m \quad (B.58)$$

$$k4 = h * (u3(i) + l3) \quad (B.59)$$

$$l4 = -h * b * \mu' * g / J_G / m \quad (B.60)$$

For  $|v| = |\omega| r$  and considering equations (3.8) and (3.7), we have:

$$q2(i + 1) = q2(i) \quad (B.61)$$

$$q1(i + 1) = q1(i) + 1/6 * (k1 + 2 * k2 + 2 * k3 + k4) \quad (B.62)$$

$$u4(i + 1) = u4(i) + 1/6 * (l1 + 2 * l2 + 2 * l3 + l4) \quad (B.63)$$

where

$$k1 = h * u4(i) \tag{B.64}$$

$$l1 = 0 \tag{B.65}$$

$$k2 = h * (u4(i) + 0.5 * l1) \tag{B.66}$$

$$l2 = 0 \tag{B.67}$$

$$k3 = h * (u4(i) + 0.5 * l2) \tag{B.68}$$

$$l3 = 0 \tag{B.69}$$

$$k4 = h * (u4(i) + l3) \tag{B.70}$$

$$l4 = 0 \tag{B.71}$$

and

$$u3(i + 1) = u3(i) + 1/6 * (l1 + 2 * l2 + 2 * l3 + l4) \tag{B.72}$$

where

$$k1 = h * u3(i) \tag{B.73}$$

$$l1 = 0 \tag{B.74}$$

$$k2 = h * (u3(i) + 0.5 * l1) \tag{B.75}$$

$$l2 = 0 \tag{B.76}$$

$$k3 = h * (u3(i) + 0.5 * l2) \tag{B.77}$$

$$l3 = 0 \tag{B.78}$$

$$k4 = h * (u3(i) + l3) \tag{B.79}$$

$$l4 = 0 \tag{B.80}$$

## B.2 Numerical Models on the Incline Plane

Applying the Runge-Kutta method to equations (2.167) and (2.168) yields expressions that determine the sphere's position and velocity between bounces in

the  $\vec{c}_1$  and  $\vec{c}_2$  directions respectively. Assuming a time step of  $h$ , we have in the  $\vec{c}_1$  direction:

$$q_{11}(i+1) = q_{11}(i) + 1/6 * (k1 + 2 * k2 + 2 * k3 + k4) \quad (\text{B.81})$$

$$u_{44}(i+1) = u_{44}(i) + 1/6 * (l1 + 2 * l2 + 2 * l3 + l4) \quad (\text{B.82})$$

where

$$k1 = h * u_{44}(i) \quad (\text{B.83})$$

$$l1 = -h * g * \sin\theta \quad (\text{B.84})$$

$$k2 = h * (u_{44}(i) + 0.5 * l1) \quad (\text{B.85})$$

$$l2 = -h * g * \sin\theta \quad (\text{B.86})$$

$$k3 = h * (u_{44}(i) + 0.5 * l2) \quad (\text{B.87})$$

$$l3 = -h * g * \sin\theta \quad (\text{B.88})$$

$$k4 = h * (u_{44}(i) + l3) \quad (\text{B.89})$$

$$l4 = -h * g * \sin\theta \quad (\text{B.90})$$

For the  $\vec{c}_2$  direction, we have:

$$q_{22}(i+1) = q_{22} + 1/6 * (k1 + 2 * k2 + 2 * k3 + k4) \quad (\text{B.91})$$

$$u_{55}(i+1) = u_{55}(i) + 1/6 * (l1 + 2 * l2 + 2 * l3 + l4) \quad (\text{B.92})$$

where

$$k1 = h * u_{55}(i) \quad (\text{B.93})$$

$$l1 = -h * g * \cos\theta \quad (\text{B.94})$$

$$k2 = h * (u_{55}(i) + 0.5 * l1) \quad (\text{B.95})$$

$$l2 = -h * g * \cos\theta \quad (\text{B.96})$$

$$k3 = h * (u_{55}(i) + 0.5 * l2) \quad (\text{B.97})$$

$$l3 = -h * g * \cos\theta \quad (\text{B.98})$$

$$k4 = h * (u_{55}(i) + l3) \quad (\text{B.99})$$

$$l4 = -h * g * \cos\theta \quad (\text{B.100})$$

Next, we apply the Runge-Kutta method to the rolling model previously developed. We list the expressions that determine the sphere's position and translational velocity in the  $\vec{c}_1, \vec{c}_2$  directions and the angular velocity in the  $\vec{c}_3$  direction respectively. Again, we must take into account the relationship between  $|v|$  and  $|\omega| r$ . For  $|v| > |\omega| r$  and considering equations (3.10) and (3.11), we have:

$$q_{22}(i+1) = q_{22}(i) \quad (\text{B.101})$$

$$q_{11}(i+1) = q_{11}(i) + 1/6 * (k1 + 2 * k2 + 2 * k3 + k4) \quad (\text{B.102})$$

$$u_{44}(i+1) = u_{44}(i) + 1/6 * (l1 + 2 * l2 + 2 * l3 + l4) \quad (\text{B.103})$$

where

$$k1 = h * u_{44}(i) \quad (\text{B.104})$$

$$l1 = -h * g(\mu' \cos\theta + \sin\theta) \quad (\text{B.105})$$

$$k2 = h * (u_{44}(i) + 0.5 * l1) \quad (\text{B.106})$$

$$l2 = -h * g(\mu' \cos\theta + \sin\theta) \quad (\text{B.107})$$

$$k3 = h * (u_{44}(i) + 0.5 * l2) \quad (\text{B.108})$$

$$l3 = -h * g(\mu' \cos\theta + \sin\theta) \quad (\text{B.109})$$

$$k4 = h * (u_{44}(i) + l3) \quad (\text{B.110})$$

$$l4 = -h * g(\mu' \cos\theta + \sin\theta) \quad (\text{B.111})$$

and

$$u_{33}(i+1) = u_{33}(i) + 1/6 * (l1 + 2 * l2 + 2 * l3 + l4) \quad (\text{B.112})$$

where

$$k1 = h * u_{33}(i) \quad (\text{B.113})$$

$$l1 = h * \frac{\mu' g b \cos\theta}{J_G/m} \quad (\text{B.114})$$

$$k2 = h * (u_{33}(i) + 0.5 * l1) \quad (\text{B.115})$$

$$l2 = h * \frac{\mu' g b \cos\theta}{J_G/m} \quad (\text{B.116})$$

$$k3 = h * (u_{33}(i) + 0.5 * l2) \quad (\text{B.117})$$

$$l3 = h * \frac{\mu' g b \cos \theta}{J_G / m} \quad (\text{B.118})$$

$$k4 = h * (u33(i) + l3) \quad (\text{B.119})$$

$$l4 = h * \frac{\mu' g b \cos \theta}{J_G / m} \quad (\text{B.120})$$

For  $|v| < |\omega| r$  and considering equations (3.13) and (3.14), we have:

$$q22(i+1) = q22(i) \quad (\text{B.121})$$

$$q11(i+1) = q11(i) + 1/6 * (k1 + 2 * k2 + 2 * k3 + k4) \quad (\text{B.122})$$

$$u44(i+1) = u44(i) + 1/6 * (l1 + 2 * l2 + 2 * l3 + l4) \quad (\text{B.123})$$

where

$$k1 = h * u44(i) \quad (\text{B.124})$$

$$l1 = h * g(\mu' \cos \theta - \sin \theta) \quad (\text{B.125})$$

$$k2 = h * (u44(i) + 0.5 * l1) \quad (\text{B.126})$$

$$l2 = h * g(\mu' \cos \theta - \sin \theta) \quad (\text{B.127})$$

$$k3 = h * (u44(i) + 0.5 * l2) \quad (\text{B.128})$$

$$l3 = h * g(\mu' \cos \theta - \sin \theta) \quad (\text{B.129})$$

$$k4 = h * (u44(i) + l3) \quad (\text{B.130})$$

$$l4 = h * g(\mu' \cos \theta - \sin \theta) \quad (\text{B.131})$$

and

$$u33(i+1) = u33(i) + 1/6 * (l1 + 2 * l2 + 2 * l3 + l4) \quad (\text{B.132})$$

where

$$k1 = h * u33(i) \quad (\text{B.133})$$

$$l1 = -h * \frac{\mu' g b \cos \theta}{J_G / m} \quad (\text{B.134})$$

$$k2 = h * (u33(i) + 0.5 * l1) \quad (\text{B.135})$$

$$l2 = -h * \frac{\mu' g b \cos \theta}{J_G / m} \quad (\text{B.136})$$

$$k3 = h * (u33(i) + 0.5 * l2) \quad (\text{B.137})$$

$$l3 = -h * \frac{\mu' g b \cos \theta}{J_G / m} \quad (\text{B.138})$$

$$k4 = h * (u33(i) + l3) \quad (\text{B.139})$$

$$l4 = -h * \frac{\mu' g b \cos \theta}{J_G / m} \quad (\text{B.140})$$

For  $|v| = |\omega| r$  and considering equations (3.16) and (3.15), we have:

$$q22(i+1) = q22(i) \quad (\text{B.141})$$

$$q11(i+1) = q11(i) + 1/6 * (k1 + 2 * k2 + 2 * k3 + k4) \quad (\text{B.142})$$

$$u44(i+1) = u44(i) + 1/6 * (l1 + 2 * l2 + 2 * l3 + l4) \quad (\text{B.143})$$

where

$$k1 = h * u44(i) \quad (\text{B.144})$$

$$l1 = -h * \frac{g b^2 \sin \theta}{J_G / m + b^2} \quad (\text{B.145})$$

$$k2 = h * (u44(i) + 0.5 * l1) \quad (\text{B.146})$$

$$l2 = -h * \frac{g b^2 \sin \theta}{J_G / m + b^2} \quad (\text{B.147})$$

$$k3 = h * (u44(i) + 0.5 * l2) \quad (\text{B.148})$$

$$l3 = -h * \frac{g b^2 \sin \theta}{J_G / m + b^2} \quad (\text{B.149})$$

$$k4 = h * (u44(i) + l3) \quad (\text{B.150})$$

$$l4 = -h * \frac{g b^2 \sin \theta}{J_G / m + b^2} \quad (\text{B.151})$$

and

$$u33(i+1) = u33(i) + 1/6 * (l1 + 2 * l2 + 2 * l3 + l4) \quad (\text{B.152})$$

where

$$k1 = h * u33(i) \quad (\text{B.153})$$

$$l1 = -h * \frac{g b \sin \theta}{J_G / m + b^2} \quad (\text{B.154})$$

$$k2 = h * (u33(i) + 0.5 * l1) \quad (\text{B.155})$$

$$l2 = -h * \frac{g b \sin \theta}{J_G / m + b^2} \quad (\text{B.156})$$

$$k3 = h * (u33(i) + 0.5 * l2) \quad (\text{B.157})$$

$$l3 = -h * \frac{gbsin\theta}{J_G/m + b^2} \quad (\text{B.158})$$

$$k4 = h * (u33(i) + l3) \quad (\text{B.159})$$

$$l4 = -h * \frac{gbsin\theta}{J_G/m + b^2} \quad (\text{B.160})$$

### B.3 Numerical Models on the Decline Plane

Applying the Runge-Kutta method to equations (2.253) and (2.254) yields expressions that determine the sphere's position and velocity between bounces in the  $\vec{a}_1$  and  $\vec{a}_2$  directions respectively. Assuming a time step of  $h$ , we have in the  $\vec{a}_1$  direction:

$$q_{111}(i + 1) = q_{111}(i) + 1/6 * (k1 + 2 * k2 + 2 * k3 + k4) \quad (\text{B.161})$$

$$u_{444}(i + 1) = u_{444}(i) + 1/6 * (l1 + 2 * l2 + 2 * l3 + l4) \quad (\text{B.162})$$

where

$$k1 = h * u_{444}(i) \quad (\text{B.163})$$

$$l1 = h * g * \sin\beta \quad (\text{B.164})$$

$$k2 = h * (u_{444}(i) + 0.5 * l1) \quad (\text{B.165})$$

$$l2 = h * g * \sin\beta \quad (\text{B.166})$$

$$k3 = h * (u_{444}(i) + 0.5 * l2) \quad (\text{B.167})$$

$$l3 = h * g * \sin\beta \quad (\text{B.168})$$

$$k4 = h * (u_{444}(i) + l3) \quad (\text{B.169})$$

$$l4 = h * g * \sin\beta \quad (\text{B.170})$$

For the  $\vec{a}_2$  direction, we have:

$$q_{222}(i + 1) = q_{222}(i) + 1/6 * (k1 + 2 * k2 + 2 * k3 + k4) \quad (\text{B.171})$$

$$u_{555}(i + 1) = u_{555}(i) + 1/6 * (l1 + 2 * l2 + 2 * l3 + l4) \quad (\text{B.172})$$

where

$$k1 = h * u555(i) \quad (\text{B.173})$$

$$l1 = -h * g * \cos\beta \quad (\text{B.174})$$

$$k2 = h * (u555(i) + 0.5 * l1) \quad (\text{B.175})$$

$$l2 = -h * g * \cos\beta \quad (\text{B.176})$$

$$k3 = h * (u555(i) + 0.5 * l2) \quad (\text{B.177})$$

$$l3 = -h * g * \cos\beta \quad (\text{B.178})$$

$$k4 = h * (u555(i) + l3) \quad (\text{B.179})$$

$$l4 = -h * g * \cos\beta \quad (\text{B.180})$$

Next, we apply the Runge-Kutta method to the rolling model previously developed. We list the expressions that determine the sphere's position and translational velocity in the  $\vec{a}_1, \vec{a}_2$  directions and the angular velocity in the  $\vec{a}_3$  direction respectively. Again, we must take into account the relationship between  $|v|$  and  $|\omega| r$ . For  $|v| > |\omega| r$  and considering equations (3.20) and (3.21), we have:

$$q_{222}(i+1) = q_{222}(i) \quad (\text{B.181})$$

$$q_{111}(i+1) = q_{111}(i) + 1/6 * (k1 + 2 * k2 + 2 * k3 + k4) \quad (\text{B.182})$$

$$u_{444}(i+1) = u_{444}(i) + 1/6 * (l1 + 2 * l2 + 2 * l3 + l4) \quad (\text{B.183})$$

where

$$k1 = h * u444(i) \quad (\text{B.184})$$

$$l1 = -h * g(\mu' \cos\beta - \sin\beta) \quad (\text{B.185})$$

$$k2 = h * (u444(i) + 0.5 * l1) \quad (\text{B.186})$$

$$l2 = -h * g(\mu' \cos\beta - \sin\beta) \quad (\text{B.187})$$

$$k3 = h * (u444(i) + 0.5 * l2) \quad (\text{B.188})$$

$$l3 = -h * g(\mu' \cos\beta - \sin\beta) \quad (\text{B.189})$$

$$k4 = h * (u444(i) + l3) \quad (\text{B.190})$$

$$l4 = -h * g(\mu' \cos\beta - \sin\beta) \quad (\text{B.191})$$

and

$$u_{333}(i+1) = u_{333}(i) + 1/6 * (l1 + 2 * l2 + 2 * l3 + l4) \quad (\text{B.192})$$

where

$$k1 = h * u_{333}(i) \quad (\text{B.193})$$

$$l1 = h * \frac{\mu' g b \cos \beta}{J_G / m} \quad (\text{B.194})$$

$$k2 = h * (u_{333}(i) + 0.5 * l1) \quad (\text{B.195})$$

$$l2 = h * \frac{\mu' g b \cos \beta}{J_G / m} \quad (\text{B.196})$$

$$k3 = h * (u_{333}(i) + 0.5 * l2) \quad (\text{B.197})$$

$$l3 = h * \frac{\mu' g b \cos \beta}{J_G / m} \quad (\text{B.198})$$

$$k4 = h * (u_{333}(i) + l3) \quad (\text{B.199})$$

$$l4 = h * \frac{\mu' g b \cos \beta}{J_G / m} \quad (\text{B.200})$$

For  $|v| < |\omega| r$  and considering equations (3.23) and (3.24), we have:

$$q_{222}(i+1) = q_{222}(i) \quad (\text{B.201})$$

$$q_{111}(i+1) = q_{111}(i) + 1/6 * (k1 + 2 * k2 + 2 * k3 + k4) \quad (\text{B.202})$$

$$u_{444}(i+1) = u_{444}(i) + 1/6 * (l1 + 2 * l2 + 2 * l3 + l4) \quad (\text{B.203})$$

where

$$k1 = h * u_{444}(i) \quad (\text{B.204})$$

$$l1 = h * g(\mu' \cos \beta + \sin \beta) \quad (\text{B.205})$$

$$k2 = h * (u_{444}(i) + 0.5 * l1) \quad (\text{B.206})$$

$$l2 = h * g(\mu' \cos \beta + \sin \beta) \quad (\text{B.207})$$

$$k3 = h * (u_{444}(i) + 0.5 * l2) \quad (\text{B.208})$$

$$l3 = h * g(\mu' \cos \beta + \sin \beta) \quad (\text{B.209})$$

$$k4 = h * (u_{444}(i) + l3) \quad (\text{B.210})$$

$$l4 = h * g(\mu' \cos \beta + \sin \beta) \quad (\text{B.211})$$

and

$$u_{333}(i+1) = u_{333}(i) + 1/6 * (l1 + 2 * l2 + 2 * l3 + l4) \quad (\text{B.212})$$

where

$$k1 = h * u_{333}(i) \quad (\text{B.213})$$

$$l1 = -h * \frac{\mu' g b \cos \beta}{J_G/m} \quad (\text{B.214})$$

$$k2 = h * (u_{333}(i) + 0.5 * l1) \quad (\text{B.215})$$

$$l2 = -h * \frac{\mu' g b \cos \beta}{J_G/m} \quad (\text{B.216})$$

$$k3 = h * (u_{333}(i) + 0.5 * l2) \quad (\text{B.217})$$

$$l3 = -h * \frac{\mu' g b \cos \beta}{J_G/m} \quad (\text{B.218})$$

$$k4 = h * (u_{333}(i) + l3) \quad (\text{B.219})$$

$$l4 = -h * \frac{\mu' g b \cos \beta}{J_G/m} \quad (\text{B.220})$$

For  $|v| = |\omega| r$  and considering equations (3.26) and (3.25), we have:

$$q_{222}(i+1) = q_{222}(i) \quad (\text{B.221})$$

$$q_{111}(i+1) = q_{111}(i) + 1/6 * (k1 + 2 * k2 + 2 * k3 + k4) \quad (\text{B.222})$$

$$u_{444}(i+1) = u_{444}(i) + 1/6 * (l1 + 2 * l2 + 2 * l3 + l4) \quad (\text{B.223})$$

where

$$k1 = h * u_{444}(i) \quad (\text{B.224})$$

$$l1 = h * \frac{g b^2 \sin \beta}{J_G/m + b^2} \quad (\text{B.225})$$

$$k2 = h * (u_{444}(i) + 0.5 * l1) \quad (\text{B.226})$$

$$l2 = h * \frac{g b^2 \sin \beta}{J_G/m + b^2} \quad (\text{B.227})$$

$$k3 = h * (u_{444}(i) + 0.5 * l2) \quad (\text{B.228})$$

$$l3 = h * \frac{g b^2 \sin \beta}{J_G/m + b^2} \quad (\text{B.229})$$

$$k4 = h * (u_{444}(i) + l3) \quad (\text{B.230})$$

$$l4 = h * \frac{g b^2 \sin \beta}{J_G/m + b^2} \quad (\text{B.231})$$

and

$$u_{333}(i + 1) = u_{333}(i) + 1/6 * (l1 + 2 * l2 + 2 * l3 + l4) \quad (\text{B.232})$$

where

$$k1 = h * u_{333}(i) \quad (\text{B.233})$$

$$l1 = h * \frac{gbsin\beta}{J_G/m + b^2} \quad (\text{B.234})$$

$$k2 = h * (u_{333}(i) + 0.5 * l1) \quad (\text{B.235})$$

$$l2 = h * \frac{gbsin\beta}{J_G/m + b^2} \quad (\text{B.236})$$

$$k3 = h * (u_{333}(i) + 0.5 * l2) \quad (\text{B.237})$$

$$l3 = h * \frac{gbsin\beta}{J_G/m + b^2} \quad (\text{B.238})$$

$$k4 = h * (u_{333}(i) + l3) \quad (\text{B.239})$$

$$l4 = h * \frac{gbsin\beta}{J_G/m + b^2} \quad (\text{B.240})$$